# Anti-counterfeiting method using synthesized Nanocrystalline Cellulose Taggants

**Yu Ping Zhang**

**Department of Electrical and Computer Engineering**
**McGill University, Montreal**

**November 21, 2012**

**A thesis submitted to McGill University in partial fulfillment of the requirements of the degree of Ph.D.**

# Abstract

For as long as economies and trade have existed, there have been people who have attempted to produce imitations of valuable goods for personal gain. Counterfeiting is a substantial drain on business, costing the U.S. economy between $200-250 billion annually, as well as billions of dollars in losses to the Canadian economy. The increased in counterfeiting attests to the limitation of present security techniques and indicates a strong need to develop more secure ones. In this contribution, we synthesize Nanocrystalline Cellulose (NCC), study the optical properties of this novel material, and propose that NCC can be used as a sophisticated anti-counterfeiting taggant.

We suggest that NCC security taggants possess multiple security features: overt iridescence, covert selective reflection, ultraviolet fluorescence, covert unique morphology, a white light diffraction pattern, and a water induced color variation. The origin of the iridescence of NCC comes from both the Bragg multilayer reflection and surface relief grating diffraction, while the covert selective reflection security feature comes from the chiral structure formed during the casting by self-assembly of NCC. In order to add another covert security feature, ultraviolet fluorescence, an Optical Brightening Agents (OBA) was incorporated into the NCC suspension, and the result is a fluorescent and iridescent NCC material. The white light diffraction pattern which arises from the morphology of the NCC taggant provides further covert security. We also show that this NCC material displays water induced color variation which may also be used as security feature.

Compared to conventional anti-counterfeiting techniques, the proposed method has several advantages: one system supports multi-level security, including overt and covert features. These features are very difficult to copy, but can be authenticated using low-cost tools, as well as a simple optical set-up when further lab tests are needed.

# Résumé

Depuis que l'économie et le commerce existent, des gens ont tenté de créer des imitations de marchandises de valeur pour leur profit personnel. La contrefaçon engendre des pertes substantielles, coûtant entre 200 et 250 milliards de dollars annuellement à l'économie des États-Unis ainsi que des pertes de milliards de dollars à l'économie canadienne. L'augmentation de la contrefaçon souligne les limites des technologies présentement utilisées pour la sécurité et indique le besoin grandissant pour le développement d'une nouvelle technologie d'authentification. Dans cette contribution, nous synthétisons la nanocellulose cristalline (NCC), nous étudions les propriétés optiques de ce nouveau matériau, et nous proposons l'utilisation de la cellule nanocristalline (NCC) comme marqueur anti-contrefaçon sophistiqué.

Nous suggérons que la NCC traceurs de sécurité possèdent plusieurs fonctions de sécurité: une irisation manifeste, une sélection de réflexions masquées, une fluorescence ultraviolette, une morphologie unique masquée et un motif de diffraction de la lumière blanche. L'origine de l'irisation de la NCC vient à la fois de la réflexion de Bragg sur de multiples interfaces et du relief sur la surface du réseau de diffraction, alors que la sélection de réflexions masquées vient de la structure chirale formée lors du moulage par autoassemblage du NCC. Afin d'inclure une autre caractéristique de sécurité masquée, la fluorescence ultraviolette, un agent azurant, est ajoutée au NCC en suspension ce qui lui apporte la fluorescence et l'irisation. Finalement, la morphologie du marqueur NCC et le motif de diffraction de la lumière blanche fournissent des éléments de sécurité masqués supplémentaires.

La méthode proposée possède de multiples avantages par rapport aux méthodes d'anti-contrefaçon conventionnelles: un système de sécurité à multiples niveaux, incluant des caractéristiques manifestes et masquées. Ces caractéristiques sont très difficiles à reproduire mais peuvent être authentifiées grâce à des outils à faible coût ainsi qu'avec un système optique simple lorsque de plus amples tests seront nécessaires.

# Publications

## List of publications

**Results of Chapter 5 have been published as refereed paper:**

Y. P. Zhang, V. P. Chodavarapu, A. G. Kirk, M. P. Andrews, "Nanocrystalline cellulose for covert optical encryption," SPIE Journal of Nanophotonics, vol. 6, art. 063516 (2012)

**Results of Chapter 5 has been published in SPIE Professional Magazine October 2012**

R&D Highlights, Editor's Recommendation "The color of money"

**Results of Chapter 6 have been published as refereed paper:**

Y.P. Zhang, V.P. Chodavarapu, A.G. Kirk, M.P.Andrews, " Structured color humidity indicator from reversible pitch tuning in self-assembled nanocrystalline cellulose films," Sensors and Actuators B: Chemical (2012)

# Contributions of Co-Authors

In this study, many attractive optical features of nanocrcytalline cellulose have been found, and some results have been published in peer-reviewed journals as listed previously. Professor Andrew Kirk, Professor Vamsy Chodavarapu and Professor Mark Andrews, co-authored all resulting publications. Except for their invaluable supervision in Nanocrystalline Cellulose (NCC) research area and correction of the manuscripts, I proposed the research objectives, established the methodologies, conducted the experiments and eventually wrote drafts of manuscript describing the results obtained.

# Acknowledgements

First and foremost, I would like to express my sincere appreciation to my advisors Dr. Andrew G. Kirk, Dr. Vamsy Chodavarapu and Dr. Mark Andrews for their continuous support and guidance throughout my PhD study. I am very grateful for their encouragement during the ups and downs of my PhD research. What I learned from them will definitely benefit my future career. I would also like to extend my appreciation to Dr. Zetian Mi who is one of my PhD committee members.

I would like to thank the following people and organizations who assisted me during the course of my research: Sebastien Ricoult from Neuro-science, Prof. Jay Nadeau from Biomedical Engineering, Petr Fiurasek from CSACS, Dr. David Liu from FEMR, Timothy Gonzalez, Mohini Ramkaran from Chemistry Department, and Dr. Judith Kornblatt from Concordia University.

Special thanks is extended to the Dr. Johns from School of Dietetics and Human Nutrition of McGill and his colleague Dr. Pat Owen for allowing me to use their Willy mill. Without their help, my study would have been further delayed.

Thanks to my photonics group colleagues who companioned me during these years.

Many thanks also go to the Faculty and Staff members of Department of Electrical and Computer Engineering.

I would like to acknowledge the financial support from the ArboraNano Network and the Fonds québécois de la recherche sur la nature et les technologies (FQRNT).

Finally, I would like to thank my family for their unconditional love, support and trust throughout these many years.

# Table of Contents

# List of Tables

# List of Figures

# ORIGINAL CONTRIBUTIONS

In this study, we demonstrated for the first time that iridescent NCC taggants can be created using a neutral NCC suspension without the need for any electric or magnetic field. This was accomplished by optimizing the sulfuric acid hydrolysis process parameters, particularly the wood species, acid-to-pulp ratio, hydrolysis time, and sonication. The neutral state is desired when NCC is going to be used in a process in which the pH is important, such as printing, without the need for concern for damage that could be caused by a strong acid. The elimination of the need for an external field, on the other hand, simplifies the iridescence formation process.

Secondly, we demonstrated for the first time that iridescence can be produced in liquid chiral nematic NCC suspension, and that one can obtain different white light diffraction patterns by controlling the NCC casting environment conditions. Moreover, these ordered structures can be transferred to a solid phase when water is evaporated. The significance of these findings are that either the self-assembly structure formed in liquid phase or the structure formed in solid phase can be used as a template to create many other possible device applications.

Thirdly, iridescent and fluorescent NCC taggants have been made in this work. This was accomplished by adding OBA, a UV fluorescent dye, into NCC and controlling the dosage of the OBA addition. We also demonstrated that OBA-doped NCC is circularly polarized, and this property adds further security to the NCC taggant.

In addition, by examining the surface morphology and the white light diffraction of the iridescent NCC, we found the surface of the NCC not only has a unique morphology but also has a unique white light diffraction pattern, both of which are features for possible security application.

Furthermore, a structured color humidity indicator from reversible pitch tuning in self-assembled nanocrystalline cellulose films has been demonstrated. The significance of this work not only gave insight into the color shift induced by moisture, but also suggests the possibility of using water to authenticate the NCC material when used as a security taggant.

Finally, by combining all the security features, such as iridescence, selective reflection, UV fluorescence, unique morphology, white-light diffraction pattern, and water induced color variation, one can arrive at a sophisticated NCC taggant. The result is a single system supporting multiple levels security features. Moreover, in this thesis, we provide authenticating methods that are low-cost and simple for brand owners and consumers. The proposed taggant is very hard to mimic because of the complexity of making these security features. Therefore, any attempt to counterfeit would require the counterfeiters to recreate the NCC synthesis process, which requires advanced chemistry techniques. Moreover, some of these techniques, such as the relationship between the chirality of NCC and iridescence, require knowhow that is not readily available in the literature.

# Chapter 1

# INTRODUCTION

## 1.1 Background and Statement of Problems

As defined in its broadest sense, counterfeiting is as old as human civilization itself. Once something of value has been produced, others have often sought to copy it. Today, counterfeiting is a major black market industry. The U.S. economy loses between $200 billion and $250 billion annually [1] and, according to another report in 2007 [2], Canadian businesses have lost billions of dollars to date. Counterfeiting can be observed in almost every aspect of society, from electronics to food and pharmaceuticals, military equipment, and most notably in currency, such as banknotes. The amount of counterfeiting activity has increased substantially over time; governments of many countries, including Canada, take this issue very seriously. The Bank of Canada issued a new polymer-based banknote in November of 2011 specifically to combat latent counterfeiters.

The importance of developing effective anti-counterfeiting methods cannot be overstated. The race between developers of anti-counterfeiting techniques and counterfeiters is an eternal one. Tireless vigilance and revision are the only means officials have to stay ahead of the counterfeiter. Unique encryption methods are currently much sought after as the best assurance of authenticity, but the attainment of any means to jump ahead of the criminal competition should also be important.

Effective anti-counterfeiting techniques are often multilayered technologies consisting features that are both overt (readily visible to the naked eye) or covert (undetectable without the use of special equipment and/or chemicals). A classic example of an overt feature is the hologram of the MasterCard® logo found on credit cards issued by various financial institutions. The average consumer can easily determine the authenticity of the cards because they are familiar with the company's advertisements or publicity. Overt features are advantageous in the sense there is no need for special equipment, and they are easily accessible to the consumer as well as the retailer. Various technologies can be used for overt security, one of the most common being security printing. Printed security features can be layered into the various printing stages and incorporated into the different materials used during the manufacturing of a product. These features include security paper, threads, and physical watermarks as well as digital watermarks and laminates. Other commonly employed overt features are the aforementioned hologram in which an image or the colors of an image change depending on the viewing angle. The problem with all overt techniques, however, is that a counterfeiter can easily study them and, given time and resources, reproduce them.

There is a much lower risk of covert techniques being replicated in this manner as they are invisible without special equipment. Indeed, most consumers are largely unaware of covert security measures and so they are not ideal techniques in situations where products pass through a large number of hands or where it is difficult to obtain a means of verification. There is great interest in developing sophisticated, inexpensive anti-counterfeiting techniques that allow officials to deploy both covert and overt techniques while keeping them ahead of the competition.

## 1.2 Thesis Objectives

In this study, we propose the use of Nanocrystalline Cellulose (NCC), a material derived from wood pulp, as the basis of a more secure and less expensive anti-counterfeiting device.

The objectives of this thesis are:

- To synthesis NCC from wood pulp
- To create iridescent NCC material
- To explore the NCC material's optical properties
- To functionalize NCC material with UV fluorescent dye
- To explore the potential for making an anti-counterfeiting device by using this newly developed NCC material.

## 1.3 Thesis Structure

This thesis is presented in eight Chapters following the sequence of the development of our security method, including an introductory and a literature review Chapter.

Chapter 3 deals with the synthesis of NCC as well as crystallite ordering and iridescence in the fluid phase. Iridescence is an optical property that potentially can be used as a security feature, iridescence in holograms being a good example. However, iridescence from NCC in fluid phase has not been well documented. Since NCC possesses liquid crystalline properties, the ordering of NCC particles may play a role in the

formation of iridescence. Wether or not this ordering and resultant iridescence formed initially in solution can be qualitatively transferred into the solid phase need to be futher explored. In this study, laser diffraction will be used to monitor the evolution of order in aqueous NCC suspension. Stereomicroscopy will be used to record the retardation lines in the bulk fluid phase and white light diffraction will be used to investigate bulk grating formation in the NCC suspension. The purpose of this study is to determine key factors that affect the formation of iridescence in the fluid phase.

Chapter 4 deals with the origin of iridescence in solid films of NCC. It has been determined that NCC made from specific wood species under certain acid hydrolysis conditions can exhibit iridescence; however the detailed reason for this behaviour is not clear. The purpose of this study is to explore the origins of iridescence in solid NCC films. It can be argued that the iridescence of NCC comes entirely from multilayer reflection; however, some optical phenomena cannot be fully explained by this assumption. We provide evidence that the iridescence of NCC comes from multilayer reflection and from diffraction by a surface grating structure. The structures of NCC films, either cross-section or surface profiles, are studied by cutting the film along different directions. Transmission Electron Microscope (TEM), Scanning Electron Microscope (SEM), Atomic Force Microscope (AFM), and polarizing microscope are used to investigate the structure of the films in detail. Ordering in the NCC suspension during the casting is monitored in situ in different containers to mitigate the effects of different external dynamic forces; in this manner the evolution of NCC from the liquid to solid phase can be recorded. Laser diffraction is used to monitor this process. AFM was used to confirm the existence of surface relief gratings in the film.

Security ink is a popular security feature that is widely used for anti-counterfeiting applications. The addition of a UV fluorescent dye into NCC presents the opportunity of a new application in this field for the material. In Chapter 5, the functionalization of NCC by the addition of a UV fluorescent dye is studied, the purpose being to determine the possibility of having a film that is both iridescent and fluorescent. The effects of concentration of the added Optical Brightening Agent (OBA) on the iridescence and optical activities of the resultant NCC films are discussed. Due to its high affinity for NCC and high UV fluorescence efficiency, a small amount of OBA may yield strong fluorescence without compromising the film iridescence.

Chapter 6 deals with the interaction between water and NCC. The possibility of using water as an authentication tool for NCC will be investigated and the possibility to make a humidity color indicator using NCC film will also be discussed.

Chapter 7 deals with the assessment of the possibility of using NCC as a security taggant. A sophisticated security device should be very complex to avoid imitation yet easily identifiable by consumers and investigators. This study attempts to create a more secure device by employing the unique optical properties of the NCC film, namely iridescence, selective reflection and fluorescence, water-induced color change, unique morphology and white-light diffraction patterns. Authentication methods of the proposed taggants are described.

Chapter 8 summarizes the overall conclusions, and offers suggestions for future research.

## 1.4 References

[1]. National Chamber Foundation report, "What are Counterfeiting and Piracy Costing the American Economy?" (2005)

[2]. http://www.cacn.ca/publications.html, "Report on Counterfeiting and Piracy in Canada: A Road Map for Change" (2007)

# Chapter 2

## LITERATURE REVIEW

### 2.1 Introduction

This Chapter gives a general overview of the thesis topic from different aspects, namely, chemical nature of cellulose, synthesis and optical properties of NCC, the chiral nematic phase of NCC liquid crystals and its applications for optical security features.

### 2.2 Cellulose

Cellulose is the most abundant renewable organic material in the biosphere with an estimated annual production of over $7.5 \times 10^{10}$ tons [1]. Cellulose is ubiquitous in larger plants (woods, flax, cottons, etc), in several marine animals (e.g. tunicates), and to a lesser degree in algae, fungi, bacteria, invertebrates and even amoeba (protozoa) [2].

Cellulose is a carbohydrate polysaccharide consisting of a linear chain of several hundred, to over ten thousand, β-(1, 4)-d-glucose residues. The chemical structure of cellulose is shown in Figure 2-1. The chemical formula of the cellulose chain can be empirically expressed as $(C_6H_{10}O_5)n$ where n is the number of repeating sugar units or Degree of Polymerization (DP). The repeat unit of the chain is actually two consecutive glucose anhydride molecules, known as a cellobiose unit. The value of n depends on the source of the cellulose in question.

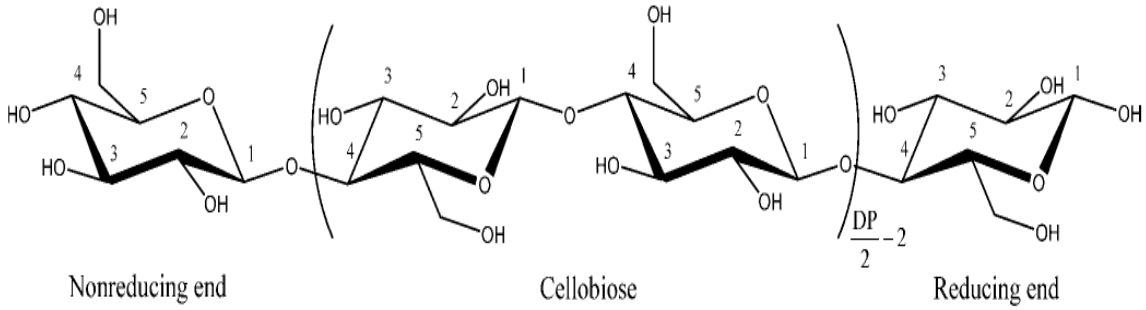


**Figure 2-1**. The structure of cellulose [2].

In contrast with the α-(1-4)-glycosidic bonds present in starch, glycogen, and other carbohydrates, all of the β-d-glucopyranose rings in cellulose adopt a chair conformation; consequentially the hydroxyl groups are positioned in the ring (equatorial) plane, while the hydrogen atoms are in the vertical axial position. This structure is stabilized by an intra- and intermolecular hydrogen bond network [3], as shown by the representative structure in Figure 2-2. The hydroxyl groups on the glucose from one chain form hydrogen bonds with oxygen molecules either on the same or on neighbouring chains, binding the chains firmly together and forming microfibrils with high tensile strength. This structure, where the microfibrils are meshed into a carbohydrate matrix, is an important source of strength that confers rigidity on plant cell walls.

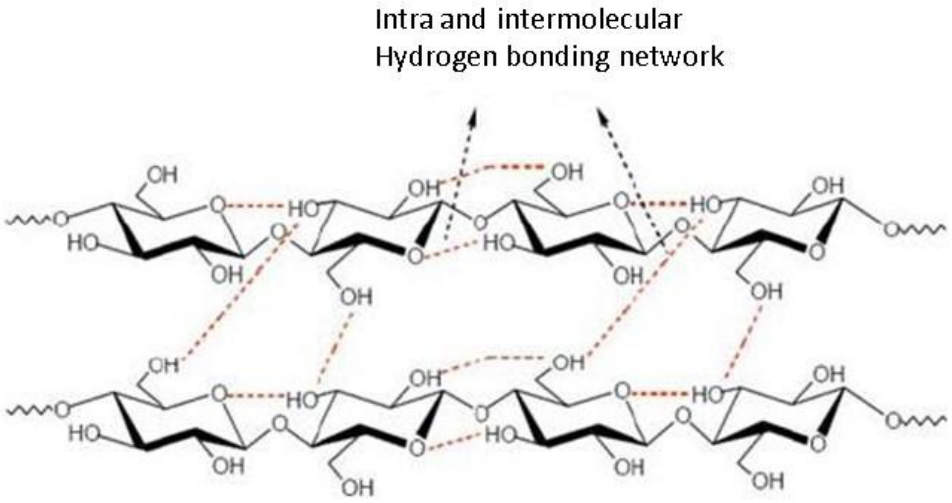


**Figure 2-2**. The intramolecular hydrogen-bonding network in a representative cellulose structure [3].

In nature, cellulose does not occur as an isolated individual molecule but as assemblies of cellulose chain-forming fibers. These fibers are spun together in a hierarchical manner at the site of biosynthesis. Approximately 36 individual cellulose molecules assemblies are brought together into larger units known as elementary fibrils (protofibrils), which then pack into larger units called microfibrils, and these in turn are assembled into cellulose fibers [4].

This hierarchical structure of cellulose as found in wood is displayed in Figure 2-3.

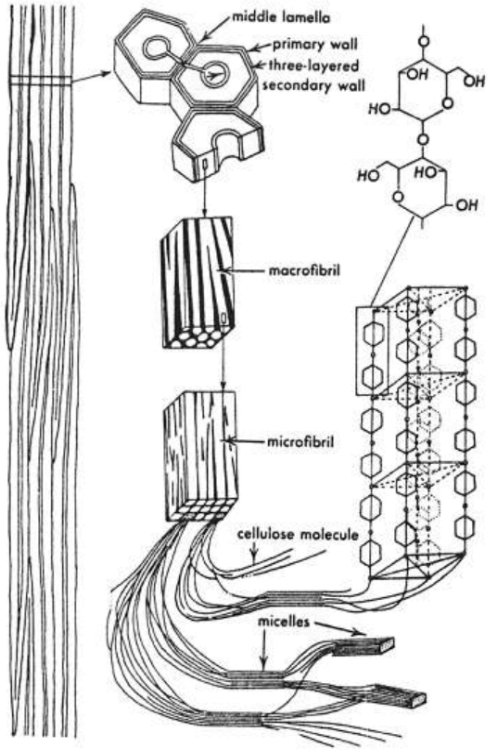


**Figure 2-3**. The hierarchical structure of cellulose fibers in wood [4].

The cross-section of the wood fiber wall is composed of a middle lamella, a primary wall and a three-layered secondary wall where the majority of the cellulose material is found. The cell wall is made up of aggregated macrofibrils (in white) and interceding noncellulosic material (in black). A macrofibril consists of aggregates of microfibrils, which are in turn aggregates of cellulose molecules. Finally the cellulose molecules are organized into series of "unit cells" where the cellobiose is present [5].

During biosynthesis, cellulose derived from different sources may occur in different packing forms as dictated by the biosynthesis conditions. The combined actions of biopolymerization fiber spinning, and crystallization conditions can organize cellulose

molecules into crystalline and amorphous regions (defects). The typical structure of this molecular organization is shown in Figure 2-4.

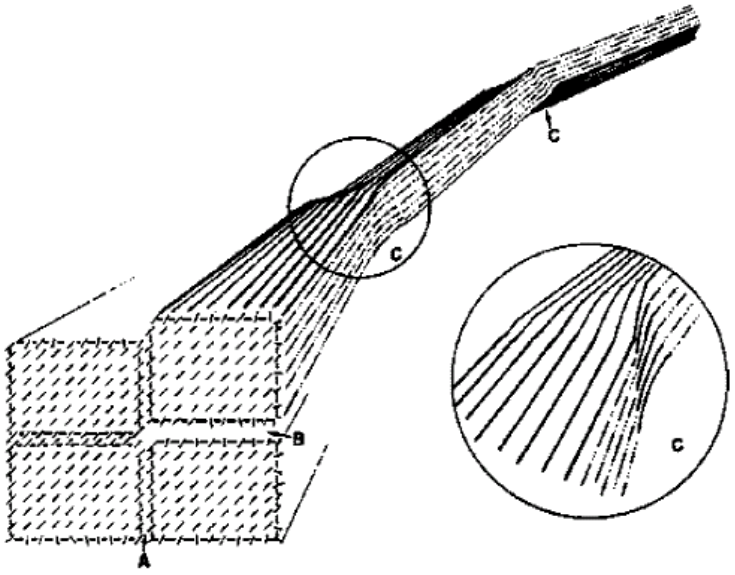


**Figure 2-4**. Schematic representation of an elementary fibril illustrating the microstructure of the elementary fibril and strain distorted regions (defects) (A) coalesced surfaces of high order, (B) slightly disordered surfaces, and (C) strain-distorted tilt and twist regions [6].

In the ordered regions cellulose chains are tightly packed together into crystallites, which are stabilized by the strong and very complex intra- and intermolecular hydrogen-bond network. These molecular networks fit together over long segments and form regions that are difficult to penetrate by solvent or reagents. By contrast the relatively amorphous defect regions are readily penetrated by solvent and therefore are more susceptible to hydrolysis reactions and thus the chain can be broken down chemically into its constituent glucose units by treating it with concentrated acids at a temperature above 45°C. Cellulose is considerably more crystalline than other carbohydrate polysaccharides

such as starch, which undergoes a crystalline-to amorphous transition when heated beyond 60-70°C in water (as occurs during cooking).

In regards to its other physical properties cellulose is odorless, hydrophilic (with a water contact angle of 20–30 degrees), insoluble in water and most organic solvents, and biodegradable.

## 2.3 NCC Synthesis

Rånby was the first to report that colloidal suspensions of cellulose can be obtained by controlled sulfuric acid-catalyzed degradation of cellulose fibers [7-9]. The presence of microscopic aggregates of needle-shaped particles in dried cellulose suspensions, having the same crystalline structure as the original fibers, was then revealed [10,11] . Battista et al. [12,13] studied the hydrochloric acid-assisted degradation of cellulose fibers followed by sonication and found that microcrystalline cellulose (MCC) can be obtained from high-quality wood pulps. MCC is thermally stable, chemically inert, physiologically inert and with attractive binding to protein property. It therefore possesses many potential applications: in the pharmaceutical industry as a tablet drug binder, in the food industry as a texturizing agent and replacement for lipids, and as an additive in paper and composite materials.

Sulfuric and hydrochloric acids have been extensively used for NCC preparation [14-17]. The use of phosphoric and hydrobromic acids has also been reported, but the resultant NCC aqueous suspensions tend to flocculate [18].

Subsequently, Marchessault et al. [19] demonstrated that colloidal suspensions of NCC exhibited nematic liquid crystalline texture. The isolation of NCC from cellulose fibers is based on strong acid hydrolysis. As described previously, the amorphous regions existing in the microfibrils can be penetrated readily by the strong acid and then undergo transverse cleavage to release crystalline cellulose, as seen in Figure 2-5.

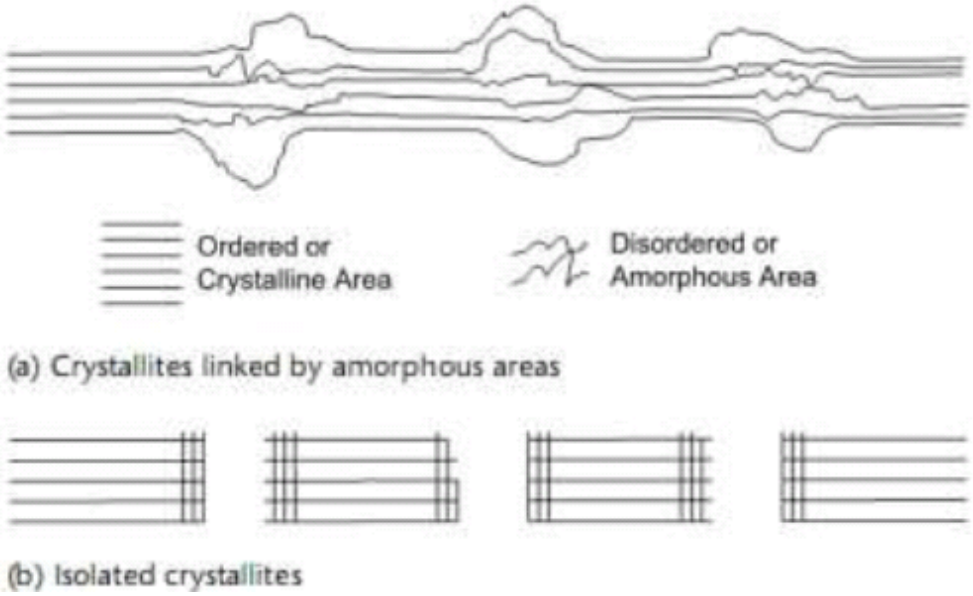


**Figure 2-5**. Schematic presentation of the transition between cellulose fibril and crystalline cellulose [16].

In addition, when sulfuric acid is used as a hydrolyzing agent, it reacts with surface hydroxyl groups of cellulose and yields charged sulfate esters on the surface that promote dispersion of the NCC in water, so that it forms stable suspensions.

NCC units are usually treated conceptually as cylinders with mean diameters and lengths in dimensional models. Geometrical dimensions (length, L, and diameter, D) of NCCs are found to vary widely, depending on the source of the cellulosic materials and

the hydrolysis conditions. Many techniques have been used to characterize the morphology of the NCC, such as the various microscopy techniques (TEM, AFM, polarized microscopy, Field Emission Scanning Electron Microscope (FESEM), and environmental SEM [40]) and light scattering methods such as Small Angle Neutron Scattering (SANS) [39] and polarized and depolarized Dynamic Light Scattering (DLS, DDLS) [20].

**Table 2-1**. **Examples of the length (L) and diameter (D) of NCCs** [2]

| source | $L$ (nm) | $w$ (nm) | technique | ref |
|---|---|---|---|---|
| bacterial | 100–1000 | 10–50 | TEM | 22 |
| | 100–1000 | 5–10 × 30–50 | TEM | 41,21 |
| cotton | 100–150 | 5–10 | TEM | 24 |
| | 70–170 | ~7 | TEM | 26 |
| | 200–300 | 8 | TEM | 28 |
| | 255 | 15 | DDL | 20 |
| | 150–210 | 5–11 | AFM | 40 |
| cotton linter | 100–200 | 10–20 | SEM-FEG | 30 |
| | 25–320 | 6–70 | TEM | 32 |
| | 300–500 | 15–30 | AFM | 33 |
| MCC | 35–265 | 3–48 | TEM | 32 |
| | 250–270 | 23 | TEM | 35 |
| | ~500 | 10 | AFM | 37 |
| ramie | 150–250 | 6–8 | TEM | 38 |
| | 50–150 | 5–10 | TEM | 23 |
| sisal | 100–500 | 3–5 | TEM | 25 |
| | 150–280 | 3.5–6.5 | TEM | 27 |
| tunicate | | 8.8 × 18.2 | SANS | 39 |
| | 1160 | 16 | DDL | 20 |
| | 500–1000 | 10 | TEM | 29 |
| | 1000–3000 | 15–30 | TEM | 31 |
| | 100–1000 | 15 | TEM | 28 |
| | 1073 | 28 | TEM | 32 |
| *Valonia* | >1000 | 10–20 | TEM | 34 |
| soft wood | 100–200 | 3–4 | TEM | 18,36 |
| | 100–150 | 4–5 | AFM | 14 |
| hard wood | 140–150 | 4–5 | AFM | 14 |

Typical geometrical characteristics of NCC, as derived from different sources of cellulose, are summarized in Table 2-1. The reported widths vary from 5 to 50 nm while the lengths span a wider range, from 100 nm to a few microns.

## 2.4 NCC, a Chiral Nematic Liquid Crystal

Liquid crystal (LC) refers to a state of matter that possesses physical properties that are intermediate between those of solids and liquids. LCs have the fluidity of a liquid but also have a degree of long-range order derived from the self-assembly properties of the LC molecules. In contrast to the long-range order found in crystalline solids, the ordering in LC media is limited, imperfect, with some structural defects. Because liquid crystal phases represent an intermediate state between conventional liquids and solids, they are also called mesophases.

From the molecular point of view, the formation of a liquid crystalline phase requires that the molecules have highly anisotropic and specific shapes, commonly found to be rod or disk-shaped. Depending on the degree and nature of the order of the phase, liquid crystals can be broadly divided into three types: nematic, smectic and chiral nematic liquid crystal.

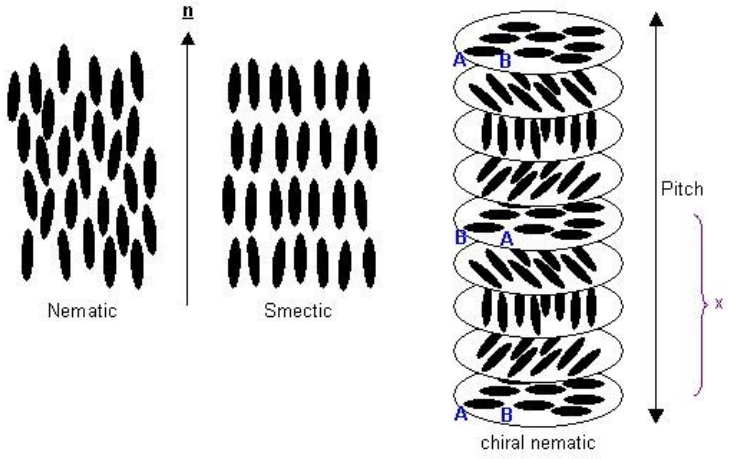


**Figure 2-6**. The three main types of liquid crystal phases.

For nematic liquid crystals, the molecules or particles are arranged with their principal axes nearly parallel. Smectic liquid crystals have an additional one-dimensional long range degree of positional order, the molecules being arranged into layers.

In the chiral nematic phase, the molecular principal axes are arranged into left or right handed helices. The helix is composed of several molecular layers that are progressively rotated and the distance required for the director to complete a full rotation is known as the pitch, as shown in the Figure 2-6.

The liquid crystal phase of NCC was first reported in 1959, when Marchessault et al. [19]. observed the formation of birefringent aqueous gels in acid-treated cellulose and chitin crystallites (microfibrils) at concentrations of cellulose greater than 13% by weight. The liquid crystalline character of these gels was attributed to the parallel alignment of the anisotropic crystallites (nematic order). No helicoidal textures were observed.

Many subsequent reports [42-44] found that most cellulose derivatives, modified celluloses, can form cholesteric liquid crystalline phases in solution or in the bulk phase. In 1986, Gerard et al. [45] studied the effect of casting conditions on the structure of the mesophase of the derivative (hydroxypropyl) cellulose and found that chiral nematic order formed during the liquid phase is preserved in the solid phase after the solvent is removed by evaporation. Moreover, they also discovered that the film showed the property of selective reflection of left-circular polarized light. The detailed reason for selective reflection is not given.

It was not until 1992, almost thirty years since the first report of the liquid crystal properties of NCC [19], that the chiral nematic phase was found in NCC suspension. Revol et al. [46] reported that a phase separation occurs in NCC suspension when the concentration of the NCC suspension is beyond a critical value. At room temperature, colloidal suspensions of cellulose separate into an upper isotropic and a lower anisotropic phase, and the anisotropic phase spontaneously forms small tactoids [47], which are ellipsoidal ordered regions that grow in size as time passes. When observed between crossed polarizers the tactoids (as shown in Figure 2-7) either appear uniformly birefringent or they display two or more equidistant bands of regions depending on their size and orientation relative to the frame of reference of the observer. They argued that an intermediate fluid phase is involved in formation of the widely observed helicoidal structure. They also reported that ordering of the NCC chiral structure could be controlled by an applied magnetic field to give a homogeneous texture.

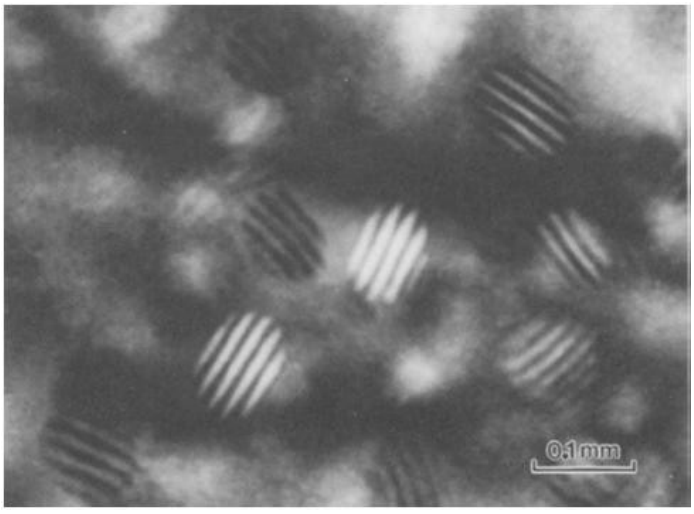


**Figure 2-7**. Tactoid structures in the anisotropic phase of NCC [47]. With time, these tactoids merge into longer “finger print” patterned line, as shown in Figure 2-8.

.

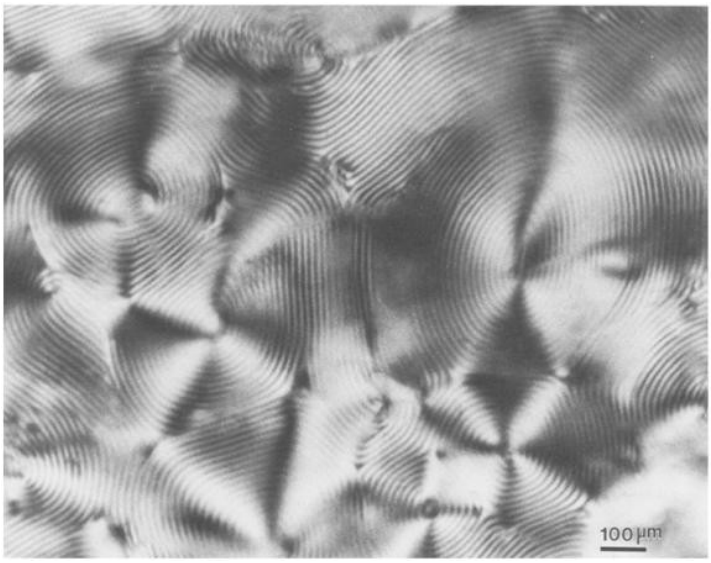


**Figure 2-8**. Finger print structure (under crossed polarizers) present in the anisotropic phase of NCC. This is the same sample as Figure 2-7 but examined after it was left standing one day [47].

## 2.5 Optical Properties of NCC

### 2.5.1 Iridescence

Iridescence is an optical phenomenon where the apparent color of the object depends upon the viewing angle of the observer. It is often seen in the world of biology, such as in the butterfly wings, carapaces of beetles, and in sea shells. The mechanism of iridescence has been extensively studied in the cases of various creatures for over a century. In 1927, using only optical microscopy, Mason [48] studied the structure of the butterfly wing and concluded that multilayer systems were primarily responsible for the iridescence present in the wing. The invention of electron microscopy then allowed for this phenomenon to be studied in greater detail than was possible before. Anderson et al. in 1942 [49] observed similar optical results as Mason by using SEM. In general the iridescence of butterfly wings is caused by the multilayer structure as opposed to pigmentation. Interference from

these structures produces the observed colors.

Iridescence studies also have been done on sea shells [50], peacock feathers [51], as well as on spider and beetle exoskeletons [52]. In a review article, Seago et al. [53] classfied the iridescence observed in beetles into three groups based on its origins: multilayer reflection, three-dimensional photonic crystal, and diffraction grating behaviour.

The iridescent properties of NCC films were first reported by Revol et al. [54] in 1998 when studying the casting process of NCC suspensions under controlled conditions. They found that a solid films produced by these casting showed iridescence. This phenomena was later explained using a theory from de Vries [55] on the basis of a helicoidal arrangement of birefringent layers. De Vries postulated that the reflected wavelength depends upon the helical pitch of the chiral nematic liquid crystal arrangement. When the magnitude of the pitch is on the order of the wavelength of the incident light, satisfying the condition $\lambda = nP$, where n is the average refractive index of the material and P is the helical pitch of the liquid crystal, then only a narrow wavelength band of the light will be reflected. De Vries limited his discussion to the case of normal incident propagation light. Revol et al. [54] subsequently extended de Vries' relationship, and concluded that an approximate relationship of $nP\cos\theta = \lambda$ could be adopted for the oblique angle situation, where, $\theta$ being the angle between the viewing angle and the normal vector of the surface. Thus, a sample with a black background that reflects red light when viewed at normal incident to the surface would appear green when viewed at 45 º.

It can be seen from the de Vries equation that the reflected iridescence color depends

mainly on the pitch of the chiral nematic structure. The pitch itself can be altered by changing many different parameters, the first being ionic strength. Dong et al. [56] studied the effect of adding various electrolytes such as HCl, NaCl and KCl during the phase separation of NCC produced during acid-hydrolysis. They found that by increasing the ionic strength of the positively charged particles, the pitch formed by the anisotropic phase of NCC LC decreases. This induces a blue-shift in the reflected light of an NCC suspension when it is cast into a solid film. The decrease in pitch was explained as a product of the reduction of the double layer thickness caused by the repulsive forces that exist between chiral nematic NCC particles. NCC crystals synthesized by acid hydrolysis have many sulfate groups on the surface of the cellulose molecules; adding electrolytes is analogous to adding counterions to the suspension. This has the effect of neutralizing the surface charge of the NCC particles in the anisotropic phase and reduces the repulsive forces. It was found that the amount of electrolyte that can be added is limited to a low concentration; high concentrations make the suspension unstable.

Later, Dong et al. [57] extended their study by adding inorganic counterions such as $K^+$, $Na^+$, $Cs^+$, and $H^+$ as well as organic ones such as ammonium, tetramethylammonium, tetraethylammonium, tetrapropylammonium, tetrabutylammonium, trimethylammonium, and triethylammonium to the NCC suspension. They found that for inorganic counterions the critical concentration for formation of the ordered phase increases in the order of H+ < Na+ < K+ < Cs+. For the organic counterions the critical concentration in general increases with increasing counterion size, suggesting that the equilibrium is governed by a balance between hydrophobic attraction and steric repulsion forces. Adding counterions also decreases the pitch of the NCC chiral nematic phase as determined by a polarized

microscopy.

The pitch can be affected by other parameters including NCC concentration, temperature, and applied magnetic field, as studied by Pan et al. [58]. They showed that the pitch increased with the NCC concentration. This was explained by the fact that increasing the concentration will increase the anisotropic phase volume and an increased suspension concentration promotes the formation of proportionately more anisotropic phase. As the volume fraction of the anisotropic phase increases, so does the pitch of the chiral nematic phase. By increasing the temperature, they found that pitch was reduced; the increased temperature will enhance the flexibility of the cellulose molecules in NCC, allowing for a greater twist angle. Finally, by drying the NCC under an applied 0.2 Tesla magnetic field an elongated pitch was observed. The increase in chiral nematic pitch may be due to the magnetic alignment of cellulose crystallites, given their anisotropic shapes and nonzero magnetic susceptibilities. This may cause the tilt angle between the directors in adjacent pseudo layers to decrease [59-60], Similar effects have been observed for DNA [61-62] and for other liquid crystals[63]. The pitch data in these studies were obtained by measuring the maximum reflection Circular Dichroism (CD) peak value.

### 2.5.2 Selective circular polarized reflection

Another unique optical property of NCC is that it selectively reflects left-circularly polarized light, meaning that the material has a stronger reflection for left-handed polarized light than for right-handed polarized light. This property is referred to as optical activity and applies to all chiral nematic liquid crystal molecules, as it is derived from the interaction of chiral materials with polarized light. This property was first observed by

Jean-Baptiste Biot in 1815 [64]. Louis Pasteur [65] deduced in 1848 that this phenomenon had a molecular basis. It was believed that the origin of this property is in the asymmetry of the molecules.

Like other chiral nematic materials NCC has strong optical activity, in the range of $10^3$ to $10^5$ deg/mm. The optical activity is measured as the angle of polarization vector rotation when linear polarized light passes through a medium. As with the iridescence exhibited by NCC films, the selective reflection of circular polarized light has also been explained by de Vries. In his model, de Vries [55] proposed that liquid crystals consist of a large number of thin layers and that light is reflected at the successive boundaries formed by these layers. Reflection at the boundary of two layers can only occur when there is a difference between the refractive indices of these layers, meaning that the medium can be thought of as a stack of double-refractive thin layers. This reflection occurs because the linear components of the light wave passing through one layer will observe a change in the refractive index of the medium when passing into the next layer. The fast component will be reflected with phase reversal, and the other component is reflected without reversal. Constructive interference will occur when the reflected electric field components are in phase with one another. From his model, de Vries concluded that only one handedness of circular polarized light can be selectively reflected by a chiral structure.

### 2.5.3 Circular Dichroism (CD) and Induced Circular Dichroism (ICD)

Circular Dichroism (CD) is a measure of the optical activity of chiral molecules and is quantified by the absorption difference between left circularly polarized light and right circularly polarized light by a chiral medium.

$$CD = AL - AR \qquad (2\text{-}1)$$

where, AL is the absorption of left-handed Circular Polarized Light (CPL) and AR, the absorption of right-handed CPL. As NCC is pure crystalline cellulose it has no chromophore [66]; absorption by the material is negligible at visible wavelength. Instead the selective reflection of NCC has been widely considered as a source of CD. If a chiral nematic sample predominantly reflects left-handed CPL then the total amount of light transmitted through the sample will be reduced by the amount of reflected light, resulting in the apparent selective absorption of left CPL. The magnitude of the CD will therefore be positive which is characteristic of a left-handed helical structure. Given that CD quantities can be directly related to material structure, in particular the chiral nematic pitch, by measuring the CD across a wide spectrum one can gain insights into the molecular structure of NCC.

The shape of a CD band depends on the degree of order and the texture of the mesophase. A uniform planar texture gives a sharp CD band, whereas a structure composed of chiral nematic polydomains yields a broad CD band [67]

Induced circular dichroism (ICD) refers to circular dichroism that is induced by the interaction of an achiral compound interacting with chiral molecules. This effect is produced by a combination of the intermolecular forces, the properties of the chiral molecule in question, and even on the chromophore itself. The ICD technique has been

widely used both as a probe for determining the interaction between chiral and achiral molecules [68] and to measure the chirality of chiral matrices [69]. NCC has been shown to display induced CD for specific dye compounds [70].

## 2.6 Optical Security Device Design

The large increase in counterfeiting in recent years demonstrates the inadequacy of current anti-counterfeiting methods. It is prudent and advisable that more sophisticated security technology should be developed to maintain an edge over counterfeiters. By sophisticated, it is often understood to mean use of multilayered technologies consisting of both overt (readily visible to the naked eye) and covert (hidden and invisible without the use of special equipment and/or chemicals); They are difficult for counterfeiters to reproduce, yet easy for consumers and field investigators to verify information.

There are many anti-counterfeiting techniques presently available to both the public at large and commercial interests, ranging from the simple to the sophisticated. Security features based on optical techniques are of particular interest, being difficult to replicate and relatively easy for customers to identify. The most popular optical security technologies are Optical Variable Device (OVD), selective reflection, and security inks.

### 2.6.1 Optical Variable Device (OVD)

The Optical Variable Device relies on changes in the optical properties of the material to certify the uniqueness of a brand. Color dependence on orientation properties are useful as a medium-level security method, as the image made of this material cannot be copied due to the fact that conventional copiers and scanners can only copy in a fixed direction. The most popular examples of OVDs are holograms, hidden images and iridescent images.

Holograms are one of the most well-known and easily recognizable anti-counterfeiting devices in the market. They were first used in 1982 [71], when they appeared on MasterCard® credit cards. Holograms are produced by recording the interference pattern created by two beams of coherent light, typically laser light. A hologram image is made up of microgrooves, which will diffract light and recreate the recorded image in the projected interference pattern.

Different types of holographic images can be formed depending on the techniques used, namely 2D and 3D holograms. The former refers to a layering of 2D images to create the holographic object, while the latter refers to a real 3D image created using holograph recording techniques. A 3D hologram has an additional dimension realized by placing objects in the foreground, midground and background; extremely complex and secure designs can be created. A high volume of holograms can be produced by hot stamping, which makes this technique more favourable in terms of cost. Further, holograms produce vibrant, iridescent 3D images that cannot be reproduced by conventional imaging techniques.

Holograms can however be copied using mechanical means such as embossing. A skilled holographer can make copies that are very difficult to distinguish from the originals [72]. For instance, it has been reported that more than half the sales of the drug artesunate in South East Asia are forged despite the use of holographic security [73-76]. Given time, any anti-counterfeiting technique can be duplicated and so companies should look to the future and work to develop more sophisticated measures.

Another technique used for making a more secure OVD is the hidden image created by using computer- generated Fourier signals. Stepien et al. [77] proposed an approach to make such an OVD by including both a rainbow holographic effect and hidden Fourier-plane images. Under typical illumination, the first element shows rainbow holographic and kinematic effects while the second element shows up as a darker image visible at an angular range different than that of the first element, being less visible under usual white light illumination conditions but appearing sharp under laser light.

The advancement of Electron-beam (E-beam) lithographic techniques makes it possible to create high resolution microstructures for use in high security OVD design. R. A. Lee [78] proposed using color-tone lithography to create micro-mirrors having directionally-dependent color reflection. In this example, the micro-mirrors were designed in such a way that the dollar and euro symbol have alternating maximum reflection depending on the viewing angle (see Figure 2-9).

**Figure 2-9**. An artwork sample to be converted into an optically variable microstructure by the color-tone lithography process [78].

### 2.6.2 Selective Reflection

Selective reflection as a security feature has been widely studied, although it is more often

seen in disclosed patents than in published papers. A few typical examples of the use of selective reflection by chiral liquid crystals for security applications will be discussed.

In US patent application No. 20100112314, Jiang et al. [79] disclose a method to make invisible ink using chiral liquid crystals. Security pigment systems are generally a composite of a reflective material, a transparent chiral birefringent material and a transparent carrier medium. The security pattern is invisible when viewed with naked eye but becomes visible as an achromatic bright mark on a dark background when viewed with a circular polarizer. Selective reflection by the chiral nematic pigment is the key to the aforementioned security feature.

Another example is a commercial product, called Helicone® made by SICPA. Helicone is a cholesteric liquid crystal polymer that has an additional secondary security feature that it selective reflects circular polarized light.

NCC possesses iridescence; therefore it can be used as an OVD in the same manner as a hologram. Revol et al. [54] first proposed a method to make security paper by adding NCC planchette into the paper. The color variation properties make for a simple authentication method to determine the authenticity of the security paper.

### 2.6.3 Security Ink

As with selective reflection, security ink is another covert security feature that usually operates in the UV or infrared band. Security ink is used to print security images on various substrates. They cannot be seen under normal lighting conditions; imaging is triggered by light induction, thermal induction, or chemical induction.

Security ink features have been widely used in various brands and product anti-counterfeiting, including bank notes and consumer product protection. A brief review of these techniques will follow.

*2.6.3.1 Light reaction ink*

Light reaction ink changes color when exposed to a specific wavelength of light, typically achieved through UV or infrared fluorescence or phosphorescence. These inks can continue to emit for an extended period of time after exposure. A typical example of phosphorescent ink can be seen in glowing watch dials, as seen in Figure 2-10.


**Figure 2-10**. Green phosphorescent watch dial (after Printcolor inc.[80]).

UV security inks are very popular today. Fluorescence from these inks can span from the visible to the infrared. They are widely used in bank notes and other official documents, and have been incorporated into almost all countries' banknote protection systems. Security paper is strictly controlled by the government; the paper being non-fluorescent as it has no optical brightening Agent (OBA). This UV-insensitive paper is useful for two reasons: one, it provides a good background for fluorescent inks and two, it is easily distinguished from commercial brightened paper [81]

Security inks can also be sensitive to IR excitation. This feature is of particular interest in that it takes advantage of the anti-Stokes emission where a shorter wavelength emission is generated by a longer wavelength excitation. Security features can be made by printing objects with both IR-active and IR-inactive ink. A typical example of this is barcode printing, where the two types of inks have been used to print the barcode simultaneously but the detectable portion is printed with IR-inactive ink. A counterfeiter who reproduced the whole visible barcode would in fact have made the wrong pattern.

*2.6.3.2 Thermal reaction ink*

Thermal-reactive inks change color when the temperature of the ink print substrate area is changed. Such inks can often be activated by body temperature or friction, a property that cannot be reproduced by a copier. Thermochromic inks are available for wet or dry offset printing and flexographic printing [82].

*2.6.3.3 Chemical reaction security ink*

Chemically reactive inks are also important; they are particularly useful for deterring forgers who may try to re-use the security ink by recovering it with solvent. When exposed to solvents such as bleach, alcohol, or acetone these inks will run, change color, or cause a stain to develop. Tampering is easily detected when chemicals or solvents are used on these inks.

The definite reaction of the ink to solvent can be used as a forensic test to determine authenticity, but this is an inherently destructive verification method. Security inks may also degrade naturally over time, depending on the chemical structure.

## 2.7 References

[1]. A. D. French, N. R. Bertoniere, R. M. Brown, H .Chanzy, D. Gray, K. Hattori, and W. Glasser. In Kirk-Othmer Encyclopedia of Chemical Technology 5th ed.; Seidel, A., Ed.; John Wiley & Sons, Inc.: New York,; Vol. 5 (2004)

[2]. Y. Habibi, L. A. Lucia, and O. J. Rojas, "Cellulose nanocrystals: Chemistry, self-assembly, and applications," Chem. Rev. 110, 3479–3500 (2010)

[3]. P. Visakh and S. Thomas, "Preparation of bionanomaterials and their polymer nanocomposites from waste and biomass," Waste and Biomass Valorization, vol.1, pp. 121-134 (2010)

[4]. A. Frey-Wyssling and K. Mühlethaler, Ultrastructural plant cytology: With an introduction to molecular biology: Elsevier Pub. Co., 1965.

[5]. G. A. Smook, "Handbook for Pulp & Paper Technologist," 3rd edition, Angus Wilde publications Inc. (2002)

[6]. S. P. Rowland, E. J. Roberts, J. Polym. Sci., Part A: Polym. Chem.10, 2447.(1972)

[7]. B. G. Rånby, "Aqueous colloidal solutions of cellulose micelles," Acta Chemica Scandinavica, vol. 3, pp. 649-650 (1949)

[8]. B. G. Rånby, "Fibrous macromolecular systems. Cellulose and muscle. The colloidal properties of cellulose micelles," Discussions of the Faraday Society, vol.11, pp. 158-164 (1951)

[9]. B. G. Rånby and E. Ribi, " Ber den feinbau der zellulose," Cellular and Molecular Life Sciences, vol. 6, pp. 12-14(1950)

[10]. S. M. Mukherjee and H. J. Woods, "X-ray and electron microscope studies of the degradation of cellulose by sulphuric acid," Biochimica et Biophysica Acta, vol. 10, pp. 499-511 (1953)

[11]. S. M. Mukherjee, J. Sikorski, and H. J. Woods, "Electron-microscopy of degraded cellulose fibres," Journal of the Textile Institute Transactions, vol. 43, pp. 196 -201 (1952)

[12]. O. A. Battista, "Hydrolysis and crystallization of cellulose," Industrial & Engineering Chemistry, vol. 42, pp. 502-507 (1950)

[13]. O. A. Battista, S. Coppick, J. A. Howsmon, F. F. Morehead, and W. A. Sisson, “Level-off degree of polymerization," Industrial & Engineering Chemistry, vol.48, pp. 333-335, (1956)

[14]. S. Beck-Candanedo, M. Roman, and D. G. Gray, "Effect of reaction conditions on the properties and behavior of wood cellulose nanocrystal suspensions,” Biomacromolecules, vol. 6, pp. 1048-1054 (2005)

[15]. D. Bondeson, A. Mathew, and K. Oksman, "Optimization of the isolation of nanocrystals from microcrystalline cellulose by acid hydrolysis," Cellulose, vol. 13, pp. 171-180 (2006)

[16]. O. A. Battista, "Microcrystal polymer science," McGraw-Hill (1975).

[17]. W. Y. Hamad and T. Q. Hu, "Structure-process-yield interrelations in nanocrystalline cellulose extraction," Canadian Journal of Chemical Engineering, vol. 88, pp.392-402 (2010)

[18]. J. Araki, M. Wada, S. Kuga, and T. Okano, "Flow properties of microcrystalline cellulose suspension prepared by acid treatment of native cellulose," Colloids and Surfaces A: Physicochemical and Engineering Aspects, vol. 142, pp. 75-82 (1998)

[19]. R. H. Marchessault, F. F. Morehead, and N. M. Walter, "Liquid crystal systems from fibrillar polysaccharides," Nature, vol. 184, pp. 632-633 (1959)

[20]. M. M. De Souza Lima, J. T. Wong, M. Paillet, R. Borsali, and R. Pecora, "Translational and rotational dynamics of rodlike cellulose whiskers," Langmuir, vol. 19, pp. 24- 29 (2002)

[21]. M. Grunert and W. T. Winter, "Nanocomposites of cellulose acetate butyrate reinforced with cellulose nanocrystals," Journal of Polymers and the Environment, vol. 10, pp. 27-30 (2002)

[22]. J. Araki and S. Kuga, "Effect of trace electrolyte on liquid crystal type of cellulose microcrystals," Langmuir, vol. 17, pp. 4493-4496, 06/19 (2001)

[23]. A. Junior de Menezes, G. Siqueira, A. A. S. Curvelo, and A. Dufresne, "Extrusion and characterization of functionalized cellulose whiskers reinforced polyethylene nanocomposites," Polymer, vol. 50, pp. 4552-4563 (2009)

[24]. J. Araki, M. Wada, and S. Kuga, "Steric stabilization of a cellulose microcrystal suspension by poly(ethylene glycol) grafting," Langmuir, vol. 17, pp. 21-27 (2000)

[25]. N. L. Garcia de Rodriguez, W. Thielemans, and A. Dufresne, "Sisal cellulose whiskers reinforced polyvinyl acetate nanocomposites," Cellulose, vol. 13, pp. 261-270 (2006)

[26]. X. M. Dong, T. Kimura, J.-F. Revol, and D. G. Gray, "Effects of ionic strength on the isotropic−chiral nematic phase transition of suspensions of cellulose crystallites,"Langmuir, vol. 12, pp. 2076-2082 (1996)

[27]. G. Siqueira, J. Bras, and A. Dufresne, "Cellulose whiskers versus microfibrils: Influence of the nature of the nanoparticle and its surface functionalization on the thermal and mechanical properties of nanocomposites," Biomacromolecules, vol.10, pp. 425-432 (2008)

[28]. L. Heux, G. Chauve, and C. Bonini, "Nonflocculating and chiral-nematic self - ordering of cellulose microcrystals suspensions in nonpolar solvents," Langmuir vol. 16, pp. 8210-8212 (2000)

[29]. M. N. Angles and A. Dufresne, "Plasticized starch/tunicin whiskers nanocomposites structural analysis," Macromolecules, vol. 33, pp. 8344-8353 (2000)

[30]. M. Roohani, Y. Habibi, N. M. Belgacem, G. Ebrahim, A. N. Karimi, and A. Dufresne, “Cellulose whiskers reinforced polyvinyl alcohol copolymers nanocomposites,” European Polymer Journal, vol. 44, pp. 2489-2498 (2008)

[31]. F. Kimura, T. Kimura, M. Tamura, A. Hirai, M. Ikuno, and F. Horii, "Magnetic alignment of the chiral nematic phase of a cellulose microfibril suspension," Langmuir, vol. 21, pp. 2034-2037 (2005)

[32]. S. Elazzouzi-Hafraoui, Y. Nishiyama, J.-L. Putaux, L. Heux, F. Dubreuil, and C. Rochas, "The shape and size distribution of crystalline nanoparticles prepared by acid hydrolysis of native cellulose," Biomacromolecules, vol. 9, pp. 57-65 (2007)

[33]. Q. Li, J. Zhou, and L. Zhang, "Structure and properties of the nanocomposite

films of chitosan reinforced with cellulose whiskers," Journal of Polymer Science Part B: Polymer Physics, vol. 47, pp. 1069-1077 (2009)

[34]. J. F. Revol, "On the cross-sectional shape of cellulose crystallites in valonia ventricosa," Carbohydrate Polymers, vol. 2, pp. 123-134 (1982)

[35]. J. R. Capadona, K. Shanmuganathan, S. Trittschuh, S. Seidel, S. J. Rowan, and C.Weder, "Polymer nanocomposites with nanowhiskers isolated from microcrystalline cellulose," Biomacromolecules, vol. 10, pp. 712-716 (2009)

[36]. J. Araki, M. Wada, S. Kuga, and T. Okano, "Influence of surface charge on viscosity behavior of cellulose microcrystal suspension," Journal of Wood Science, vol.45, pp. 258-261 (1999)

[37]. L. Pranger and R. Tannenbaum, "Biobased nanocomposites prepared by in situ polymerization of furfuryl alcohol with cellulose whiskers or montmorillonite clay," Macromolecules, vol. 41, pp. 8682-8687 (2008)

[38]. Y. Habibi, A.-L. Goffin, N. Schiltz, E. Duquesne, P. Dubois, and A. Dufresne, "Bionanocomposites based on poly (ε-caprolactone)-grafted cellulose nanocrystal by ring-opening polymerization," Journal of Materials Chemistry, vol. 18, pp. 5002-5010 (2008)

[39]. P. Terech, L. Chazeau, and J. Y. Cavaille, "A small-angle scattering study of celluloswhiskers in aqueous suspensions," Macromolecules, vol. 32, pp. 1872-1875 (1999)

[40]. A. F. Miller and A. M. Donald, "Imaging of anisotropic cellulose suspensions using environmental scanning electron microscopy," Biomacromolecules, vol. 4, pp.510-517 (2003)

[41]. M. Roman and W. T. Winter, "Effect of sulfate groups from sulfuric acid hydrolysis on the thermal degradation behavior of bacterial cellulose," Biomacromolecules, vol. 5, pp. 1671-1677 (2004)

[42]. M. Bagheri and S. Shateri, "Synthesis and characterization of novel liquid crystalline cholesteryl-modified hydroxypropyl cellulose derivatives," Journal of Polymer Research, Volume 19, Number 3 (2012)

[43]. Y. Nishio and Y. Fujiki: Liquid-crystalline characteristics of cellulose derivatives: Binary and ternary mixtures of ethyl cellulose, hydroxypropyl cellulose, and acrylic acid, Journal of Macromolecular Science, Part B: Physics, 30:4, 357-384 (1991)

[44]. Y. Onogi, J. L. White, and J. F. Fellers, "Structural Investigations of Polymer Liquid-Crystalline Solutions: Aromatic Polyamides, Hydroxy Propyl Cellulose, and Poly (y-Benzyl-L-Glutamate)," Journal of Polymer Science: Polymer Physics Edition, Vol. 18,663482 (1980)

[45]. G. Charlet and D. G. Gray, "Solid Cholesteric Films Cast from Aqueous (Hydroxypropy1)cellulose," Macromolecules,20, 33-38 (1987)

[46]. J. F. Revol, L. Godbout, X. Dong, D.G. Gray, H. Chanzy and G. Maret, "Chiral nematic suspensions of cellulose crystallites; phase separation and magnetic field orientation," Liquid Crystals, 16:1, 127-134 (1994)

[47]. J. F. Revol, H. Bradford, J. Giasson, R. H. Marchessault, D. G. Gray, "Helicoidal self-ordering of cellulose microfibrils in aqueous suspension," Int. J Biol Macromol. 14(3):170-2 (1992)

[48]. C. W. Mason, "Structural colours in insects. II. Iridescent colour," J.Phys. Chem. 31, 321-354 (1927)

[49]. T. F. Anderson and A. G. Richards, “An electron microscope study of some structural colours of insects,” J. appl. Phys. 13, 748-758 (1942)

[50]. D.J. Brink, N.G. van der Berg, and A.J. Botha, "Iridescent Colors on Seashells: an Optical and Structural Investigation of Helcion pruinosus," Appl. Opt. 41, 717-722 (2002)

[51]. S. Yoshioka and S. Kinoshita, ‘Effect of Macroscopic Structure in Iridescent Color of the Peacock Feathers,” Forma, 17, 169–181 (2002)

[52]. M. L. M. Lim and D. Li, “Extreme ultraviolet sexual dimorphism in jumping spiders (Araneae: Salticidae),” Biological Journal of the Linnean Society,89, 397–406 (2006)

[53]. A. E. Seago, P.a. Brady, J. Vigneron, and T.D. Schultz, “Gold bugs and beyond: a review of iridescence and structural colour mechanisms in beetles (Coleoptera),” J R Soc Interface. April 6; 6(supp2): S165–S184 (2009)

[54]. J.F. Revol, L. Godbout &, D. G. Gray, “Solid self-assembled films of cellulose with chiral nematic order and optically variable properties,” J. Pulp Pap. Sci. 24, 146–149 (1998)

[55]. H. de Vries, “Rotatory power and other optical properties of certain liquid crystals,” Acta Cryst.4, 219-226 (1951)

[56]. X. M. Dong, T. Kimura, J. F. Revol, and D. G. Gray, “Effects of Ionic Strength on the Isotropic-Chiral Nematic Phase Transition of Suspensions of Cellulose Crystallites,” Langmuir, 12, 2076-2082 (1996)

[57]. X. M. Dong, and D. G. Gray, "Effect of Counterions on Ordered Phase Formation in Suspensions of Charged Rodlike Cellulose Crystallites," Langmuir 13, 2404–2409 (1997).

[58]. J. Pan, W. Hamad and S. K. Straus, "Parameters Affecting the Chiral Nematic Phase of Nanocrystalline Cellulose Films," Macromolecules,43 (8), pp 3851–3858 (2010)

[59]. R. B. Meyer, "Distortion of a Cholesteric Structure by a Magnetic Field," Appl. Phys. Lett., 14 (7), 208–209 (1969)

[60]. J. P., Hurault, "Static Distortions of a Cholesteric Planar Structure Induced by Magnetic or Ac Electric-Fields," J. Chem. Phys., 59 (4), 2068–2075 (1973)

[61]. M. W., Davidson, Liquid Crystalline DNA. Arch. Fam. Med., 2 (10), 1067(1993)

[62]. Y. M., Yevdokimov, "Double-stranded DNA liquid-crystalline dispersions as biosensing units," Biochem. Soc. Trans., 28 (2), 77–81 (2000)

[63]. V.Domenici; C. A., Veracini; V., Novotna; R. Y. Dong, "Twist grain boundary liquid-crystalline phases under the effect of the magnetic field: a complete 2H and 13C NMR study," Chem-Phys Chem, 9 (4), 556–66 (2008)

[64]. A. Lakhtakia, selected papers on natural optical activity, SPIE, Bellingham, WA (1990)

[65]. L. Pasteur (1848). "Researches on the molecular asymmetry of natural organic products," English translation of French original, published by Alembic Club Reprints (Vol. 14, pp. 1-46) in 1905, facsimile reproduction by SPIE in a 1990 book

[66]. X. M. Dong and D. G. Gray, "Induced Circular Dichroism of Isotropic and Magnetically-Oriented Chiral Nematic Suspensions of Cellulose Crystallites," Langmuir, 13, 3029-3034 (1997)

[67]. Z. Yue, and J. G. Cowie, "Preparation and Chiroptical Properties of a Regioselectively Substituted Cellulose Ether with PEO Side Chains," Macromolecules, 35, 6572-6577 (2002)

[68]. F, Zsila, Z, Bikádi, M. Simonyi "Induced circular dichroism spectra reveal binding of the antiinflammatory curcumin to human alpha1-acid glycoprotein," Bioorg Med Chem. Jun 15;12(12):3239-45 (2004)

[69]. J. X. Guo and, D. G. Gray, "Induced circular dichroism as a probe of handedness in chiral nematic polymer solutions," Liquid Crystal, Vol.18, No.4, 571-580 (1995)

[70]. C.D. Edgar and D. G. Gray," Induced circular dichroism of chiral nematic cellulose films," Cellulose 8: 5–12 (2001)

[71]. http://www.ihma.org/history

[72]. S. P. McGrew "Holographic Technology for Anti-Counterfeit Security: Present and Future," Holo-pack*Holo-print Asia (Singapore), July (1996)

[73]. Dhar R. "Anti counterfeit packaging technologies. A strategic need for the Indian industry. Confederation of Indian Industry," pp.1–47 (2009).

[74]. A.K. Deisingh Pharmaceutical counterfeiting. Tutorial Review. [last cited on 2010 Sep 10];The Analyst. The Royal society of chemistry. 2005 130:271–9. Available from: http://www.rsc.org/analyst

[75]. P.N. Newton, M.D. Green, F. Fernandez, N.J. White. Counterfeit anti-infective drugs. Lancet. 6:602–13 (2006)

[76]. P.N. Newton, R McGready, F. Fernandez, M.D. Green, M. Sunjio, C. Bruneton, et al., "Manslaughter by fake artesunate in Asia-will Africa be next?" PLoS Med. 3(6):e197.(2006)

[77]. P. J. Stepien, R. Gajda and T. Szoplik, "Computer-generated optically variable devices containing hidden information," Proc. SPIE 2659, 218 (1996); http://dx.doi.org/10.1117/12.235466

[78]. R.A. Lee, " Colourtone lithography", Microelectronic Engineering 61–62 105–111 (2002)

[79]. Y. Jiang and A. Hochbaum, "Invisible Pigments and Ink", US 20100112314

[80]. www.printcolor.ch, "Phosphorescent Inks – Great effects with white and colorless ink"

[81]. R.D. Warner, R.M. Adams II. Introduction to Security Printing. Pennsylvania: PIA/GATF Press, (2005) Print.

[82]. http://xpedx.edviser.com/default.asp?req=knowledge/article/245,last accessed on May (2012)

# Chapter 3

# ORIGIN OF IRIDESCENCE IN LIQUID CHIRAL NEMATIC PHASE NANOCRYSTALLINE CELLULOSE

## 3.1 Introduction

Iridescence refers to the property of some surfaces to change color with viewing angle, and might be used for security applications. Iridescence is described as a color travel phenomenon or a structural color phenomenon. The latter designation is meant to indicate that the optical effect occurs when electromagnetic radiation encounters some sort of ordered spatial variation in the material dielectric constant (refractive index), where the spatial variation is on the order of the wavelength of light. Iridescence is manifested in nature in the exoskeleton of the scarab beetle, in butterfly wings, feathers, and oyster shells [1]. Iridescence found in nature has stimulated research to develop optical coatings, luster pigments, cosmetics and security features for anti-counterfeiting [2]. The underlying physical mechanisms by which iridescence manifests itself are complex and are only now beginning to be detailed by multidisciplinary groups of researchers. 1D variations in the refractive index give rise to Bragg mono-grating-like responses, while 2D and 3D variations produce responses characteristic of photonic crystal fibers, bi-gratings and full photonic crystals [3, 4]. Since the discovery by Revol et al. [5] of iridescence from nanocrystals of cellulose, there has been significant interest from forest sector in exploring the potential of Nanocrystalline Cellulose (NCC) in a wide range of technological applications, including optics [6]. A series of seminar papers by Gray and

co-workers have documented features of iridescence from solid films and deposits of NCC materials [7]. Our interest is in developing new kinds of encryption inks from NCC materials. Knowledge of parameters giving rise to self organization of the chiral nematic NCC composition in the fluid phase may be important for print applications for encryption that rely on a fluid vehicle to transport luster pigments like NCC aggregates. In this Chapter, we try to explore the evidence for iridescence from a bulk fluid liquid crystal phase of NCC. Our hypothesis is that the iridescence in this case appears to originate in the reflective diffraction from an underlying self-organized bulk grating structure. Stereomicroscopy, polarized microscopy, laser diffraction and reflectance spectroscopy are used to reveal the detail information of this structure.

## 3.2 Experimental

### 3.2.1 Materials

Whatman ashless cotton cellulose powder was purchased from Anachemia. Sulfuric acid (95 –98%) for hydrolysis was purchased from Fisher Scientific. Purified water (Millipore Milli-Q purification system) was used throughout.

### 3.2.2 Preparation of Nanocrystalline Cellulose

The NCC suspension was produced by hydrolysis of cotton fiber with sulfuric acid. The hydrolysis procedure was adapted from Beck et al. [8]. Briefly, a sulfuric acid to pulp ratio of 17.5 ml/g of pulp was used to prepare the NCC. Accordingly, pulverized cotton was mixed to 64% diluted acid and the mixture maintained at 45 ˚C with constant stirring. The reaction was terminated by adding a ten-fold excess of deionized water. The NCC suspension was isolated by centrifugation in repeated wash cycles to remove excess acid.

The pellet was re-suspended in water and dialyzed (spectro/Por membrane, molecular weight cutoff of 12000-14000 Daltons). Dialysis continued for three days until the dialysis water was pH neutral. The resultant NCC particles were then dispersed by sonication (Vibracell Sonics & Materials Inc, Danbury, CT) for about 5 minutes. The colloidal dispersion was finally combined with a mixed bed ion exchange resin (Sigma-Aldrich) for up to 3 days. NCC particle size typically depends on hydrolysis time (see text below).

### 3.2.3 Characterization of NCC using TEM

One drop of diluted (0.1% w/w) NCC suspension was deposited onto a copper grid (Cu-300LC) from Pacific Grid Tech, dried at room temperature (24°C) for one minute. The TEM graphs of NCC particles were acquired with Philips CM200 at 200 kV at McGill University.

### 3.2.4 Flat cell filling and positioning

VitroCom flat cells (100 x 10 x 1 mm, Fiber Optic Center Inc.) were used to hold NCC suspensions in water. Typically 5 wt% NCC in water suspensions were introduced to the flat cell by syringe, injecting sample first to the bottom of the cell, then gradually withdrawing the needle tip as the sample chamber filled. The cell was then fixed in a vertical position, sealed against water loss and allowed to stand at room temperature.

### 3.2.5 Polarized light microscopy

Phase separation of the NCC suspension in the flat cell was detected with polarized light. Polarized optical microscopy (POM) was carried out with a Nikon Optiphot microscope connected to a SonyXCD-X710CR CCD camera equipped with Instrumentation & Industrial Digital Camera (IIDC) image capture software. The light source on the

microscope was equipped with a 530 nm wave plate. to increase image contrast. Flat cells were placed on the microscope rotation stage with the long axis parallel to the polarizer direction.

### 3.2.6 Laser diffraction studies

Ordering of NCC in liquid crystal phase was monitored in time by diffracting a 632.8 nm HeNe laser beam. The NCC suspension was mounted vertically to allow the beam to pass through the flat cell normal to the plane of the cell.

### 3.2.7 Spectrometry

An Ocean Optics 2000 spectrometer was used to record iridescence from the fluid ordered NCC. A xenon lamp light source was directed through a rectangular shaped aperture, focused by a microscope objective lens, then passed through an diaphragm aperture before impinging on the flat cell at 45 degrees to the normal of the cell flat surface. The flat cell was mounted on a holder which was located at the focal point of the objective lens. A multimode optical fiber with 200 μm core diameter was mounted on a Newport micrometer stage, and the color spectrum was recorded by scanning the first order iridescence spectrum as the micrometer stage was rotated.

## 3.3 Results and Discussion

### 3.3.1 Phase separation

Figure 3-1 shows an image of the two-phase system of the lower chiral nematic phase NCC exhibiting a sharp interface with the isotropic upper phase in the flat cell. Phase separation is driven by the anisometric rod-like (high aspect ratio) shape and negative surface potential of the NCC (see Figure 3-2) when concentrated above a critical value.

The transition is readily described by Onsager [9]. The region of phase separation depends on the species from which the NCC is derived and can cover a range of concentrations varying from 1-15 % w/w. Chiral nematic liquid crystals comprise rods arranged in pseudo-layers. Rods are thought to align parallel to one another and parallel to the plane of the layer. Since each layer is rotated slightly with respect the plane above and below, a helix of layers is produced. The pitch P of the helix is the distance required for the NCC assembly to make one complete rotation about an axis perpendicular to the layers.

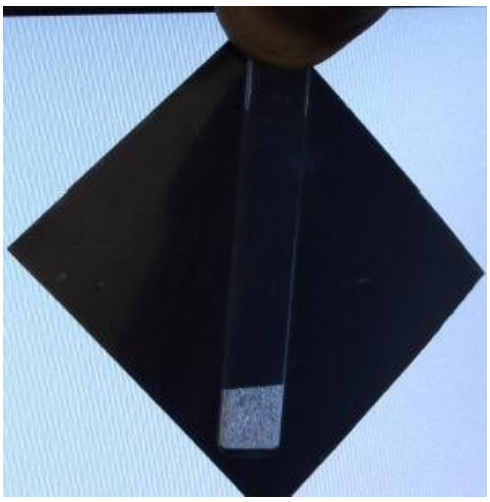

**Figure 3-1**. Photograph of the chiral nematic phase (bottom bright region of the flat cell) sandwiched between cross-polarizer. A sharp boundary can be seen from chiral nematic phase and the isotropic phase.

Aqueous NCC suspensions can be evaporated to yield thin solid translucent films that retain the chiral nematic order. Iridescence from such films originates by reflecting left-hand circularly polarized light over a wavelength band determined by the chiral nematic pitch (P) and the refractive index of the film such that $\lambda = nP\cos\theta$. Here, $\lambda$ is the reflected wavelength, n is the refractive index and $\theta$ is the angle of reflection relative to the normal of the film surface. Clearly, the reflected wavelength diminishes at more oblique viewing

angles. The reflectance is rationalized in terms of Bragg scattering from the helicoidal arrange-

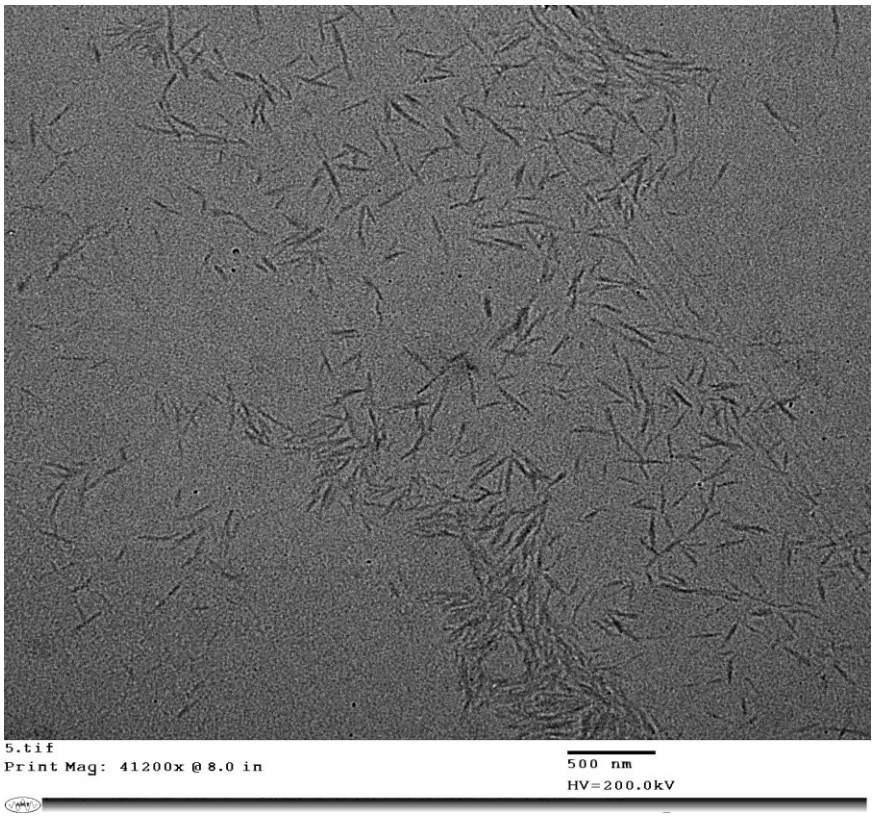


**Figure 3-2**. TEM image of synthesized NCC.

-ment of the (birefringent) NCC layers. If the helicoidal pitch is on the order of the wavelength of light, color structure iridescence evolves which alters with the angle of reflection. Iridescence from NCC suspensions can be blue-shifted by adding salts to the solution. The salts have the effect of screening the negative surface potential so that the NCC particles can approach one another more closely. This approach reduces the chiral nematic pitch and shifts the iridescence to shorter wavelength. The chiral nematic pitch also depends on the hydrolysis conditions and on the size of the NCC particles. Smaller NCC particles produce phases with a smaller pitch. Desulfation by heating or perhaps by

ultrasound (but see below) might also reduce the pitch. Figure 3-3 shows the progressive evolution of the chiral nematic phase and the boundary between the nematic and the isotropic phases. Initially there is no phase sharp boundary. At t=0 minutes, birefringent tactoids with quasi-nematic order are visible.

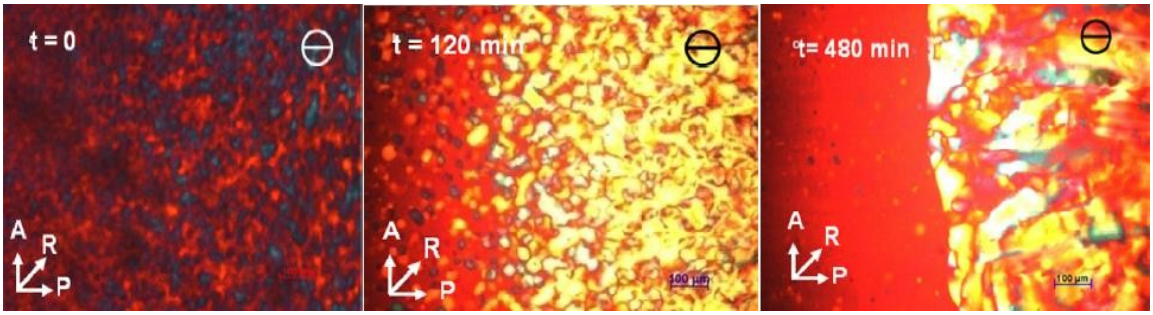


**Figure 3-3**. Left to right. Progressive evolution of the boundary separates the chiral nematic and isotropic phases of 5 wt% NCC in water in a flat cell. The direction of the Polarizer (P) and Analyzer (A) and retarder (R) are indicated. All images taken under crossed polarizers with 530 nm retarder.

Tactoids in Figure 3-4 exhibit periodic birefringent bands typical of chiral nematic order. Colors detected with the quarter wave plate indicate that the NCC rods lie in planes parallel to the birefringent bands. The chiral nematic axis must therefore lie perpendicular to the bands. Tactoids gradually merge with other tactoids and sediment toward the bottom of the flat cell where they produce fingerprint-like texture typical of liquid crystalline order. We find that if the flat cell containing NCC is oriented horizontally, phase separation occurred with parabolic focal conic shape defects [10] and with no long range grating structure.

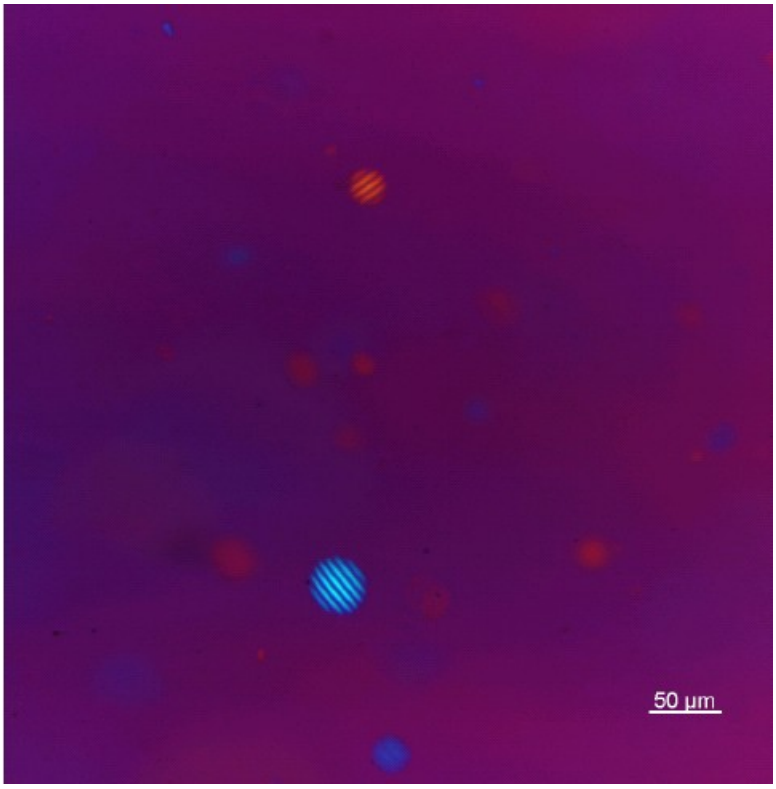


**Figure 3-4**. Tactoids exhibiting chiral nematic order as indicated by the birefringent bands.

We have remarked above that phase separation is also affected by parameters such as concentration, hydrolysis time, surface charge, particle size and sonication. We found that when the NCC concentration is less than 2% or higher than 9% no phase separation occurs. At higher concentration, there is a tendency to form a gel. We found that long hydrolysis times (> 120 min) did not further reduce the particle size. We observe that as hydrolysis time increases, the nanocrystallite size is reduced (size measured as length because there is negligible change in particle width ~20-25 nm). When the hydrolysis time is increased over 120 minutes, the particle size reaches a steady value of about 150 nm. The table also shows that increase in NCC concentration increases the tendency to form the chiral nematic phase.

**Table 3-1.The results of the hydrolysis for 45 minutes or greater, followed always with 5 minutes sonication**.

| Hydrolysis Time (min) | Particle length | Chiral nematic phase at 3% concentration overnight | Chiral nematic phase At 8% concentration Over week |
|---|---|---|---|
| 45 | 300nm+/-75nm | no | no |
| 60 | 251nm+/-70nm | no | yes |
| 75 | 207nm+/-55nm | no | yes |
| 90 | 152nm+/-60nm | yes | yes |
| 120 | 150nm+/-70nm | yes | yes |

Increasing the sonication time reduces the size of particle aggregates, but usually 5 minutes sonication is enough to disperse them into smaller elements. We found that lenger sonication times alters the NCC particles in some manner as indicated by the fact that one observes an order transition from chiral nematic to nematic phase only. Revol and Marchessault [11] observed that variations in the degree of N-sulfonation of chitin nanocrystallites significantly impacted aggregation behaviour where N refers to the amino groups formed from the Nitrogen in chitin. At low concentrations of sulfonation, no tactoids were formed. We first conjectured that long time sonication might similarly cause desulfonation of the NCC particles, which in turn would interfere with the formation of the chiral nematic phase because of changes in surface charge density. Recent work by Beck et al. [12] showed that sonication hinders anisotropic phase formation, but appears not to alter the sulfur content of the NCC components. Sonication causes small changes in conductivity of the suspensions which appear to correlate with peak wavelength redshift in reflectance from dried NCC films. The authors argued that sonication liberates ions trapped in the bound water layer and possibly also in a gel-like layer of polysaccharide at the surface of the nanocrystal. If the electric double layer (EDL) is responsible for

screening the chiral interaction among rods, then loss of ions from the bound water and gel layers would allow the EDL to expand, weakening chiral interactions and opening the pitch. Similarly, swelling of the gel surface after expulsion of ions might produce larger excluded volume in the NCC particles and increase the pitch.

### 3.3.2 Ordering by self-assembly in the bulk fluid phase: grating formation

Phase separation of the NCC suspension is accompanied by large scale ordering towards a fingerprint texture. Figure 3-5. shows a typical order evolution of the suspension imaged through polarizing optics. Shortly after a 5% w/w NCC suspension is introduced to the flat cell tactoids are visible (Figure 3-4, t=0 minutes).

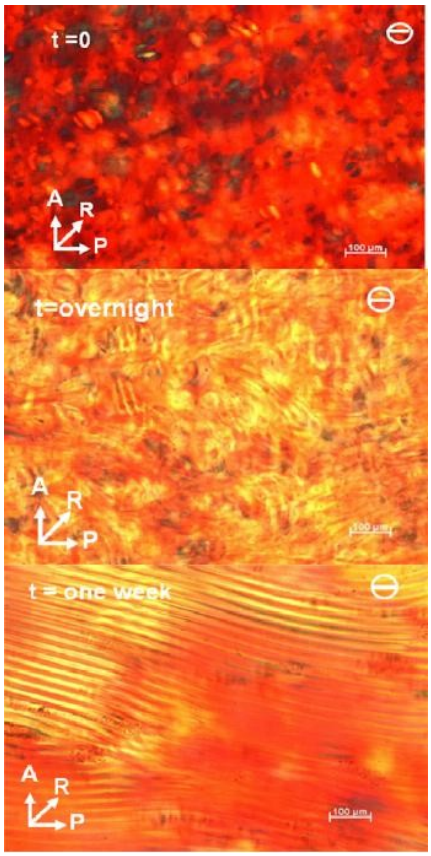


**Figure 3-5**. Evolution of chiral nematic phase fingerprint texture in 5% w/w NCC in water.

As tactoids evolve, coalesce and sediment, longer range order appears (bottom two images of Figure 3-4). Ordering of the suspension may occur not only near the flat surfaces of the cell, but also within the volume at different depths of the suspension; in other words, phase separation may occur in a three dimensional space. Volume ordering may therefore impact iridescence from the bulk liquid phase chiral nematic NCC suspension. The bottom of Figure 3-5 shows the classic fingerprint texture (regular retardation lines) of the liquid crystal NCC. The lines inherit the chirality of the tactoids. The length of the lines increases over time, some of which extend up to 20 millimeters. The retardation lines in the fingerprint texture are not always continuous. Disclinations due to defects in the orientation of the director are observed. It is usually argued that iridescence arises from the chiral nematic pitch P through, $\lambda = nP\cos\theta$, where $\lambda$ is the wavelength, n is the refractive index and $\theta$ is the angle of reflection relative to the normal of the film surface. If the texture should propagate through the bulk of the chiral nematic phase fluid, then a bulk grating structure might form. Stereomicroscope provides spatial, three dimensional images of the NCC phase micro-topography because it uses two separate optical paths with two objectives and two eyepieces to provide slightly different viewing angles to the left and right eyes. As evidence of three dimensional order, Figure 3-6 shows a depth of field image of the retardation lines acquired with no polarizer in place.

**Figure 3-6**. Stereomicroscope image (100X) of fingerprint texture in the bulk of a 5 %w/w NCC ordered phase.

As further evidence for bulk ordering we cite the findings of Shopsowitz and coworkers [13], who showed that chiral nematic NCC solutions will template the growth of ordered 3-dimensional mesoporous silica. The calcined silica exhibits iridescence over the visible domain and into the near infrared. Color travel arises from the stacked layers of silica grating structure due to the imposition of the helical pitch from the LC NCC template. Encouraged by these findings, we used 632.8 nm (HeNe) laser diffraction to follow the time evolution of volume phase separation, and examine the ordering formation of NCC in the flat cell. The results are collected in the series of images shown in Figure 3-7.

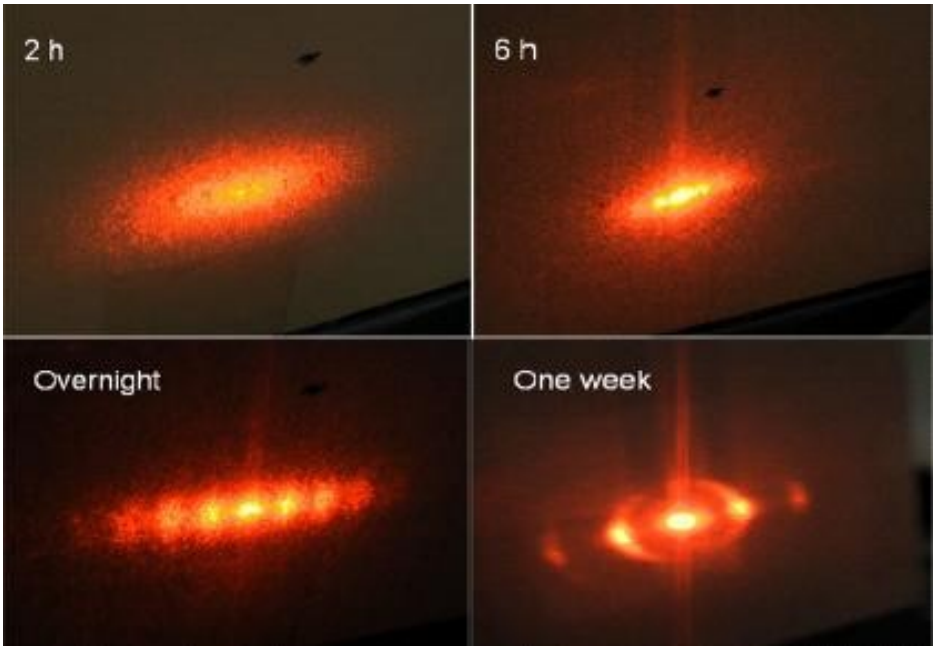


**Figure 3-7**. Time evolution of diffraction from 5% w/w NCC in water in a flat cell.

About 2 hours after introducing a 5 % w/w NCC suspension to the flat cell, we observed diffraction but no clear evidence of grating structure. With time (one week) the diffraction pattern confirmed vertical alignment of the LC phase along the long axis of the flat cell. At this stage, a volume grating structure appears to be complete.

### 3.3.3 Iridescence from the bulk liquid phase

We used white light to examine diffraction and iridescence from the ordered fluid phase. Figure 3-8 shows two images from the anisotropic region of the flat cell which was tilted to reveal the change in iridescence. The width of the cell is 10 mm, and the length of the sample anisotropic phase in the cell is about 20 mm. Birefringent threads visible in the iridescent fluid arise from hydrodynamic flow.

In order to obtain optical information from the anisotropic fluid in three dimensions, we measured the angular response of diffracted white light from the same sample as shown in Figure 3-8.

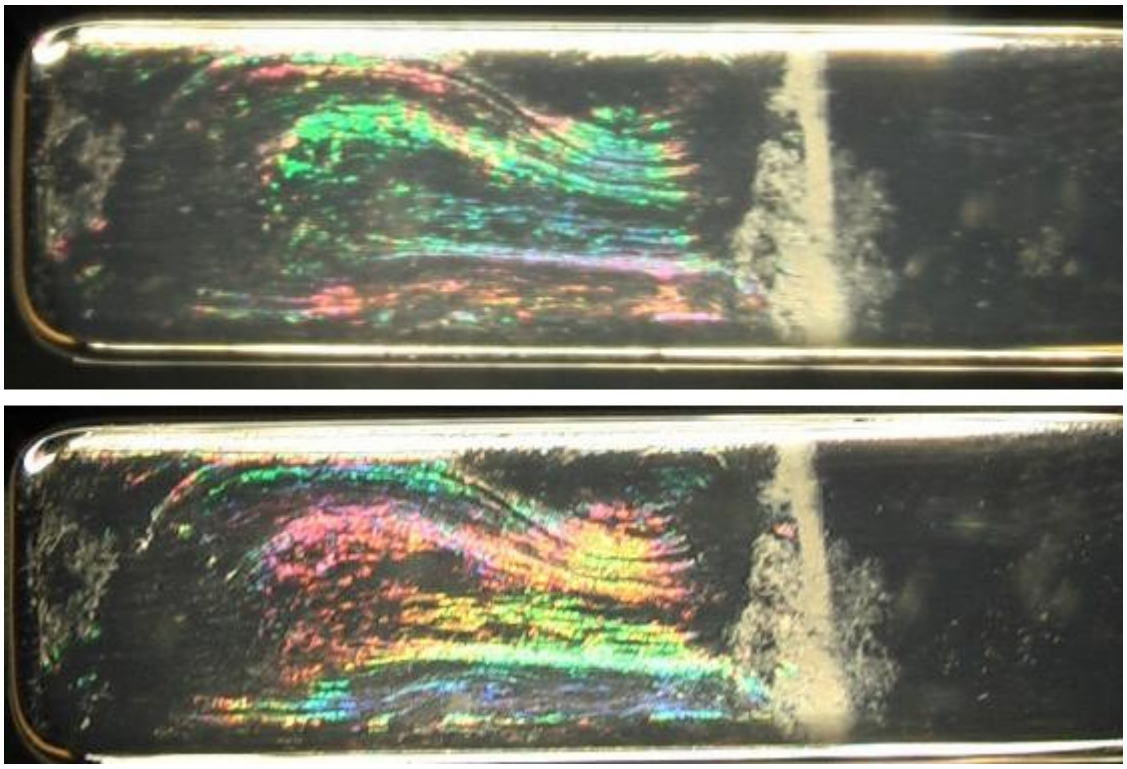

**Figure 3-8**. Iridescence of ordered NCC (anisotropic phase) in flat cell were acquired with digital camera under white light illumination. Iridescent color green and blue (top) transforms to yellow and reddish hues when the sample is tilted (bottom).

Light diffracted from the bulk was recorded using a color CCD camera with a window size of 6.5 x 4.9 mm². Figure 3-9 shows the diffracted white light pattern.


**Figure 3-9**. Iridescence recorded from white light diffracted from the anisotropic fluid phase of the flat cell of Figure 3-8.

It can be seen that the iridescence spectrum covers the visible band, from blue to red, and that the pattern is vertical, and relatively homogeneous. The first diffraction order on the left is accompanied by second order diffraction as the image progresses to the right. The iridescence is left circularly polarized.

The first order angular distribution of the color spectrum diffracted from the fluid was also measured. This was accomplished by mounting the flat cell on a rotation stage. As described in the experimental section 3.2.6, white light was imaged onto the sample and the scattered light was collected at a range of polar angles by an optical fiber mounted on the rotation stage. The light was delivered to a spectrometer. The spectral response is shown in Figure 3-10.

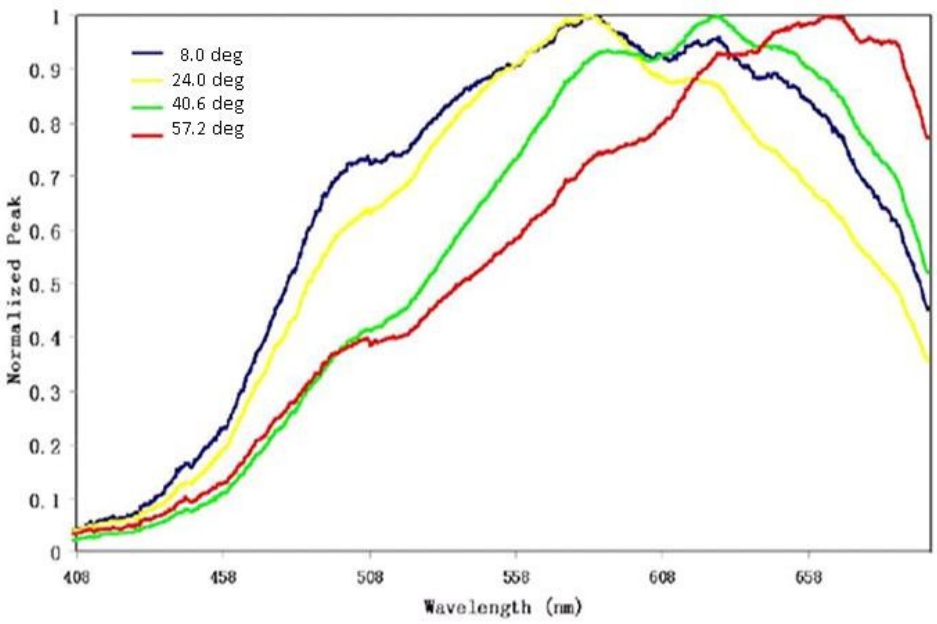


**Figure 3-10**. White light diffraction spectra from the chiral nematic fluid phase in flat cell. Legend values correspond to the angle of diffraction color band maximum from the center white spot. Iridescent band peaks from blue to reddish were recorded by the fiber detector mounted on the rotation stage.

## 3.4 Conclusions

Chiral nematic liquid crystal phase from cotton fiber NCC suspension exhibits iridescence in a narrow concentration range. The iridescence appears to emerge from grating diffraction originating from ordered phases in the bulk of the anisotropic fluid.

## 3.5 References

[1]. M. Meadows, M. Butler, N. Morehouse, L. Taylor, M. Toomey, K. McGraw, and R. Rutowski., "Iridescence: views from many angles," J. R. Soc. Interface 6, S107-S113 (2009)

[2]. Committee on Technologies to Deter Currency Counterfeiting, National Research Council, A Path to the Next Generation of U.S. Banknotes: Keeping Them Real, National Academic Press (2007)

[3]. P. Vukusic, and D.G. Stavenga, “Physical methods for investigating structural colors in biological systems,” 32 J. R. Soc. Interface, 6, S133-S148 (2009)

[4]. A. Seago, P. Brady, J-P. Vigneron, and T. Schultz, "Gold bugs and beyond: a review of iridescence and structural colour mechanisms in beetles (Coleoptera)," J. R. Soc. Interface, 6, S165-S184 (2009)

[5]. J.-F. Revol, L. Godbout, and D. G. Gray, “solid self-assembled films of cellulose with chiral nematic order and optical variable properties ,” J. Pulp Paper Sci. 24 (5), 146–149 (1998)

[6]. W. Hamad, "On the development and applications of cellulosic nanofibrillar and nanocrystalline materials," Can. J. Chem. Eng.,84, 513-519 (2006)

[7]. E. Cranston, and D. G. Gray, "Morphological and optical characterization of polyelectrolyte multilayers incorporating nanocrystalline cellulose," Biomacromolecules, 7, 2522-2530 (2006)

[8]. S. Beck-Candanedo, M. Roman, and D. G. Gray, “Effect of reaction conditions on the properties and behavior of wood cellulose nano crystal suspensions," Biomacromolecules, 6,1048-1054 (2005)

[9]. L. Onsager, “The effects of shape on the interaction of colloidal particles”, Annals of the New York Academy of Sciences, Vol.51, pp 627-659 (1949)

[10]. M. Roman, and D.G. Gray, "Parabolic Focal Conics in Self-Assembled Solid Films of Cellulose Nanocrystals", Langmuir**,** 21, 5555-5561 (2005)

[11]. R.H. Marchessault and J.F. Revol, "In vitro chiral nematic ordering of chitin crystallites," Intl. J. Biol. Macromol.,15, 329-335 (1993)

[12]. S. Beck, J. Bouchard, and R. Berry, "Controlling the Reflection Wavelength of Iridescent Solid Films of Nanocrystalline Cellulose," Biomacromolecules, 12 (1), pp 167–172 (2011)

[13]. K.E. Shopsowitz, H. Qi, W.Y. Hamad, and M.J. MacLachlan, "Free-standing mesoporous silica films with tunable chiral nematic structures," Nature, 468, 422-426 (2010).

# Chapter 4

## STRUCTURED CHIRAL NEMATIC GRATINGS BY SELF-ASSEMBLY OF NANOCRYSTALLINE CELLULOSE

### 4.1 Introduction

In the previous Chapter we studied factors contribute to the iridescence within anisotropic liquid crystal phase of NCC, the result showed that the iridescence came from the diffraction of light by bulk grating formed by NCC self-assembly. In this Chapter, we will explore the iridescence in solid NCC films by creating ordered structures. Structural coloration is a scattering phenomenon that refers to the spectral reflection response produced by the physical interaction between light and meso-, micro-, and nano-scale variations in the geometric patterning of matter. There has been a surge of research into structural coloration in biological systems [1-3], and in turn these researches have stimulated biomimetic design and fabrication in materials and optical science [4-5]. These structures are very important because of their potential applications in photonics, paints, inks, cosmetics, textiles, and encryption. Iridescence is a structured color that shows changes in hue of the object with variations in the viewing angle. In the biosphere, iridescence is diversely distributed for communication, like species identification, intraspecific chromatics for sexual recognition, encoding of age, and for flocking, mimicry, and camouflage. Multilayer reflection, photonic crystals and diffraction gratings can give rise to iridescence [1-2]. Diffraction gratings are of particular interest in encryption. Gratings belong to the class of so-called optically variable devices (OVDs) that have been invented to deter fraud. For example, super-structured Bragg gratings with

pseudorandom modulation for optical encryption have been proposed to offer security by transforming noise like patterns in the optical domain [6]. Interference colors can be expressed by chiral nematic (CN) liquid crystals that act as one-dimensional Bragg reflectors (or equivalently as photonic crystals) at visible wavelengths when the periodicity of the helix matches the wavelength of light. CN phases figure prominently in structural biology. They include collagen in bone [7], cornea [8], or fish scales [9], in DNA [10], in chitin *in vitro* [11-12], and *in vivo* on crab [13] and insect cuticle [14], and in polysaccharides and cellulose derivatives [15-17]. Iridescence exhibited by certain insects has been linked to Bragg reflections from ordered helicoidal phases that may be templated by chiral nematic chitin. Indeed, *in vitro* ordering of chitin crystallites in water produces birefringent bands in tactoids typical of chiral nematic organization [11-12]. Due to its strong negative diamagnetic anisotropy, Nanocrystalline Cellulose has been shown to deposit self-assembled films in the presence of strong magnetic fields with good planar chiral nematic order [17]. Iridescent cellulose films produced in this manner show structured color that appears to depend on the chiral nematic pitch, making the films attractive for use in OVDs [17]. The primary mechanism for iridescence in this case is thought to be selective reflectance of (left) circularly polarized light whose wavelength depends on the pitch $P$ and mean refractive index $n$ of the chiral nematic structure through the relationship, $\lambda = nP$. This is the de Vries relationship [18] that holds when a uniformly ordered film is viewed along the chiral nematic (helicoid) axis. Indeed, the peak iridescence wavelength can be tuned by adjusting the pitch by adding electrolyte to screen Coulombic repulsions among the negatively charged cellulose nanocrystals [17,19].

Iridescence from surface relief gratings is common among invertebrates [20], and CN reflection is used by scarabaeid beetles to produce color [14]. Yet we know of no biological examples that show the combination of CN Bragg reflection with surface relief gratings. Certainly, diffraction from a physical grating will lead to a modified angular dependence of the reflection properties. The combination of structured chiral nematic Bragg filters is little explored in optical science and engineering [20,21]. With a rising interest in "green" photonics, the use of environmentally benign and renewable materials like cellulosics for device fabrication is attractive.

If one unifying principal for structured color in some biological systems is the formation of a chiral nematic liquid crystal phase and another is the creation of structured gratings, this suggests a biomimetic approach to structured color that combines the two. In this Chapter, we will deposit nanocrystalline films of cellulose and explore their optical properties, and study how its ultrastructure impacts optical response. We propose that surface and subsurface physical convexo-concave Bragg gratings arise spontaneously during film formation. These gratings are randomly oriented by virtue of the defected assembly of the film from tactoids and coalesced tactoids in the absence of applied electric or magnetic fields. The result is a film that expresses both iridescence from multilayer Bragg reflection and diffraction from randomly oriented surface relief physical gratings.

## 4.2 Experimental

### 4.2.1 Synthesis and Characterization of Nanocrystalline Cellulose (NCC).

Sheets of softwood spruce fiber (Temalfa93, Tembec Inc, Temiscamingue, QC) were cut into 3 x 0.5 cm pieces and ground in a Willy mill, then passed through a 20-mesh screen. The NCC suspension was produced by hydrolysis with sulfuric acid (Fisher). Same procedure described in Chapter 3 has been used for synthesizing NCC. The final NCC suspension was concentrated to 4-5% by evaporation. NCC particle size was determined by transmission electron microscopy (see chapter 3) to be approximately 120 nm x 25 ± 3 nm, polydisperse by a distribution primarily around the length (± 20%).

**4. 2.2 Microscopy.**

Same polarized optical microscopy (POM) as described previously in Chapter 3 was used for image capture. Images were captured either as stills or from a video sequence. Video of the dynamics of tactoid diffusion, coalescence and immobilization in the sedimenting NCC chiral nematic material was acquired as the film emerged over time. Samples for scanning electron microscopy (SEM) were first coated with 2-4 nm of gold palladium and images were collected with a Hitachi S-4700 FEGSEM. Cross sections of films were obtained by cutting the film in North-South and East-West directions and at $45^{o}$ to these cardinal points. Scanning probe microscopy was performed with a Nanosurf Easy Scan 2 AFM enhanced with an Image Metrology A/S SPIP 5.0.1 software for data acquisition and analysis. Dry imaging of the films was performed in Tapping Mode. The near subsurface layers were imaged by SEM and AFM after carefully peeling off the top surface of the NCC film with adhesive tape.

**4.2.3 White light diffraction.**

The light spectrum diffracting from the film surface was investigated using an Ocean Optics-2000 fiber spectrometer. White light from Xe lamp was focused and direct onto

the film surface with an angle 10 deg from the normal, and the measurement of diffracted light spectrum was performed using a fiber optical detector mounted onto a rotational micro-stage located 12 centimeter away from the sample, and the maximum diffraction peak intensity was recorded at corresponding polar angle of the peak maximum position to the normal of the film surface. The diffracted color spectrum was normalized to the color peak intensity to facilitate the positioning of the peak.

### 4.2.4 Laser diffraction.

Ordering of NCC in the fluid phase was monitored in real time by the diffracted light at 632.8 nm from a HeNe laser beam. The NCC suspension was mounted to allow the unpolarized 1.5 mm beam to pass vertically or horizontally through a 10 mm path length precision optical cell or normal to the plane of the solid NCC film. Diffraction images were projected onto a white background or the surface of the optical table where they were digitally photographed.

## 4.3 Results and Discussion

### 4.3.1 Iridescent NCC film and its white light diffraction.

Figure 4-1 shows a sample of iridescent NCC film that was produced after 48 h nominal drying in a 3.5 cm Petri dish at room temperature at ambient humidity.

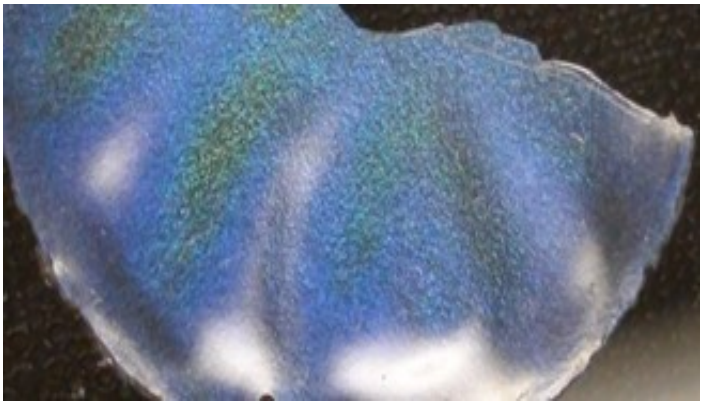

**Figure 4-1.** Image of iridescence from a nominally dry NCC film.

The film exhibits broad deformation undulations in the surface due to internal stresses that accumulate as the film undergoes shrinkage and delamination from the substrate during the drying process. These undulations produce different angles at which light is reflected from the surface so that various metallic hues are directly visible in Figure 4-1. The film reflects left circularly polarized light since the film appears dark when viewed through a right handed circular polarizer. This is to be expected from the chiral nematic liquid crystal phase of NCC from which the solid films are derived [22]. Nevertheless, as shown below the iridescence in this case cannot be fully explained by Bragg reflection on the periodic helical structure of the film when the chiral nematic pitch $P$ is comparable to the wavelength of light.

The left image Figure 4-2A is an optical photomicrograph of the same film under crossed polarizers. The film texture is far from planar since the CN phase is unable to reach equilibrium alignment during the drying process. Quasi-planar regions appear as light patches in the film. Close inspection of the image reveals that the surface is textured throughout with fingerprint patterns which owe their origin to the optical retardation lines associated with the helicoid pitch of CN NCC produced in water. These patterns are

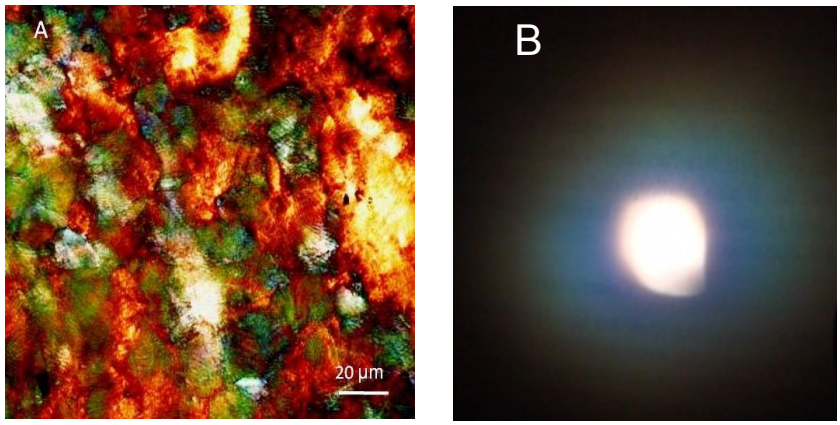


**Figure 4-2.** A) Polarized optical microscopy image (200x) of the NCC film from Figure 4-1. B) White light diffraction from the same film.

distributed randomly not only at the surface but also within the depth of the film. The pitch measured from the lines is approximately 2 μm for this particular solid film sample. As shown below, this spacing was confirmed by SEM and AFM measurements.

White light was directed at the film surface at an angle of 10 degrees off normal, i.e., at near normal incidence in order to measure the reflectance spectra. The reflected and diffracted light was projected onto a white screen located 12 centimeter away from the sample, and the image was taken using Sony digital camera. The diffract pattern image in Figure 4-2B shows a central white region of about 1 mm diameter surrounded by a halo of iridescence. The center white spot is due to specular reflection from the NCC film while the halo iridescence is caused by a combination of Bragg multilayer reflective interference and diffraction from the surface relief grating. The spectrum of light diffracted from the film was investigated using an Ocean Optics-2000 fiber spectrometer. Measurements were performed by recording each monochromatic spectrum peak using a fiber optical

detector fixed on a rotational micron step stage. The results are collected in Figure 4-3, where the diffraction intensity is expressed as normalized to the peak intensity of each color.

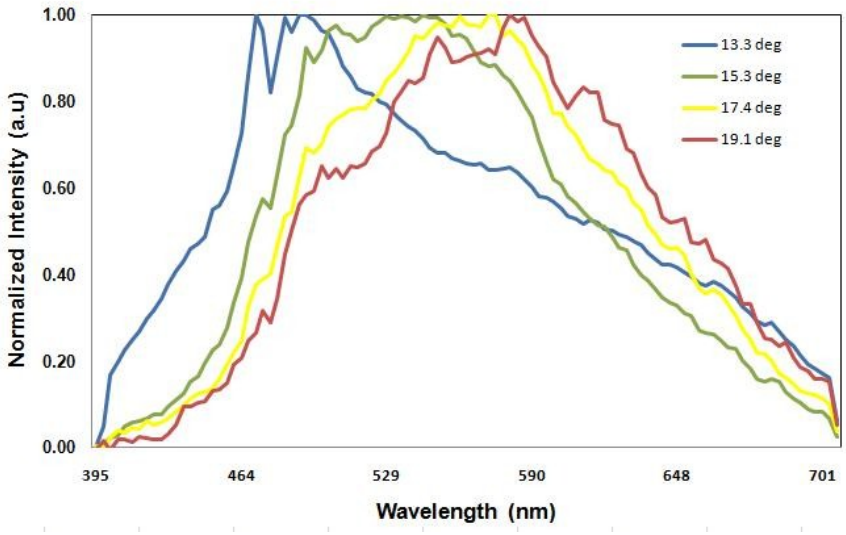


**Figure 4-3.** Spectra of light diffracted from iridescent NCC solid film. Maximum of each circular color band was recorded, value indicates the angle of the color band maximum positioned away from the center white spot (see Figure 4-2B).

The diffraction band spans from blue to yellow to red (ie, to longer wavelength) as the collection angle increases. This iridescence originates from rather complex structural color and cannot be attributable to Bragg multilayer interference alone. The origins of the structural color can be rationalized by examining specific morphological properties of the film.

### 4.3.2 Morphological origins of structural color.

Detailed studies of the morphology of the NCC film were undertaken. This involved examination of the pristine film surface by optical microscopy, AFM and SEM,

explorations of the texture revealed by careful removal of surface layers by adhesive tape, and studies of cross-sections of the film.

Figure 4-4A shows an optical micrograph of a portion of the NCC film surface. Evident in the optical micrograph are contrasting light and dark bands that appear.

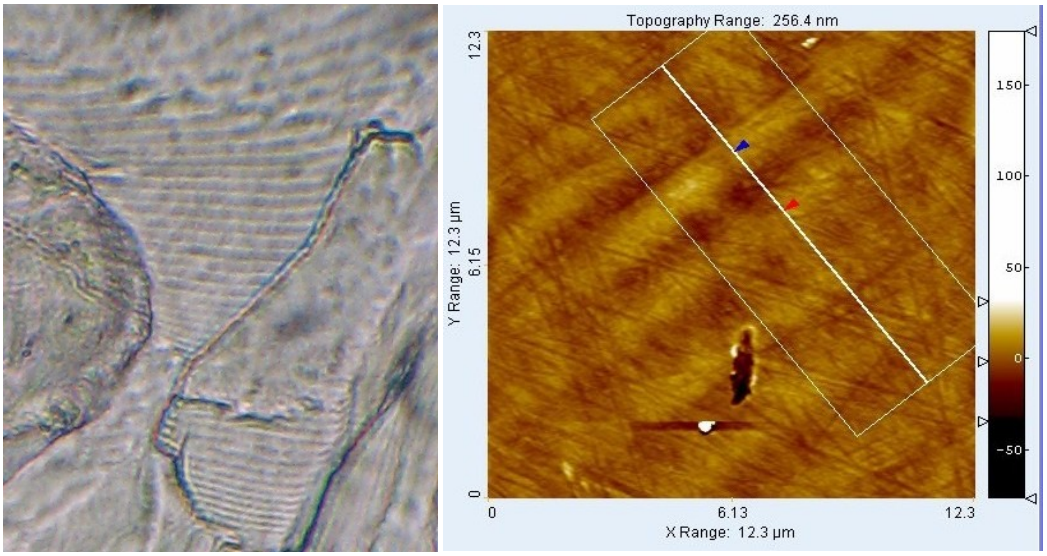


**Figure 4-4.** A) Optical micrograph of surface of NCC film exhibiting periodic birefringence. B) AFM peak-to-peak spacing is ~ 2 µm.

The periodic spacing appears to decrease in some areas because the film surface is uneven and tilts away in places from the plane. The pattern resembles the fingerprint texture observed in the precursor aqueous anisotropic phase of NCC.

AFM images in these regions show that these stripes of optical contrast are in fact physical gratings with 4 nm amplitude and spaced by approximately 2 µm (Figure 4-4B) saw-tooth with very small tilt angles of about 0.0025 radians. We observed that the grating structures propagate with a given orientation for some distance before

encountering other grating structures oriented at different angles. The picture is that of surface texture "roughened" with randomly oriented physical grating structures.

These findings suggest that under our film forming conditions, the optical response of the film may be a combination of Bragg reflection from the helicoid structure and diffraction from randomly oriented physical gratings on the surface and in the subsurface of the film. We next investigated by SEM the internal structure of the film and the surface that was revealed after peeling and fracturing the top of the film.

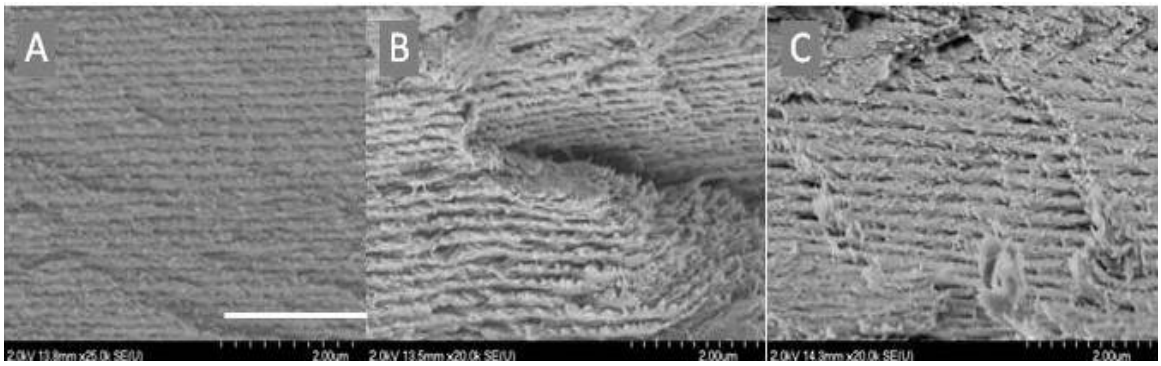


**Figure 4-5.** SEM cross-sections of NCC film. A) Corresponds to an East-West section, B) to North-South section, and C) is a cut at 45 degrees to the compass directions. (Scale bar = 2 μm for all images).

Figure 4-5 shows three nominally vertical SEM cross-sections through the NCC film. Left to right, the cuts correspond to East-West (A), North-South (B), and $45^0$ (C) to the cardinal points. The left hand side image, Figure 4-5A shows periodic layers with a thickness of 150 nm on average. The central image, Figure 4-5B yields layer thicknesses on the order of 120-200 nm, whereas analysis of the angled cut C sample yields a layer thickness of about 150 nm. At lower magnification (not shown) the layered structure exhibits remarkable periodic order, regardless of the direction of the cut. The layers, or

plies, extend over lateral distances of tens of microns and remain more or less parallel to each other. Lower magnification images also reveal that the action of the knife blade is not always vertical to the periodic layer structure: regions of cutting through obliquely oriented layered inclusions and cutting almost parallel to the plies can be discerned. It is evident that the film is actually made of regions of layered aggregates (inclusions) that intersect other layered aggregates at tilt angles. From top to bottom of the 40 μm thick film, section profiles show that there are lacunae, tears and fissures throughout. This suggests that the film is made up of helicoid inclusions with boundaries derived from sedimented precursor tactoids or multidomain features exhibiting chiral nematic order that have been frozen in during film growth [11,15]. This makes sense, since the polarized light micrograph in Figure 4-2 confirms that the film is anisotropic with respect to the helicoid director orientation.

The edges of the sectioned layers in Figures 4-5 and 4-6 are very ragged. This arises likely because the knife is more apt to cut between crystallites than through them. A parabolic (nested arc) texture is discernible within many of the layers in Figure 4-6. Some planar regions are tilted out of the horizontal periodic stacking plane. The tilt is not an artifact of the action of the knife, but gives evidence about how the film is assembled from the fluid chiral nematic phase.

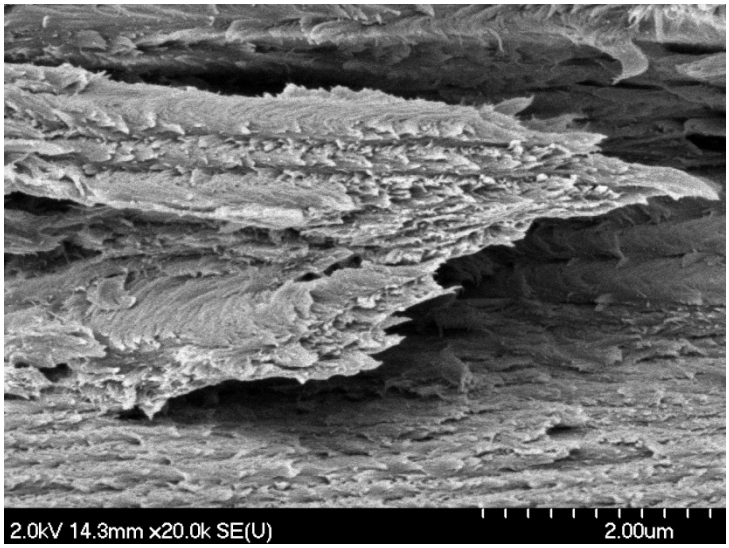


**Figure 4-6**. Section showing periodic pseudo-layers and parabolic texture with layers tilted in different directions.

The solid NCC film is rather brittle so that sections can be pulled away by applying and carefully withdrawing adhesive tape at the top surface of the film. The resulting texture is revealed in the collage of Figure 4-7. In Figure 4-7A, we note that the resulting surfaces are periodically terraced and that the terraces comprise geographical domains that intersect at different angles to give defects and discontinuities. Figures 4-7B and C show increasing magnifications of the terraced regions. The period between the ragged edged terraces is about 2 μm in Figure 4-7B and about 500 nm in Figure 4-7C, where the parabolic texture is clearly visible. Figure 4-7C was acquired at a 45 degree tilt observation angle. Over a large data set of SEM images, the measured period seems to depend on the tilt angle of the domain, i.e., the angle at which the helicoid structure is kinetically quenched as the film evolves. On closer inspection of Figure 4-7C one observes that there are fibril features assembled into arced plies on the surface of each layer. The finer structures on top of each layer surface were formed by the aggregation of

NCC particles whose helicoid features are compressed during the evaporation. We suggest that the nested arcs and terraces are visible by virtue of the fact that the deposition of tactoids and coalesced tactoids occurs at different angles or trajectories with respect to the surface normal of the Petri dish.

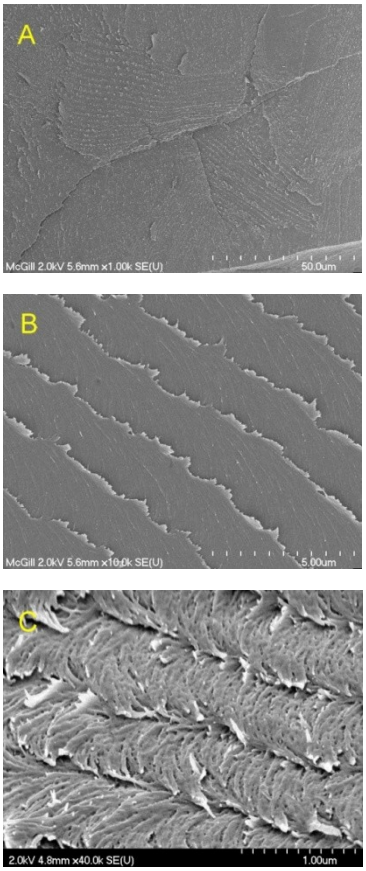


**Figure 4-7.** SEM images of top surface of NCC film (B is higher magnification of A). Section of NCC film in C) viewed at 45 degrees.

This is not to say that these terraced features in Figure 4-7 are the source of the grating structure that is linked to the iridescence. They are in fact revealed by the action of peeling away the surface layers with the adhesive tape. This can be understood as described next.

The images of Figures 4-5, 4-6 and 4-7 are reminiscent of the so-called "twisted plywood architectures" or "Bouligand features" observed in sections of insect cuticle and plant cell walls, or of solid films grown from solutions of nanocrystallites assembled into the CN phase [9,11,24,28]. Indeed, transmission electron microscopy on ultra-thin sections of chitin [11] and NCC [15] nanocrystallite films prepared under similar conditions from CN suspensions appear to be layered and manifest similar parabolic features when microtomed in oblique section. In contrast, it has been shown[15] that precise *vertical* sectioning of samples parallel to the helicoid axis of microfibrillar shrimp or crab chitin yield no parabolic texture for sections in which the helicoid axis is vertical [11]. The action of the adhesive tape in our experiments in revealing the staircased parabolic textures in Figure 4-7 in tilted inclusions can be explained as follows, if the helicoid axis is not perpendicular to the surface of the film, then the adhesive tape will create an oblique fracture. The nested parabolic arcs correspond to fracture planes that are oblique with respect to the chiral nematic strata. The arcs result from the regular succession of microfiber orientations in projection onto the oblique plane. The origin of this kind of pattern has been carefully scrutinized in the literature[24-28].

Based on this evidence we propose that a given periodic light and dark band that appears in cross-sections of Figure 4-5 corresponds to the half pitch of the chiral nematic solid phase in a highly defected film. Between successive planes the director must make a full turn of $2\pi$ along the helicoid axis for reflection. As we observe reflection (iridescence) from the film in the visible, the half pitch should be on the order of 150-250 nm, which is precisely the spacing we observe. This argument of course does not mean that the film as a whole has uniform planar texture.

In summary, the film surface is decorated with randomly oriented physical grating structures with a period on the order of 2 μm. These gratings are derived from the fingerprint patterns expressed in the precursor chiral nematic fluid phase. The gratings are distributed through the bulk of the film. In addition to the physical gratings, there are periodic bands that are broadly distributed and which arise from the chiral nematic NCC assembles that have undergone compression during condensation, consolidation and drying. When viewed in approximately vertical section, the helicoid assembly gives the appearance of periodic bands whose pitch corresponds to the visible wavelengths of light. Because the overall texture of the film is not planar, tilted periodic structures appear under fracture, and these are reminiscent of oblique sections of insect and arthropod cuticle that exhibit the well documented plywood architecture.

### 4.3.3 Fluid phase antecedents to grating and layer structure formation.

We conducted two experiments to explore self-assembly in solution as a precursor to the formation of order in solid state NCC films. In the first experiment, 5 ml of a 5% w/v NCC suspension was layered into Petri dish where the evolution of order was monitored by video POM. The initial solution was isotropic and non-birefringent. After 10 hours, uniformly birefringent structures emerged under crossed polarizers as spherical, ovoid or rod-like objects on the order of 5 μm against an isotropic background. Gradually, these objects manifested fringe patterns (circled features highlighted in Figure 4-8A). Colors observed through a quarter wave plate indicate that the chiral nematic axis is perpendicular to the bands so the long axis of the NCC rods lies in the plane parallel to the birefringent bands. After 12 hours, the tactoids were observed to coalesce to form even

larger tactoids with an approximate size of 40 μm (Figure 4-8B). Many of these eventually merged to create the defected fingerprint texture (Figure 4-8C) which was conferred on the dry film in Figure 4-8D, albeit with a decrease in pitch.

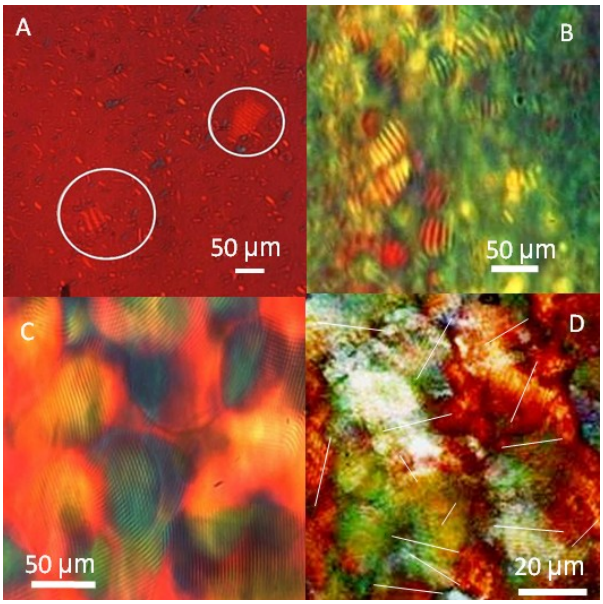


**Figure 4-8.** POM images of the self-assembly evolution from the fluid (A-C) to solid phase film (D) of NCC. In A) circles enclose tactoids exhibiting birefringent bands. B) Crossed polarizers of tactoids on the order of 40 μm distributed in water. (C) Anisotropic mesophase after aging the suspension derived from B. Birefringent multidomains are visible with superimposed retardation lines (fingerprint texture). These have a spacing of 3μm, corresponding to half the chiral nematic pitch. Image D) is the solid film from derived from the same solution in C. The white lines indicate the direction of the intersecting and overlaid the fingerprint texture that is distributed over the surface of and within the film.

A laser light scattering study of NCC at 5% w/v in water was conducted to further investigate layer and grating structure formation as the solid film evolved. For diffraction

from suspensions of NCC in an optical cell, patterns were obtained that depended on whether the beam interrogated the sample from the side (horizontal) or the top (vertical orientation) of the sample. The results are collected in Figure 4-9.

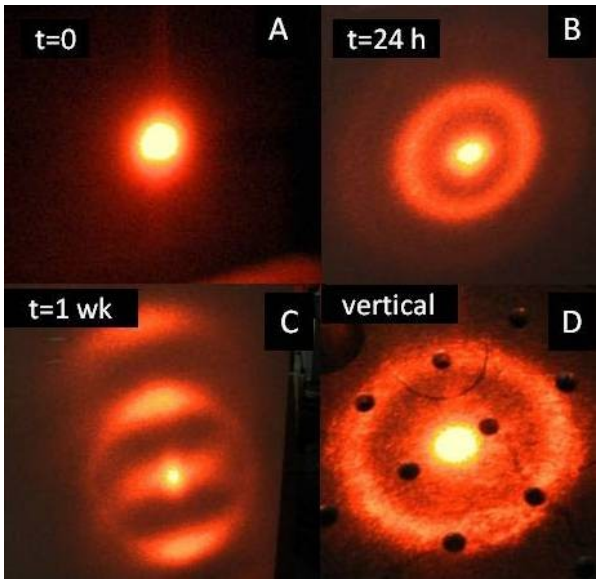


**Figure 4-9**. Time evolution of diffraction from 5% w/w NCC in water in 10 mm path length optical cell. Images A), B) and C) show the evolution of the diffraction pattern when laser beam is incident from side of the quartz wall. Image D is diffraction pattern obtained for sample C) when laser beam passes vertically through the cell from top to bottom.

Just after introducing the sample to the cell, the suspension shows only Rayleigh scattering. After 24 hours, concentric rings appear (Figure 4-9B) due to scattering from the randomly distributed birefringent domains in suspension. Rings were observed regardless of whether the laser propagated through the top or the side of the sample cell. After one week, the sample separated into an isotropic and anisotropic phase. The anisotropic component in the bottom portion of the cell formed some kind of layered structure that diffracted the horizontally injected beam in a manner like a 1D grating to

give the pattern in Figure 4-9C. We believe that this layer structure forms as the NCC undergoes gelation and sediments during evaporation. Figure 4-9D shows the diffraction pattern that results when the laser beam was injected through the top of the sample that had been allowed to stand for one week. The pattern consists of concentric rings in contrast to that of Figure 4-9C. This indicates that the diffraction ring arises from the mesophase CN structure and not from the layered structure. The solid film also showed a single diffraction ring when the beam impinged on the sample normal to the surface.

### 4.3.4 Optics of NCC film chiral nematic grating and structured grating

We [29] and others [30-32] have shown that a CN phase multidomain fingerprint texture that persists in three dimensions in solution can be transferred to the bulk solid film as periodic texture that echoes its chiral nematic phase precursor state. To account for the iridescence from the film of Figure 4-1, we need to include contributions from randomly oriented physical gratings and the chiral nematic reflector. We have argued that the physical grating is derived from the fingerprint texture which is induced from tactoids, while the layered structure comes from the emergence of compressed helicoid structure that emerges from collapsed tactoids during evaporation.

Figure 4-10 is a schematic of the grating structure which arises from the grooved structure of the surface of the collapsed fingerprint tactoids.

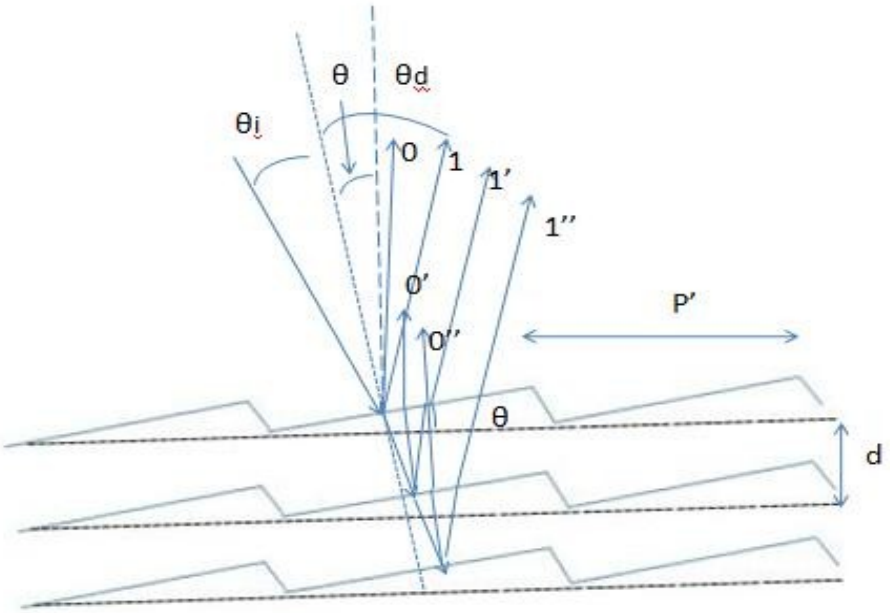


**Figure 4-10**. Schematic of grating and layer structure of NCC film. Where 0, 0′,0″ are 0 order diffraction, 1, 1′, and 1″ are first order diffraction , P′ is pitch of surface grating, θ is the angle of incline of grating, and d is the thickness of each layer.

In Figure 4-10, θ is the angle of incline of the grating plane, and from the angle of the grating height difference measured by the AFM this incline is ~0.0025 radians, which is very small. The gratings are therefore nearly convexo-concave planar. In this case the grating equation is,

$$P'(sin\theta_i + sin\theta_d) = k\lambda \qquad (4\text{-}1)$$

Here, $\theta_i$ is the angle of incidence, $\theta_d$ is the diffraction angle, k is the diffraction order, λ is the wavelength, and P′ is the (compressed) surface grating pitch. To verify, we calculated the diffraction angle using the above equation and compared it with experimental data measured from our white light diffraction experiment. We observed that tilting the NCC film within angles of $\pm 10^o$ from normal did not alter the diffraction pattern. In order to

take a picture of the image without blocking the incident light, we collected the image from an angle of $10^o$ left from the normal; however the diffraction angle is calculated for normal light incident diffraction for simplification. For normal incidence, $\theta_i$ is zero, and only the first order diffraction can be seen for this particular sample, so, k=1. Therefore, Equation 4-1 simplifies to,

$$P'(sin\theta_d) = k\lambda \qquad (4\text{-}2)$$

From the SEM and AFM data, $P'$ is 2 μm, and for blue light, λ=0.4 μm. From Equation 4-2, the first diffraction angle $\theta_d$ must be $13.3^o$ which was measured by white light diffraction test (Figure 4-3). For other wavelengths, we obtain diffraction angles that correspond to experimental data. These findings suggest that the physical grating model is a reasonable representation for features we observe on surface of our iridescent NCC films.

## 4.4 Conclusions

In this Chapter, we studied the microscopic detail of Nanocrystalline Cellulose films deposited from solution in the absence of applied electric or magnetic fields, and the results reveal the existence of randomly distributed structured gratings having a period on the order of 2 μm. The surface gratings are prefigured in the fingerprint texture of the chiral nematic fluid phase from which the solid film is derived. The film is assembled from sedimenting and coalescing tactoids whose trajectories to the evolving film surface are such that the helicoid axes of the condensing species are randomly oriented with respect to the surface normal to the plane. Evidence of structural ordering in solution was provided by laser light diffraction. The resulting texture is far from planar, and a convexo-

concave structured grating is distributed over three dimensions. The film is iridescent by a combination of multilayer Bragg reflective interference and a diffraction of surface relief gratings.

## 4.5 References

[1]. S. Kinoshita, S. Yoshioka, "Structural Colors in Nature: The Role of Regularity and Irregularity in the Structure," Chem. Phys. Chem.,6, 1443-1459 (2005)

[2]. V. Sharma, M. Crne, J. O. Park , M. Srinivasarao, "Structural Origin of Circularly Polarized Iridescence in Jeweled Beetles," Science, 325, 449-452 (2009)

[3]. A. E. Seago, P. Brady, J. P. Vigneron, T. D. Schultz, "Structural Colors in Nature: The Role of Regularity and Irregularity in the Structure," J. Roy. Soc. Interface, 6, S165-S184 (2009)

[4]. O. Deparis, C. Vandenbem, M. Rassart, V. L. Welch, J.-P. Vigneron "Color-selecting reflectors inspired from biological periodic multilayer structures,"Opt. Express, 14, 3547-3555 (2006)

[5]. O. Deparis, M. Rassart, C. Vandenbem, V. L. Welch, J.-P.Vigneron, S. Lucas, "Structurally tuned iridescent surfaces inspired by nature," New J. Phys.,10, 013032-1-11 (2008)

[6]. J.M. Castro, I. B Djorjevic, D. F. Geraghty, "Novel Super Structured Bragg Gratings for Optical Encryption," J. Lightwave Technol.,24, 1875-1885 (2006)

[7]. M. M. Giraud-Guille, "Twisted Plywood Architecture of Collagen Fibrils in Human Compact Bone Osteons," Calcif. Tissue Int.,42, 167-180 (1988)

[8]. R. L. Trestad, "The Bilaterally Asymmetrical Architecture of the Submammalian Cornea1 Stroma Resembles a Cholesteric Liquid Crystal," Dev. Biol., 92, 133-134 (1982)

[9]. M. M. Giraud, J. Castanat, F. J. Meunier, Y. Bouligand, The fibrous structure of Coelacanth scales: a twisted 'plywood', Tissue Cell, 10, 671-686 (1978)

[10]. D. H. Van Winkle, M. W. Davidson, W.-X. Chen, R. L. Hill, "Cholesteric Helical Pitch of Near Persistence Length DNA," Macromol.,23, 4140-4148 (1990)

[11]. J.-F. Revol, R. H. Marchessault, "In vitro chiral nematic ordering of chitin crystallites," Int. J. Biol. Macromol., 15, 329-335 (1993)

[12]. E. Belamie, P.Davidson, M. M. Giraud-Guille, Structure and Chirality of the Nematic Phase in r-Chitin Suspensions, J. Phys. Chem. B, 108, 14991-15000 (2004)

[13]. Y. C. R. Bouligand, "Sur une architecture torsadde repandue dans de nombreuses cuticules d'arthropodes," Acad. Sc. Paris Ser D, 261, 3665-3668 (1965)

[14]. A. C. Neville, S. Caveney, "Scarabaeid beetle exocuticle as an optical analogue of cholesteric liquid crystals," Biol. Rev., 44, 531-562 (1969)

[15]. J.F. Revol, H. Bradford, J. Giasson, R.H. Marchessault, D. G. Gray, "Helicoidal self-ordering of cellulose microfibrils in aqueous suspension ," Intl. J. Biol. Macromol., 14, 170-172 (1992)

[16]. D. G. Gray, "Chiral nematic ordering of polysaccharides ," Carbohydr. Polym., 25, 277-284 (1994)

[17]. J. F. Revol, L. Godbout, D. G. Gray, "Solid self-assembled films of cellulose with chiral nematic order and optical variable properties ," J. Pulp. Paper Sci., 24, 146-149 (1998)

[18]. H. De Vries, Rotatory power and other optical properties of certain liquid crystals, Acta Cryst., 4, 219-226 (1951)

[19]. J. Pan, W. Hamad, S. K. Strauss, "Parameters Affecting the Chiral Nematic Phase of Nanocrystalline Cellulose Films ," Macromol., 43, 3851-3858 (2010)

[20]. A. R. Parker, "515 million years of structural colour ," J. Opt. A: Pure Appl. Opt., 2, R15-R28 (2000)

[21]. D. J. Broer, "Creation of Supramolecular Thin Film Architectures with Liquid-Crystalline Networks ," Mol. Cryst. Liq. Cryst., 261, 513-523 (1995)

[22]. T. Scharf, "Static birefringent microlenses ," Opt. Laser Eng., 43, 317-327 (2005)

[23]. C.D. Edgar, D.G. Gray, "Formation of cellulose-based electrostatic layer-by-layer films in a magnetic field,"Cellulose,8, 5-10 (2001)

[24]. A. C. Neville, "Molecular and mechanical aspects of helicoid development in plant cell walls," Bio Essays, 3, 4-8 (1977)

[25]. M.M. Giraud-Guille, Direct visualization of microtomy artefacts in sections of twisted fibrous extracellular matrices, Tissue Cell,18, 603-620 (1986)

[26]. F. Livolant, Y. Bouligand, Freeze-Fractures in Cholesteric Mesophases of Polymers, Mol. Cryst. Liq. Cryst., 166, 91-100 (1989)

[27]. P. M. Hughes, “Insect cuticular growth layers seen under the scanning electron microscope: A new display method ,” Tissue Cell, 19, 705-712 (1987)

[28]. D. Gubb, “A direct visualisation of helicoidal architecture in Carcinus maenas and Halocynthia papillosa by scanning electron microscopy,” Tissue Cell, 7, 19-32 (1975)

[29]. Y.P. Zhang, V. P. Chodavarapu, A. G. Kirk, M. P. Andrews, M. Carluer, G. Picard, “Origin of iridescence in chiral nematic phase nanocrystalline cellulose for encryption and enhanced color ,” SPIE Proc., 7955, 7955-10-18 (2011)

[30]. K.E. Shopsowitz, H. Qi, W.Y. Hamad, and M.J.MacLachlan, “Free-standing mesoporous silica films with tunable chiral nematic structures,” Nature, 468, 422-426 (2010)

[31]. I. I. Smalyukh, O. D.Lavrentovich, “Three-dimensional director structures of defects in Grandjean-Cano wedges of Cholesteric liquid crystals studied by fluorescence confocal polarizing microscopy ,” Phys. Rev. E, 66, 051703-1-16 (2002)

[32]. Y. Dong, Q.Yuan, Y. Mu, M. Wang, “Fine structure in cholesteric fingerprint texture observed by scanning electron microscopy,” Polym. Bull., 44, 85-91 (2000)

# Chapter 5

## NANOCRYSTALLINE CELLULOSE FOR COVERT OPTICAL ENCRYPTION

## 5.1 Introduction

It is estimated that counterfeiting costs North American businesses over $250 billion in annual losses [1,2]. Counterfeiting affects not only banknotes, but has insinuated itself into the electronics, food, and pharmaceutical industries. To combat counterfeiting, a variety of encryption methods have been developed. Among these methods, security inks have emerged as a growth area in printed security options. Encryption inks come in many varieties: thermochromic, fluorescent, electrochromic, holographic, optically variable, invisible, water fugitive, solvent reactive and penetrating. Most contain a molecular species that can be read by a spectrometer when excited by an appropriate wavelength of light. Some respond to infrared (thermochromic), while others respond to electrochemical events (electro-chromic). Holographic inks offer 3D encryption, though these are not printed directly as holographic images. Biomaterials for green photonics is a new area where optics and photonics can recruit renewable materials and processes for communications and sensing. Nanocrystalline Cellulose (NCC) is a renewable resource material derived from wood pulp and other cellulose sources. NCC is attracting broad interest in part because of its unusual optical properties. NCC films can exhibit bright and color saturated iridescence that originates in the chiral nematic texture that can be produced in solid films. Iridescence from such films originating by reflecting left-circularly polarized light over a wavelength band determined by the chiral nematic pitch, P, and the refractive index of the film has been studied in previous Chapters, and the

selective reflection of circularly polarized light as a unique optical feature could be used for security applications. In this Chapter, we will add second covert security, UV fluorescence, into the NCC film, and to explore the potential of NCC to be used in developing encryption inks. An Optical Brightening Agent (OBA), TINOPAL (Figure 5-1) will be used as the dye in these experiments. OBAs are known to form strong hydrogen bonds with cellulose and this property simplifies bonding to the NCC particles without resorting to multi-step covalent attachment at the NCC surface. OBAs are widely used in the pulp and paper industry to enhance the whiteness of paper. The compound in Figure 5-1 exhibits strong fluorescence under UV excitation [3] and a high affinity for the cellulose surface [4].

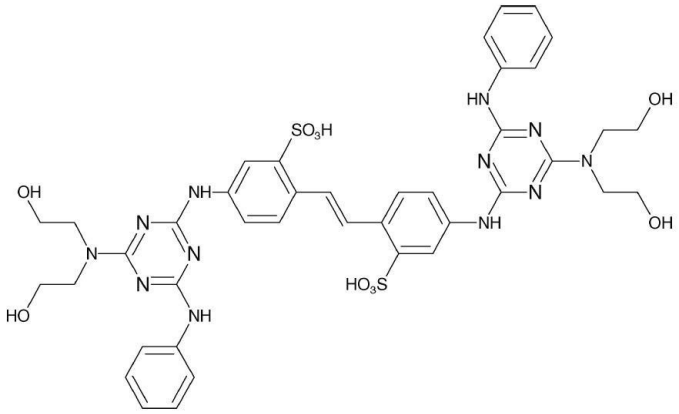


**Figure 5-1**. TINOPAL Optical Brightening Agent.

## 5.2 Experimental

### 5.2.1 Materials

Dissolving-grade softwood sulfite pulp (Temalfa93) lap sheets were purchased from Tembec Inc, Temiscamingue, QC. Sulfuric acid (95–98%) for hydrolysis was purchased

from Fisher Scientific. Purified water (Millipore Milli-Q purification system) was used throughout. Tinopal HW OBA solution was purchased from Ciba and used as received.

### 5.2.2 Preparation of Nanocrystalline Cellulose

The NCC suspension was produced by hydrolysis of softwood spruce fiber (Temalfa93) with sulfuric acid using same procedure previously described in Chapter 4.

### 5.2.3 OBA addition

0.5% TINOPAL OBA by weight was added to a 3% w/w NCC suspension with constant stirring (Thermolyne Maxi MixII mixer) to achieve dye concentrations of 50 ppm, 100 ppm, and 150 ppm.

### 5.2.4 CD Spectropolarimeter

A calibrated Jasco 710 Circular Dichroism spectropolarimeter was used to evaluate the effect of the adding OBA on the optical activity of the NCC film.

### 5.2.5 Zeta-potential analyzer

A Zeta-plus Zeta potential analyzer from Brook Haven Instruments Corporation was used to measure the Zeta potential after mixing different concentrations of OBA with NCC.

## 5.3 Results and Discussions

### 5.3.1 Overt security by Iridescence

Figure 5-2 shows a sample of iridescent NCC film that was produced with 24 h nominal drying after casting at room temperature at ambient humidity. The film shows

deformation undulations in the surface due to internal stresses that result when the film undergoes shrinkage and delamination from the substrate during the drying process. These undulations produce different angles from which light is reflected at the surface so that various metallic hues are directly visible in the Figure. The film reflects left circularly polarized light since the film appears brighter when viewed through a left-handed circular polarizer and appears darker when viewed through a right-handed circular polarizer. This is to be expected from the chiral nematic liquid crystal phase of NCC from which the solid films are derived.

**Figure 5-2**. Iridescence from NCC solid film image under room light.

It is well known that colloidal NCC suspensions can form liquid crystalline phases when the concentration of the suspension reaches a critical value [5]. Chiral nematic structures formed in NCC show high rotatory power and reflect left-handed circularly polarized light in a narrow wavelength band [6]. For a model of helically arranged particles, de Vries [7] showed long ago that the reflected wavelength, $\lambda$, depends on the chiral nematic pitch P of the chiral nematic structure through the relationship, $\lambda = nP$, where, n is the refractive

index of the liquid crystal suspension. In studies of the self association of NCC particles during evaporation, we [8] and others [9] found that part of chiral nematic texture formed in the liquid phase can be preserved when the solvent is evaporated to a make solid film. The film inherits strong rotation power and selective reflection optical properties. As it is written, the de Vries equation applies to normal incidence light. For non-normal incidence, Revol et al. [6] extended the equation to $\lambda = nP\cos\theta$, where $\theta$ is the angle between the normal of the surface and the viewing angle. Accordingly, when the incident angle is other than normal, a different color can be observed. This gives the film its rich iridescent color. Iridescent inks abound and are widely made from metal flakes. NCC iridescence is unique, however, in that it reflects left-circularly polarized light. Thus the overt iridescence of NCC carries a covert component through its polarized light response.

### 5.3.2 Covert security accomplished by adding OBA to NCC

TINOPAL HW is built around a *trans*-stilbene core that is elaborated with triazene substituents. The stilbene moiety in Figure 5-1 is a 2,2′ disulfonic acid and the triazine units are equipped with *bis*-hydroxyethylamino groups and aniline functionalities. The disodium salt was used in our studies (see below). The nitrogen, hydroxyl and sulfonic acid groups are responsible for the strong hydrogen bonding to the cellulose surface[10]. Figure 5-3 shows that TINOPAL OBA absorbs near 360 nm and emits strong fluorescence maximizing at 450 nm. The intensity of absorption and emission spectra are not comparable, but the two spectra are shown in one graph in order to emphasize the absorption and emission peak position only. This emission translates into a covert opportunity when the NCC film is excited in the UV. This is evident from Figure 5-4

which shows a sample of iridescent NCC film under conventional white light illumination (left image) and under UV excitation (right image).

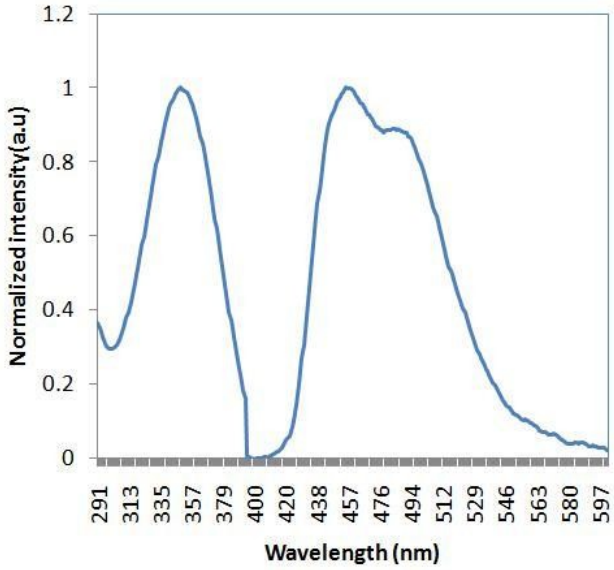


**Figure 5-3**. TINOPAL OBA absorption (left band) and emission (right band) spectra.

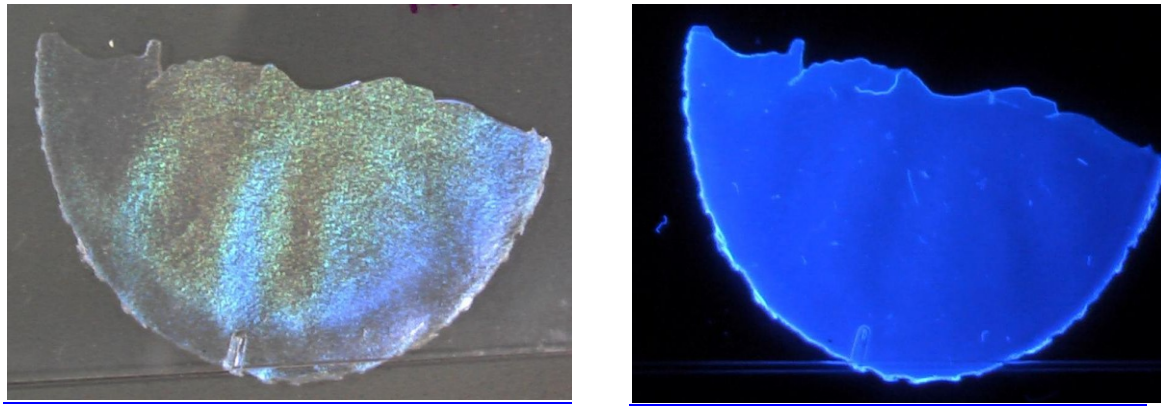

**Figure 5-4**. Iridescent NCC film doped with 50 ppm TINOPAL OBA. (left) under conventional illumination and excited with UV light (right).

### 5.3.3. Effect of adding OBA on Circular Dichroism

Circular Dichroism (CD) refers to the differential absorption of left and right circularly polarized light:

$$CD = AL - AR \qquad (5\text{-}1)$$

where AL is the absorption of left-handed Circular Polarized Light (CPL) and AR, the absorption of right-handed CPL. For chiral nematic samples that reflect visible light, the sign of the apparent CD signal resulting from the reflection of circularly polarized light gives the handedness of the chiral nematic helicoidal structure [11]. A circular selective reflection can easily be distinguished using a circular polarizer if the optical reflection contrast is high. High contrast is desirable if the material is to be used for security authentication. For our purposes, CD provides an index of the film reflection contrast with respect to polarized light. If a covert OBA signature is added to the NCC deposit, it is important to study the effect of doing so on the optical activity of the material. The shape of a CD band depends on the degree of order and the texture of the mesophase. A uniform planar texture gives a sharp CD band, whereas a structure composed of chiral nematic polydomains yields a broad CD band [12]. We used the sodium salt of TINOPAL for additions to the NCC suspensions. We surmised that increasing amounts of OBA might affect the ability of NCC to undergo an isotropic to nematic phase transition (steric effect) and that the salt might alter the pitch of the chiral nematic phase. These effects might manifest themselves in changes to the CD spectra. Figure 5-5 shows CD spectra of NCC plotted as a function of NCC concentration. When the TINOPAL OBA concentration reached 150 ppm, broadening occurred in the CD spectrum. Additions of increasing

amounts of OBA also induce a red-shift in the maximum of the CD signal (Figure 5-6). The red shift signifies elongation in the pitch with increasing concentration of OBA.

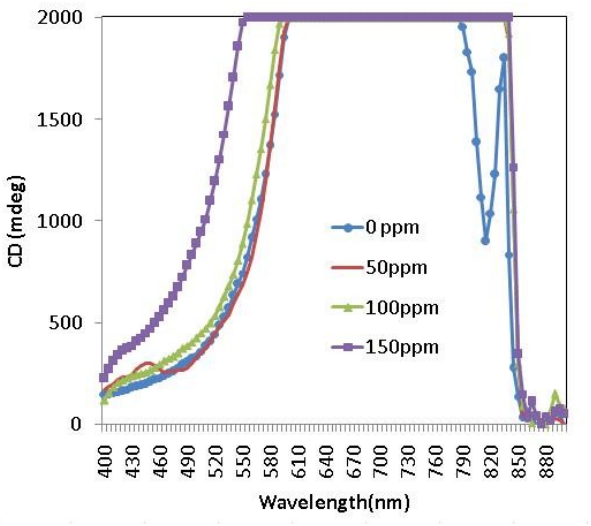


**Figure 5-5**. Effect of increasing amounts of TINOPAL OBA on CD spectral features. Note the sudden increase in width of the CD response between 100 (triangle symbols) and 150 (square symbols) ppm OBA.

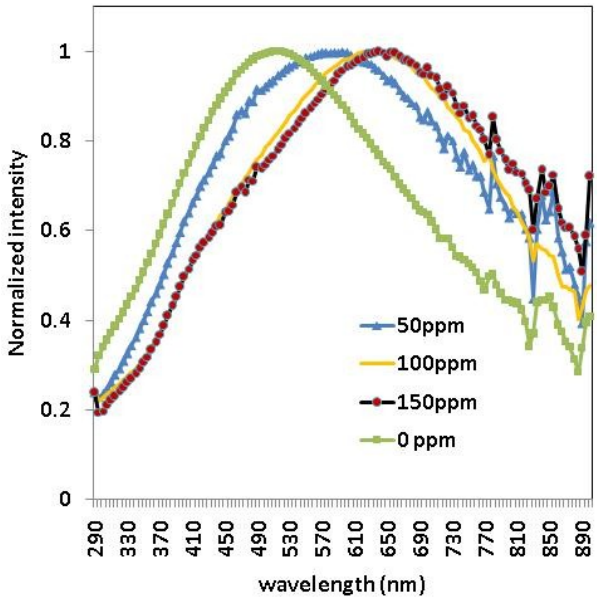


**Figure 5-6**. Red-shift in the peak maximum of the normalized CD spectra with increasing concentration of OBA in NCC.

Polarized optical microscopy gives additional insight into changes in the pitch and chiral nematic texture induced by additions of OBA. Figure 5-7 reveals two effects. 1) The pitch increases with increasing TINOPAL OBA concentration. (Table 5-1); and 2) there is a qualitative increase in the poly-domain texture with increasing OBA.

**Table 5-1. Effect of adding OBA on the chiral nematic pitch**

| OBA concentration (ppm) | Chiral nematic pitch (μm) |
|---|---|
| 0 | 2.1±0.5 |
| 50 | 3.3±1.1 |
| 100 | 5.1±2.1 |
| 150 | 7.1±2.2 |

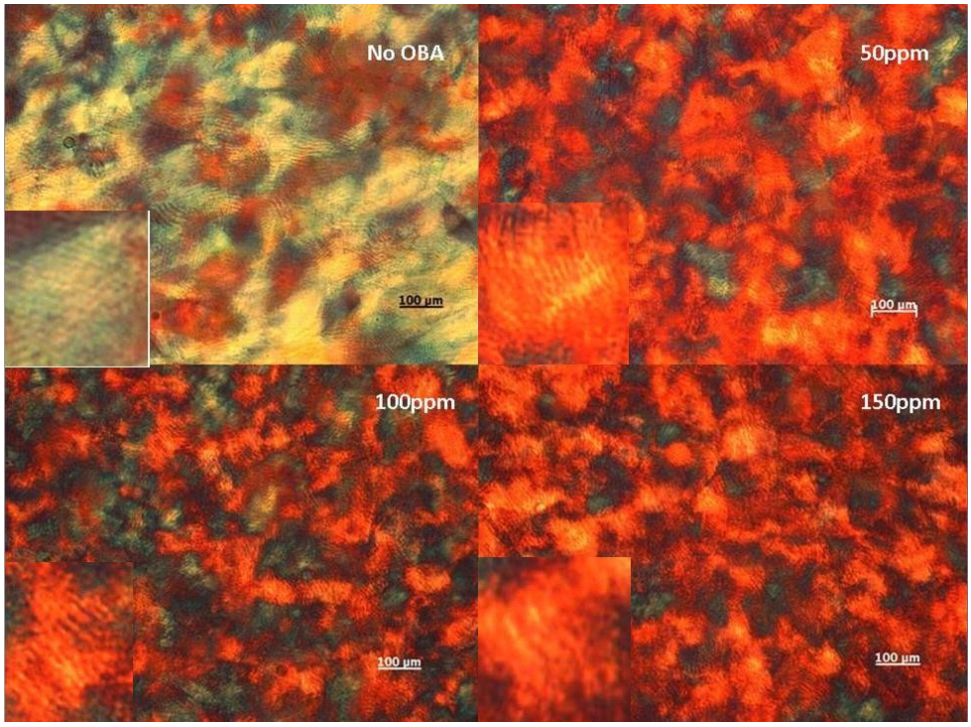


**Figure 5-7**. Polarized optical micrographs of the texture of NCC films with increasing amounts of TINOPAL OBA. Note that the chiral nematic pitch increases with addition of OBA.( see inset on each image for a magnified portion ).

### 5.3.4 Variation in the zeta potential of NCC with added OBA

The zeta potential is a measure of the electrokinetic potential of a colloidal system. More precisely, the zeta potential is the electric potential in the interfacial double layer (DL) at the location of the so-called “slipping plane” versus a point in the bulk fluid away from the interface. Thus, the zeta potential is the potential difference between the dispersion medium and the stationary layer of fluid attached to the dispersed NCC particle. Measurement of the zeta potential gives evidence of the surface charge on the colloidal particle. The stability of the suspension can be dominated by surface charge. The effect of

surface charge variation induced by adding charge (hence, colloidal stability) can be monitored by measuring the zeta potential of the suspension.

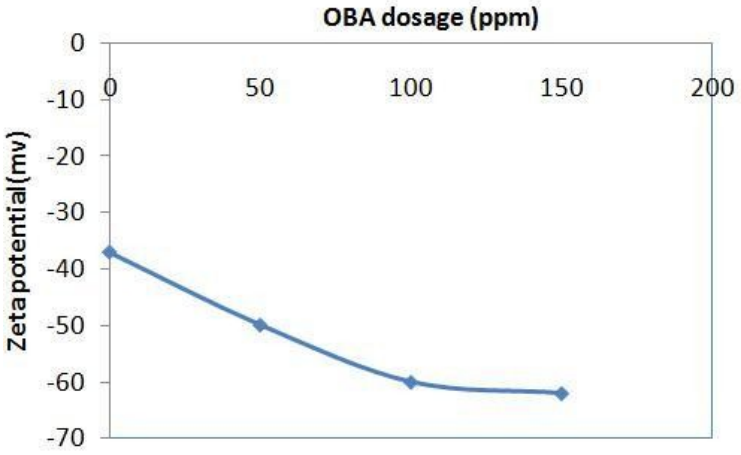


**Figure 5-8**. Evolution of the zeta potential of with increasing amounts of OBA added to the NCC suspension.

When negatively charged TINOPAL OBA was added to the NCC suspension, its adsorption will confer more negative charge on the NCC surface. The zeta potential of the suspension will become increasingly negative with increasing concentration of OBA. Figure 5-8 shows indeed that this is the case. An increase in negative potential will in turn increase the repulsive force among NCC particles, making close approach energetically unfavourable, driving the system to greater pitch, as we observed.

## 5.4 Conclusions

Nanocrystalline Cellulose may offer some potential for optical encryption applications. This potential lies in the overt level of encryption it can provide based on iridescence that

originates in the multidomain chiral nematic texture of the solid film. It offers an additional level of covert encryption because it reflects left circularly polarized light. A third level of (covert) encryption can be included by binding dye molecules that fluoresce when excited by ultra-violet light. The result is one system that supports multiple potential security features: overt security (iridescence) and covert security (selective circular reflection and fluorescence). TINOPAL Optical Brightening Agent was used as a prototype dye molecule. The OBA exhibits high fluorescent efficiency. Additions of small amounts of OBA can yield intense fluorescence with little impact on polarized light or iridescent properties. Quantities of OBA in concentrations greater than 100 ppm increase the chiral nematic pitch, broaden circular dichroism spectra and degrade chiral nematic texture in the films. Measurement of the spacing in the retardation lines of NCC films by polarized optical microscopy shows that the pitch increases with increasing OBA concentration. Simultaneously, the zeta potential becomes increasingly negative. These findings are consistent with increasing pitch caused perhaps by a combination of steric and charge effects. Future studies will establish how ink-jet printing can be used to print patterns containing all three levels of encryption.

## 5.5 References

[1] http://www.iacc.org/about-counterfeiting/the-truth-about-counterfeiting.php, International Anti-counterfeiting Coalition (IACC) (2010)

[2] http://www.cacn.ca/publications.html “Report on Counterfeiting and Piracy in Canada: A Road Map for Change” (2007)

[3] J. Hughes, and M. E. McCull, "The Use of an Optical Brightener in the Study of Plant Structure," Stain Technology 50, 151-158 (1975)

[4] B. W. Crouse, and G. H. Snow, "Fluorescent whiteness agents in the paper industry," TAPPI J. 64, 87–89 (1981)

[5] X. M. Dong, T. Kimura, J. F. Revol, and D.G. Gray, "Effects of Ionic Strength on the Isotropic-Chiral Nematic Phase Transition of Suspensions of Cellulose Crystallites," Langmuir 12, 2076-2082 (1996)

[6] J. F. Revol, L. Godbout, and D. G. Gray, "Solid self-assembled films of cellulose with chiral nematic order and optically variable properties," J. Pulp Paper Sci. 24, 146-149 (1998)

[7] H. de Vries, "Rotatory power and other optical properties of certain liquid crystals," Acta Cryst. 4, 219-226 (1951)

[8] Y.P. Zhang, V.P. Chodavarapu, A.G. Kirk, M. P. Andrews, M. Carluer, and G. Picard, "Origin of iridescence in chiral nematic phase nanocrystalline cellulose for encryption and enhanced color," Proc. SPIE 7955, 79550-79558 (2011)

[9] L. Neimo, Ed., "Papermaking Science and Technology, Book 4, Papermaking Chemistry," Fapet Oy publishers, Helsinki, Finland (1999)

[10] C.D. Edgar, and D.G. Gray, "Induced circular dichroism of chiral nematic cellulose films," Cellulose 8 5–12 (2001)

[11] Z. Yue, and J. G. Cowie, "Preparation and Chiroptical Properties of a regioselectively Substituted Cellulose Ether with PEO Side Chains," Macromolecules, 35, 6572-6577(2002)

# Chapter 6

## WATER-INDUCED COLOR CHANGE OF NANOCRYSTALLINE CELLULOSE FILMS, FOR A STRUCTURED COLOR HUMIDITY INDICATOR OR A COVERT SECURITY FEATURE

### 6.1 Introduction

Color indicators have broad appeal for monitoring the quality, freshness and shelf life of packaged foods, pharmaceuticals and chemicals. In particular, disposable indicators offer ease of visual readout with no need for electronic circuitry. Moreover, advances in flexographic and gravure tools to print functional inks create opportunities for both the print and packaging industries to create what can be viewed as one of the simplest of "indicator displays" – a symbol, a surface area or a design that changes color on exposure to an analyte. Humidity sensors are desirable in the food industry, which makes conflicting demands with respect to moisture content [1]. Thus while excess moisture can accelerate decomposition of meats, most water laden fruits and vegetables are best stored under 95% relative humidity (RH) at near $0^{o}$C; but sugar and salt lose texture and desirable flow characteristics if the moisture content is too high. Grains can become rancid when the RH is too low. Archival materials like books and paintings require careful monitoring to prevent mould and bacterial decomposition. For some technological hardware, the functionality of electronic components can be compromised if the RH is too high.

Conventionally, humidity sensors are made from electronic hygrometers based on capacitive or resistive systems that measure the change in conductivity of a polymer or ceramic film as a function of relative humidity [2]. Such devices have limitations in their

operating conditions and can be expensive and bulky to use [3]. Colorimetric humidity indictors are advantageous because color change is easily detected visually, obviating the use of any electronics or instruments. There has been a number of proposed colorimetric relative humidity indicators, the majority of which are based on the use of inorganic salts such as cobalt(II)chloride. A typical commercial form of the latter is the Humitector® Humidity Indicator Card (Chemie Inc., USA). Hybrid polymer/CoCl2 nanocomposites have been used in combination with lithographically prepared diffraction gratings for humidity sensing [4]. Despite the simplicity of the CoCl2 indicator, cobalt-free humidity cards have been advocated as replacements to satisfy the European Chemical Bureau REACH directive [5]. Elsewhere, polymer-based colorimetric inks have been suggested as potential low cost alternatives [6]. Some of these are based on chromogenic dyes [7], while others offer polymer-based photonic crystals [8]. The latter are interesting in view of the ways that ordered materials can interact with light to produce a variety of optical effects collectively known as structured color. Structured color is caused by scattering that arises from spectral reflection due to the physical interaction between light and the geometric patterning of matter over different length scales. Changes in structured color can be used for a variety of sensing applications, though the underlying mechanisms by which the color changes evolve can differ. In the biosphere, the longhorn insect species, Tmesisternus isabellae, constructs its own colorimetric humidity indicator from periodic alternating layers of dense melanoprotein and inhomogeneous layers of melanotprotein nanoparticles and air voids [9]. Constructive multilayer interference gives rise to a gold iridescence in the dry state. Water sorption and infiltration swell the multilayers and alter the refractive index and layer spacing. Simultaneously, the reflectance exhibits changes in

iridescence from gold at low RH to red in the wet state. Photonic crystals belong to the category of structured color materials as well. Indeed, recent research [10] has shown that oblique vapor phase deposition produces mesoporous $TiO_2$ films suitable for photonic crystal humidity sensing. Shi et al. [8] developed a nanoporous one-dimensional polymer photonic crystal colorimetric sensor based on holographic interference patterning of a polymer dispersed liquid crystal. Changes in RH altered the refractive index contrast between nonporous and nanoporous regions, and thus the transmittance and bandgap position. Liquid crystal (LC) materials are of interest because their optical response is controlled by self-assembly, ie, a nonlocal response to a perturbation which might be in the form of electric, optical, or mechanical field forces. The combination of self-assembly with colorimetric sensing is attractive because it can reduce sensor cost and sensor assembly complexity. Chiral nematic (CN) liquid crystals are candidates for colorimetric sensing because they can exhibit brilliant colors without the use of absorbing or emitting chromophores. A planar, uniformly textured CN material behaves as one-dimensional self-organized chiral photonic crystal. In the CN phase, the long axis of the LC-forming species rotates in a plane about a perpendicular helix. The CN phase shows a periodic variation in refractive index, allowing it to be used to filter circularly polarized incident light of the same handedness as its helix. A single-pitch (single domain planar texture) CN material will selectively reflect light at the Bragg wavelength centered at $\lambda = nP$. CN films having non-uniform pitch distribution, where the pitch lengths and helicoid tilt axes are different in different regions, will reflect light with much wider bandwidth than single-pitch CN films. The pitch length P of the helix corresponding to a $2\pi$ molecular rotation is determined by several factors that can include concentration, helical twisting power and

even charge in the case of ions. For colorimetric sensing, if analyte binding changes the pitch (expands or contracts the helix), there should be a corresponding change in the reflectance. In this context, Saha et al. [11] constructed a colorimeter humidity-sensing device based on doping an high helical twisting power binapthyl moiety, bis-[binaphthylen-(2,2′)-dioxy]-silan, into a nematic liquid crystal phase. Colored films of the composite behaved as irreversible integrating sensors since the pitch, hence the color, changed irreversibly on hydrolysis of the binaphthylene silicon alkoxide linkages.

Nanocrystalline cellulose derived from forest resources is well known to form a chiral nematic liquid crystal phase [12]. Maclachlan and co-workers [13] have used nanocrystalline cellulose as a lyotropic template to control polycondensation of bridged alkoxysilanes to prepare flexible chiral nematic mesoporous silica films. The visible reflection spectral response (iridescence) of these films is reversibly lost due to close matching of the refractive index of the organosilica walls by vapors that invade the lacunae. But if nanocrystalline cellulose can be a template for a periodic mesoporous silica humidity sensor, then perhaps a simpler construct is the bio-resource NCC itself when cast as a broad band non-uniform pitch film. The concept is appealing because the colorimetric indicator is derived solely from insoluble cellulose nanocrystallites, which are nonetheless hydrophilic. The rod-like crystallites can undergo an Onsager-type phase transition in fluid medium yielding an iridescent chiral nematic texture. Films cast from CN NCC suspensions exhibit planar texture when aligned in a magnetic field [12], or multi-domain texture when cast from solution in the absence of a coercive field. In this Chapter we will investigate the interaction between NCC and water molecular. The objective of this study is not only to explore the color shift induced by the moisture, and

its potential as humidity colorimeter indicator sensor, but also to find out the possibility of using water to authenticate NCC material when it is used as a security taggant.

## 6.2 Experiments

### 6.2.1 Synthesis and NanoCrystalline Cellulose (NCC) film formation

The NCC suspension was produced by hydrolysis of softwood spruce fiber (Temalfa93) with sulfuric acid using same procedure previously described in Chapter 4. 3 ml of this NCC suspension was filled into a 5 cm diameter petri dish and allowed to evaporate over a 48 hour period at ambient temperature to yield an iridescent NCC film.

### 6.2.2 Microscopy

The thickness of the film in its dry and wet state was measured via polarized optical microscopy (POM), and carried out with a Nikon Optiphot microscope connected to a SonyXCD-X710CR CCD camera equipped with Instrumentation & Industrial Digital Camera (IIDC) image capture software. The microscope was equipped with a 530 nm wave plate to enhance image edge contrast for film thickness measurement. An Hitachi 4700-S field emission gun scanning electron microscope (FEGSEM) was used to analyze the cross-sectional structure of the film. Films were sectioned perpendicular or fractured oblique to the film surface

### 6.2.3 Spectral monitoring under controlled humidity

Color changes in NCC films were captured by digital camera. An Ocean Optics-2000 fiber spectrometer was used to monitor the spectrum of white light reflected from the NCC film. Reflection peaks from sample films were collected via optical fiber positioned at the center of the reflection color peak position with a light incident angle of $25^{o}$ from

normal. In this work, RH was measured at 20$^{o}$C. Humidity effects on the color spectrum of the NCC film were detected by observing changes in spectral reflectivity for RH exposures of 70% or 95%. Two identical squares of NCC film with a surface area of 1 cm$^2$ were cut from the uniform center portion of cast NCC films. Films were attached to glass slides and the edges sealed to prevent penetration of water from the back side and edges. Water vapor was introduced via plastic tubing (cross-section area of 3 cm$^2$) connected to an ultrasonic humidifier. The relative humidity was measured with a calibrated traceable digital hygrometer having 0.1% resolution and ±2% accuracy ( Fisher Scientific).

## 6.3 Results

### 6.3.1 Structural characterization and dry state iridescence

NCC films cast using the method described in the experimental section show pronounced iridescence under unpolarized room light. The film in Figure 6-1A exhibits deformations in the surface due to internal stresses that accumulate as the film undergoes shrinkage and delamination from the petri dish during the drying process. These deformations produce different angles at which light is reflected from the surface so that various metallic hues are directly visible in the Figure. Scanning electron microscopy of vertical sections cut by knife through the films reveals the periodic layer structure (Figure 6-1B) that forms by self-assembly of the nanocrystallites. An interpretation of how this layer structure is constructed is given in Figure 6-7. Periodic striations have been widely observed in chiral nematic liquid crystals [14]. Extensive TEM and SEM studies reveal a good correlation between the half pitch of the CN mesophase and periodicity of the lamellar structure. The

periodic direction of the striations has been argued to arise by intercepting the helical twist structure whose axis runs parallel to the fracture surface. The striations therefore lie parallel to the layers of the ordered cellulose nanocrystals. Low magnification SEM

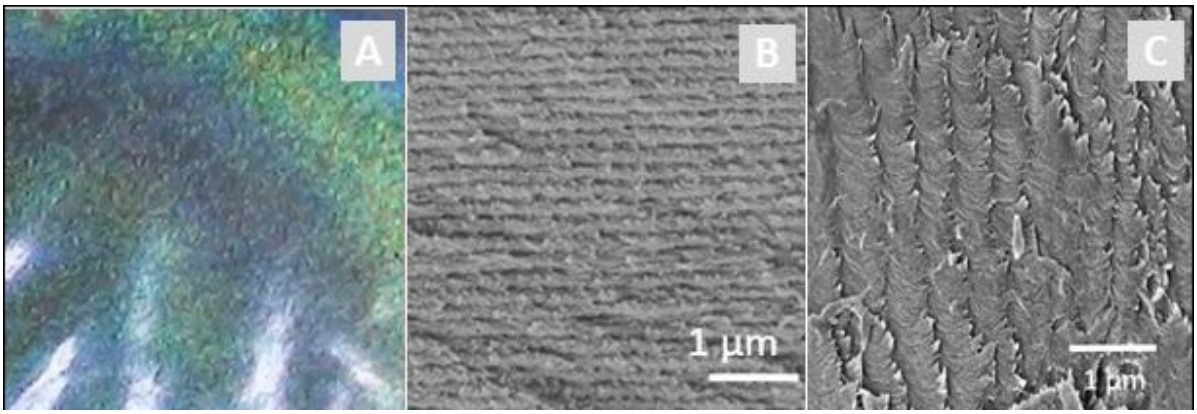


**Figure 6-1.** Image of the dry state iridescent NCC film (A) under white light illumination. SEM image of its cross-section multilayer structure (B). Oblique sectional view at high magnification showing periodic layering of left-handed chiral nematic texture (C).

analysis (not shown) indicates that the layers remain more or less parallel to each other over distances of tens of microns. We observe that the action of the knife blade is not always vertical to the periodic layer structure. Obliquely oriented layers can be discerned in some fracture sections (Figure 6-1C). The film comprises layered helicoid inclusions with boundaries

derived from sedimented precursor tactoids or multidomain features exhibiting chiral nematic order that have been frozen in at various tilt angles during film growth. This makes sense, since polarized light microscopy confirms that the film is anisotropic with respect to the helicoid director orientation. The edges of the sectioned layers in Figures 6-1B and 6-1C are very ragged. This arises likely because the knife is more apt to cut

between nanocrystallites running parallel to the knife edge than through them. The chiral nematic order in the NCC film is clearly evident in Figure 6-1C. We observe a curved texture with a director that rotates in a left-handed (counterclockwise) sense. This is the origin of the long range helicoidal order that gives rise to selective reflection. Thus the repeating bands in Figure 6-1B correspond to a 2π rotation of the director (half the helical pitch, P/2). When white light impinges on the film, multilayer reflective interference will occur, with strong selective reflection of the (left circularly polarized) light that matches the pitch of the layers. This produces the observed iridescence. Neglecting refraction, reflections are peaked at de Vries wavelength,

$$\lambda = nPcos\theta \qquad [6\text{-}1]$$

here, $n$ is the average refractive index of the NCC and θ is the angle between the surface normal and the incident ray. Clearly, a change in either $n$ or P at fixed θ can cause a change in reflected wavelength.

The description of iridescence from imperfectly textured, or multidomain, chiral nematic films are more complex because the helicoid axes are distributed with different orientations of the different domains. Nevertheless, it is clear that our films exhibit a predominantly blue iridescence. Making the reasonable assumption of an average refractive index of $n$ = 1.5, then the reflection wavelength can be determined by the thickness between two layers, ie, half of the chiral nematic pitch. Analysis of Figure 6-1B shows that the periodic planar structure of the NCC film has a layer thickness on the order of 160 ± 16 nm after correction for calibration of magnification of the microscope. The Bragg condition for this multilayer structure yields a bluish reflected color for normal incidence light.

### 6.3.2 Color change caused by moisture

From the previous section we know that the reflected color of the multilayer structure depends on the CN pitch and refractive index through equation [6-1]. Since NCC films are hydrophilic, absorption of water might cause swelling of the film which can manifest itself in changes in the CN pitch. It is this property that can be used to make a humidity color indicator. Figure 6-2 shows the color transition of the NCC film after immersion in water. Figure 6-2A is an image of the film in its dry state. It shows strong reflection in the blue at near normal viewing angles. Because the film is not flat, one observes a transition from a dark to pale blue in the image A running from the top right to the bottom left. Figure 6-2B on the right is a record image of the same film after having been immersed in water. The dry state color changes from blue to yellow en

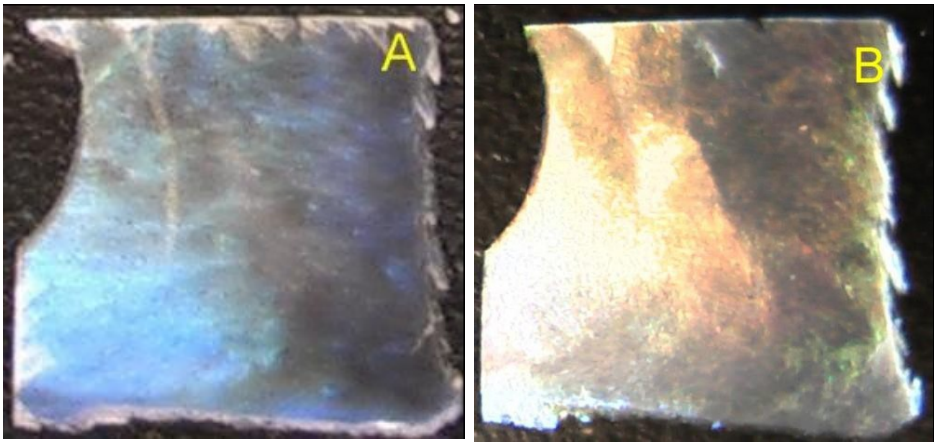


**Figure 6-2.** Color change observed when a dry NCC film (A) is immersed in water (B).

route to the final red-orange hue. The blue hue is recovered when the film is removed from the water and allowed to desorb water under ambient conditions for about 5 minutes. This process can be carried out repeatedly. NCC is expected to undergo swelling when

hydrated since the cellulose base material is hygroscopic. We observed by polarized optical microscopy that a film that is approximately 22 μm thick in its dry state expands to roughly 32 μm in the wet state. The accompanying shift in the reflectance is due primarily to expansion of the self-assembled nanocrystal matrix. Note that thinner films undergo the same color transition in less than 2 seconds. Figure 6-3 shows the reflected color spectra that accompany the dry/wet state changes for this film.

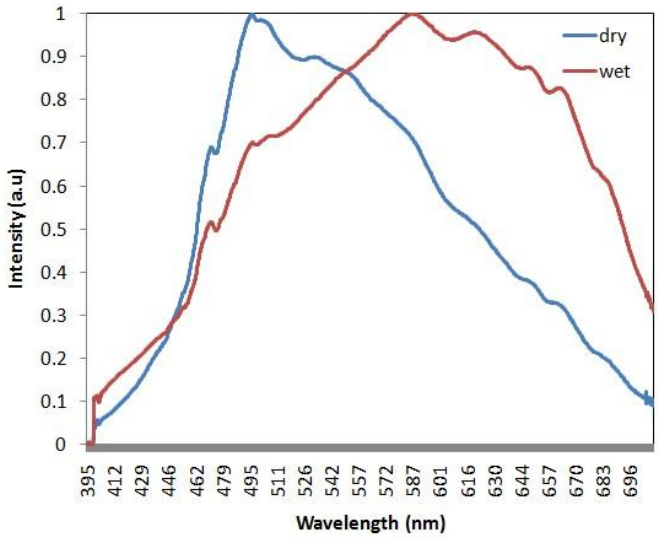


**Figure 6-3.** Reflected colour spectrum of the NCC film of Figure 6-2 under dry and wet state conditions.

### 6.3.3 Effect of humidity on white light spectral reflection

NCC films were exposed either to 70% or 95% RH cycling at constant temperature of 20 $^{o}$C. The spectral responses of the NCC films are collected in Figure 6-4 and Figure 6-5.

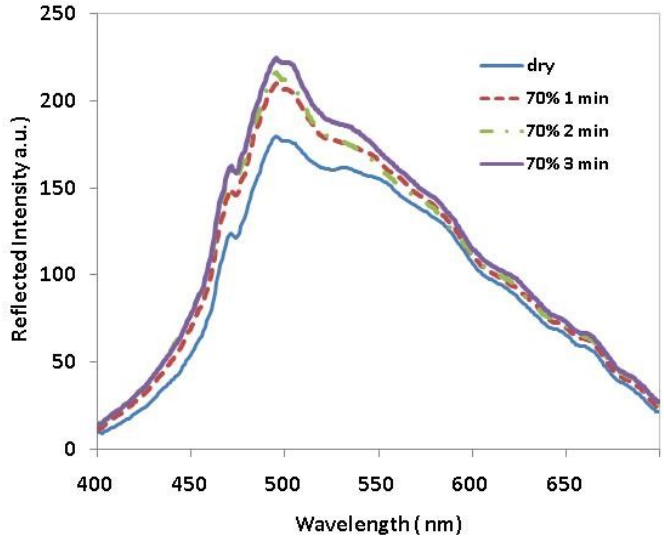


**Figure 6-4.** Time evolution of the reflection spectrum of an NCC film under 70% relative humidity.

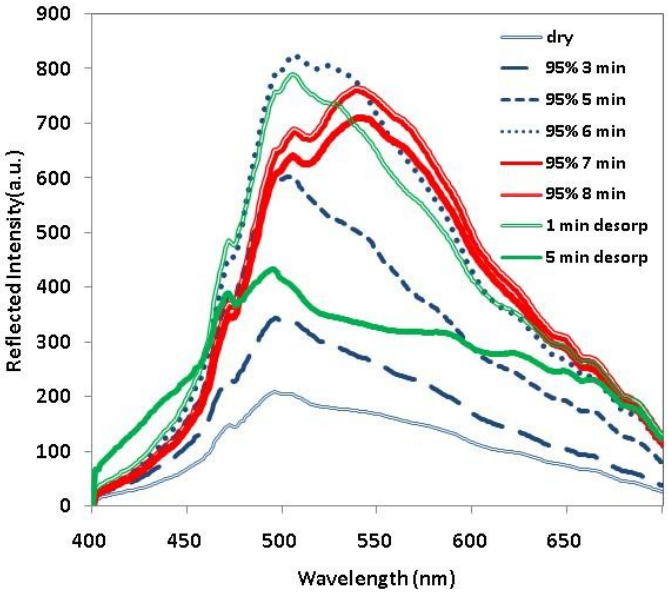


**Figure 6-5**. Time evolution of the reflection spectrum of an NCC film under 95% relative humidity.

For the first 3-6 minutes after exposure of films to either 70% or 95% RH, we

observed an increase in the reflectance from the film. Over the same time period, the reflectance peak maximum remained fixed. At 70% RH, the reflection intensity increased approximately 27% in 3 minutes, while for 95% RH, it increased 75% in the same period of time. The increase in reflectivity for both levels of RH at short times might be connected with adsorption and clustering of water at strongly binding hydroxyl

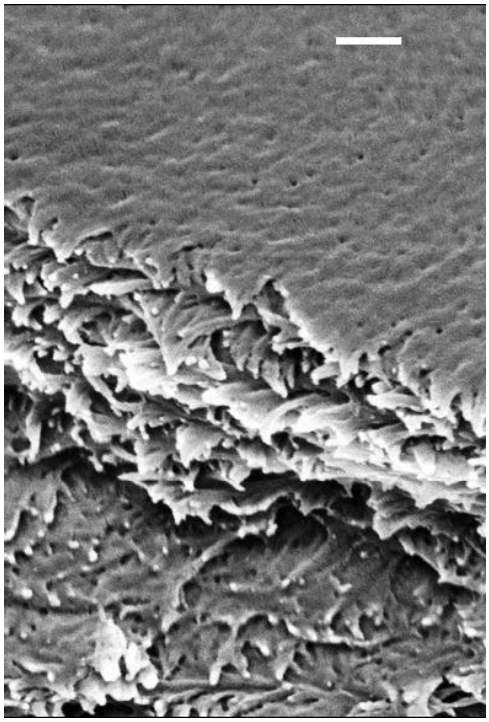

**Figure 6-6.** Scanning electron micrograph (FEG-SEM) of a film of self-organized NCC. The top surface of the film has terminated at a fractured edge where the underlying twisted helical organized layer structure is clearly visible. (Scale bar = 0.2 μm).

group sites on the cellulose nanocrystal film surface. At the early stage of exposure (< 5 min), there may be little diffusion into the film (see below) where strongly binding sites become occupied. Water clusters accumulating at the surface can act as specular reflectors whose response is added to the reflectivity of the surface. Smaller enhancements in the

reflection might be expected at the lower RH where it is possible that less of the available sites are occupied by water. The color change from blue to red-orange is much faster under the 95% RH condition, and for clarity we show only the early time data for the 70% RH case.

It is worth considering the two RH data sets in the context of phenomenological sorption models [15-17]. To our knowledge there has been only one study of water sorption behavior of cellulose nanocrystals [18]. This study was conducted on sample NCC films made from sisal fibers that had not been deposited to give multi-domain CN iridescent texture. The sisal NCC film surface shows a rod-like porous structure, similar to what is observed for paper sheet. By contrast, our films (Figure 6-6) are densely matted and populated with nanosized pores. Despite the morphological differences between sisal NCC films and our dense CN textured films, it is reasonable to assume with Dufresne et al. [18] that the water sorption and transport characteristics of our films are dominated by the surface, as was found in studies of the former. Sorption is a complex phenomenon that depends on the magnitude of the water activity coefficient (equilibrium RH), which in turn depends on surface and structural features of the film, including permeation, diffusion, water monolayer and multilayer formation, chemical bonding and capillary forces. These are not well understood for cellulosics. A two-state parallel exponential kinetic (PEK) model for cellulosics [17] suggests two different states of “bound” and “free” water, or more generally, slow and fast sorption sites or kinetic processes. At low water activity (low RH), it is argued [15,18] that Langmuir-type sorption takes place at specific immobilizing sites like hydroxyl and ionic centers, which eventually saturate. Langmuir sorption leads to a decrease in diffusion kinetics because of strong binding to

preferred sites like hydroxyl. At moderate water activity, Henry's Law-type random sorption occurs on the cellulose nanocrystals and voids with no specific interaction will lead to swelling and enhanced diffusion. Clustering of water molecules at relatively high activity (low cluster mobility) can again reduce diffusion in the films. Dufresne et al. [18] offer evidence that the surface of the sisal NCC actually acts as a diffusion barrier by structuring water directly on the external film surface. This might explain the induction period for the 70 and 95% RH exposures before a color change is observed in our films. In a two-state model, the faster response of the iridescent film to 95% RH might also be explained by the more rapid saturation of sites at the surface with a faster characteristic time, followed necessarily by an earlier conversion in time to second stage diffusion kinetics that involves slower sorption and swelling inside the sample. Figure 6-5 records the red-shift in the spectral reflectance at 95% RH in a three minute period on reaching peak reflectivity after 6 minutes. During the seventh minute, the reflection peak changed from a blue to yellow hue. The process is somewhat reversible in stages. After one minute at 22% RH the reflectance peak maximum blue shifts and then drops in intensity as the film recovers its blue iridescence, although after 5 minutes the reflectance is not equal to that of the starting dry state form.

The change in reflectance we observe is most likely due to changes in the multilayer period of the helicoid reflection grating that underlies the layered structure shown in Figures 6-1B and 6-6. The swelling of the film is due to sorption of water by the constituent cellulose nanocrystals. The latter are insoluble in water owing to the strong hydrogen bonding between the cellulose chains. Atomic force microscopy has shown that cellulose nanocrystals are resistant to water penetration [19], so the swelling must be due

to adsorption and clustering of water on the crystallite surfaces. Accumulation of water will cause a change in the layer spacing (pitch) and therefore a shift in the reflectance spectrum. Expansion of the pitch (due to swelling) will drive the peak reflectivity to the red, which is what we observe. The situation is reminiscent of dynamic photonic band gap tuning in chiral nematic liquid crystals [20], where dopant molecules or electric fields are used to adjust the pitch and therefore the optical response. An interpretation of the sorption/desorption tuning of the pitch and the accompanying color changes is given in Figure 6-7.

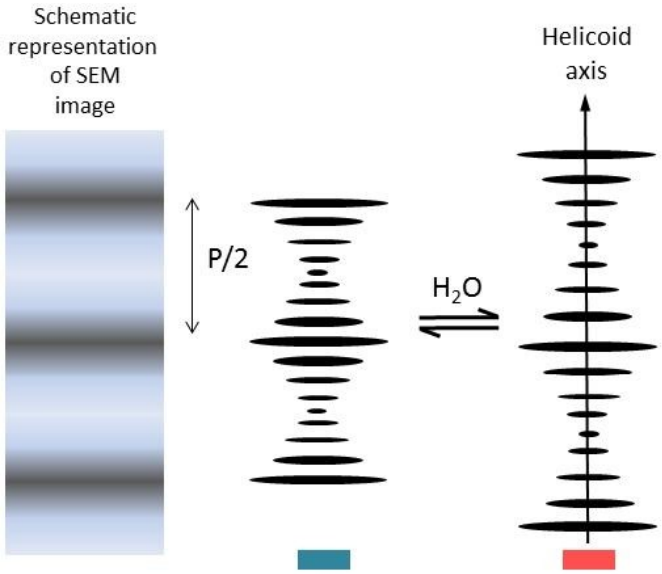


**Figure 6-7.** Proposed correspondence between NCC rigid rod assembly orientation in one domain of the chiral nematic phase solid film and the periodic structure observed in the SEM of Figure 6-1B. The pitch P increases and decreases reversibly on sorption and desorption of water, with a concomitant change in color.

Our evidence showed the differences from that exhibited by the longhorn beetle [9] where the reflectance changes are caused by infiltration of water that expands

proteinaceous nanoporous inhomogeneous layers periodically interspersed with dense homogeneous melanoprotein layers. Swelling of the beetle elytra scale structure changes the reflectance that is understood within a simple model of thin film multiply reflecting stacks.

## 6.4 Conclusions

A humidity color indicator has been prepared from self-assembled nanocrystalline cellulose. The reversible color transition is based on sorption-desorption tuning of the chiral nematic pitch which shifts the reflectance in a mechanism that resembles band tuning in classical chiral nematic liquid crystals. Films are observed to expand and contract during the sorption-desorption process. Thick films on the order of 20 μm or more show an induction period where the reflectance first increases in intensity prior to a sudden color change. The induction period may relate in complex ways to the manner in which water vapor is taken up in NCC films and a role has been assigned to dominant surface effects, although this needs to be confirmed. By reducing the thickness of the film, color transitions on the order of seconds are observed. The color system indicator is interesting in that it uses no pigments, and is constructed from self-assembling nanocrystallites derived solely from cellulose. Moreover, the unique optical property of NCC film reacting to water can be used as a simple way to authenticate the genuine of the NCC material for security application.

## 6.5 References

[1]. R. Esse, A. Saari, “An active moisture-management packaging system for food and other products: a case study,” in: J. Kerry, P. Butler (Eds.), Smart Packaging

Technologies for Fast Moving Consumer Goods, John Wiley & Sons, West-Sussex, , pp. 130–149 (2008)

[2]. N. Yamazoe, Y. Shimizu, "Humidity sensors: principles and applications," Sensors and Actuators, 10, 379–398 (1986)

[3]. S. Neethirajan, D. S . Jayas, S. Sadistap, "Carbon Dioxide (CO2) Sensors for the agri-food industry—a review," Food Bioprocess. Technol., 2, 115–121 (2009)

[4]. A.Tsigara, G. Mountrichas, K. Gatsouli, A. Nichelatti, S. Pispas, N. Madamopoulos, N.A. Vainos, H.L. Du, F. Roubani-Kalantzopoulou, "Hybrid polymer/cobalt chloride humidity sensors based on optical diffraction," Sensors and Actuators B, 120 ,481–486 (2007)

[5]. M. Benas, K. Fujisawa, R. R. Madsen, R. Mathur, T. Yeakley, "Cobalt dichloride free humidity indicator cards," Texas Instruments Application Report, SLVA410 1-8 (2010)

[6]. A. Mills, P. Grosshans, D. Hazafy, "A novel reversible relative-humidity indicator ink based on methylene blue and urea," Analyst, 135, 33–35 (2010)

[7]. J. Kunzelman, B. R. Crenshaw and C. Weder, "Self-assembly of chromogenic dyes—a new mechanism for humidity Sensors," J. Mater. Chem., 17, 2989–2991 (2007)

[8]. J. Shi, V. K. S. Hsiao, T. R. Walker, T. J. Huang, "Humidity sensing based on nanoporous polymeric photonic crystals," Sensors and Actuators B 129, 391–396 (2008)

[9]. F. Liu, B. Q. Dong, X. H. Liu, Y. M. Zheng, J. Zi, "Structural color change in longhorn beetles Tmesisternus isabellae," Opt. Express, 17, 16183–16191 (2009)

[10]. M. Hawkeye, M. Brett, "Optimized photonic crystal colorimetric humidity sensor fabricated using glancing angle deposition," Adv. Funct. Mater., 21,3652-3658 (2011)

[11]. A. Saha, Y. Tanaka, Y. Han, C. M.W. Bastiaansen, D. J. Broer, R. P. Sijbesma, "Irreversible visual sensing of humidity using a cholesteric liquid crystal," Chem. Commun., 48, 4579–4581 (2012)

[12]. J. F. Revol, L. Godbout, D. G, Gray, "Solid self-assembled films of cellulose with chiral nematic order and optically variable properties," J. Pulp Paper Sci, 24,146-149 (1998)

[13]. K. E. Shopsowitz, W.Y. Hamad, M. J. MacLachlan, "Flexible and iridescent chiral nematic mesoporous organosilica films," J. Amer. Chem. Soc., 134, 867−870 (2012)

[14]. V. Arrighi, J. M. G. Cowie, P. Vaqueiro, K.A. Prior, "Fine structure and optical properties of cholesteric films prepared from cellulose 4-methylphenyl urethane/N-vinyl pyrrolidinone solutions," Macromolecules**,** 35, 7354-7360 (2002)

[15]. F. Gouanvé, S. Marais, A. Bessadok, D. Langevin, M. Métayer, "Kinetics of water sorption in flax and PET fibers," Eur. Polym. J. 43,586–598 (2007)

[16]. R. Kohler, R. Dück, B. Ausperger, R. Alex, "A numeric model for the kinetics of water vapor sorption on cellulosic reinforcement fibers," Composite Interfaces, 10, 255–276 (2003)

[17]. R. Kohler, R. Alex, R. Brielmann, B. Ausperger, "A new kinetic model for the water sorption isotherms of cellulosic materials," Macromol. Symp., 244, 89–96 (2006)

[18]. S. Belbekhouche, J. Bras, G. Siqueira, C. Chappey, L. Lebrun, B. Khelifi, S. Marais, A. Dufresne, "Water sorption behavior and gas barrier properties of cellulose whiskers and microfibril films," Carb. Polym. 83, 1740-1748 (2011)

[19]. R. R. Lahiji, X. Xu, R. Reifenberger, A. Raman, A. Rudie, R. J. Moon, "Atomic force microscopy characterization of cellulose nanocryustals," Langmuir, 26, 4480-4488 (2010)

[20]. M. E. McConney, T. J. White, V. P. Tondiglia, L. V. Natarajan, D. Yang, T. J. Bunning, "Dynamic high contrast reflective coloration from responsive polymer/cholesteric liquid crystal architectures," Soft Matter, 8, 318 (2012)

# Chapter 7

# ASSESSMENT OF NCC FOR POSSIBLE SECURITY TAGGANT APPLICATION

## 7.1 Introduction

There are many anti-counterfeiting technologies available to manufacturers and brand owners, ranging from the very simple but effective, through to the highly sophisticated and extremely secure. Though many anti-counterfeiting technologies are available in the market, the increasing number counterfeit products, including food, medicine, military, and electronic parts indicates the limitations of present technology and the need for new security device development. The most successful security technology today includes optical security features that allow one to see and recognize by naked eye that it is a genuine product. Among them, holograms are the most widely accepted security feature, first demonstrated and successfully used by MasterCard®, and still widely used today. However holograms as an overt security technology have drawn much attention from counterfeiters, and they are being attacked more and more. Reports have shown that, even with holograms, some products have been counterfeited [1], therefore, it is necessary to add more covert security features along with the overt ones to fight counterfeiting.

As a rule of thumb, three important levels of security should be considered in new security device design [2]. The first-level features, recognizable by human senses – sight and touch - are the most important. A security device should be designed with a consistent set of security features with strong level-one features. Beyond this, level-two features can

be seen using simple equipment such as a UV lamp or a magnifying glass to view the micro text, level-three features requires specific, sophisticated equipment and special laboratory tools to analyze hidden tracers.

Present anti-counterfeiting technologies in the market so far can be broadly classified into four types: overt, or visible features, covert or hidden feature, forensic techniques and track and trace techniques. By carefully selecting these security features, a sophisticated device can be obtained.

A sophisticated anti-counterfeiting technology should be very complex to copy and easy to see, recognize and identify.

In this Chapter, we present the unique optical security features of the NCC taggant for the first time, and assess the possible security application by comparing its security features and the authentication method with other popular optical security techniques on the market. The comparison includes a discussion of the security features and the simplicity of authentication methods, the ease of duplication, and applies five-criteria to assess the quality of the proposed anti-counterfeiting technique. We claim that NCC taggants have significant advantages over conventional techniques due to the fact that this system supports multiple security features and provides simple solutions to authentication.

## 7.2 Experimental

### 7.2.1 Material

The NCC film was made using a procedure as describe previously in Chapter 5, while the

method for developing the security taggant is described in following sections.

### 7.2.2 Taggant preparation

The taggants were made using a Cricut Expression tool equipped with Easycut software. The NCC film was first attached to double-sided tape and then the desired taggant shape was designed using Easycut software and the pattern was cut using this special tool. The cut security taggants can be easily attached to any product that needs protection. In this thesis, a triangular pattern was selected as a taggant example.

## 7.3 Assessment of NCC for Possible Security Taggant Application

### 7.3.1 Unique security features of proposed NCC taggant

#### *7.3.1.1 Overt security—Iridescence and Authentication*

Iridescence of NCC has been studied in Chapter 3 and 4; here the possibility of this property as a security feature is assessed. The iridescence of NCC is a structural color, with no dye involved, and reflection spectrum depends on the chiral nematic pitch of the chiral structure formed by self-assembly. The color originates both from the Bragg reflection—caused by the multilayer structure within self-assembled NCC—and from the diffraction of surface relief gratings of NCC (see Chapter 4 for details). In fact, both structures are related to the chiral nematic pitch, which can be controlled by optimizing the processing conditions, such as wood species, hydrolysis time, temperature, sonication power, and film casting environmental conditions, as described previously in Chapter 4.

Figure 7-1 shows the iridescence of NCC. When the viewing angle changed the reflected color changed as well.

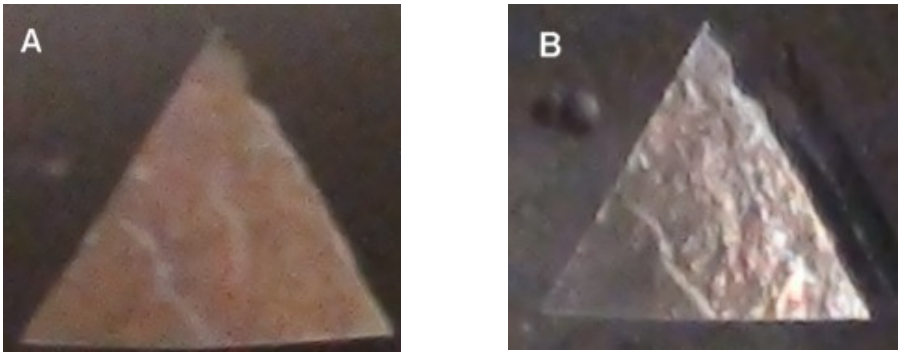


**Figure 7-1**. Iridescent NCC taggants (A: reddish color in normal viewing position, B: bluish color is shown when viewing angle is at 15° from normal).

Conventionally, security taggants are usually designed with a hidden format that is not visible to the eye to prevent any reverse engineering of the taggants, whose existence must be verified under a microscope with high magnification or special tools [3-4]. The taggant security feature can be implemented either by chemical tagging, DNA tagging, magnetic tagging with a trace amount of material or by using a radio frequency identification (RFID) microchip. We propose a new concept to eliminate the size constraint related to traditional taggant design: the proposed taggant size is about a millimeter, taking advantage of the iridescence as an overt security feature while retaining all other covert security features: selective reflection, unique morphology, and the white light diffraction pattern. To observe the taggant's iridescence by eye, a minimum size is required; below this size, the iridescence will be hard to recognize. The smallest size that can be seen by the naked eye depends on the individual, but the average size at which one

can see the shape and color is about a millimeter. This size allows the taggant to have strong iridescence, distinguishable from other polymer films.

Furthermore, our preliminary results show that iridescent color has a strong relation with the chirality of NCC which will be discussed in the next section. The chirality test can be combined with iridescence together to authenticate the genuineness of NCC taggants.

#### *7.3.1.2 Covert Security: Selective Reflection and Authentication*

Selective reflection refers to the fact that the NCC taggant has a stronger reflection for left-handed circularly polarized light than for right–handed circularly polarized light; the reflectance difference of NCC for two orthogonally circularly polarized incident beams will produce a light intensity contrast that can be used as a technique to assess the genuineness of the material. The reflection intensity contrast of the two orthogonally polarized beams incident on the taggants' surface can be represented by the chirality of the NCC. Chirality of the NCC taggants can be defined as follows,

$$C = \frac{(I_{lcp} - I_{rcp})}{(I_{lcp} + I_{rcp})} \qquad (7\text{-}1)$$

where, $I_{lcp}$ and $I_{rcp}$ represent the reflected light intensity of left-handed and right-handed circularly polarized light respectively.

It can be seen from Equation (7-1) that the chirality of the NCC taggant is a measureable parameter; by measuring the reflection intensity difference of the circularly

polarized light on the material, one can verify the genuineness of the taggant. This gives several advantages in distinguishing NCC taggants from other materials.

The first advantage of the chirality test is that a simple and low-cost circular polarization analyzer can be used to authenticate the genuineness of NCC. Figure 7-2 shows NCC taggant images viewed through low-cost circular polarizers. The big difference in the reflection intensity of NCC taggant over left-handed circularly polarized light and right-handed circularly polarized light under normal position characterize the unique feature of this material.

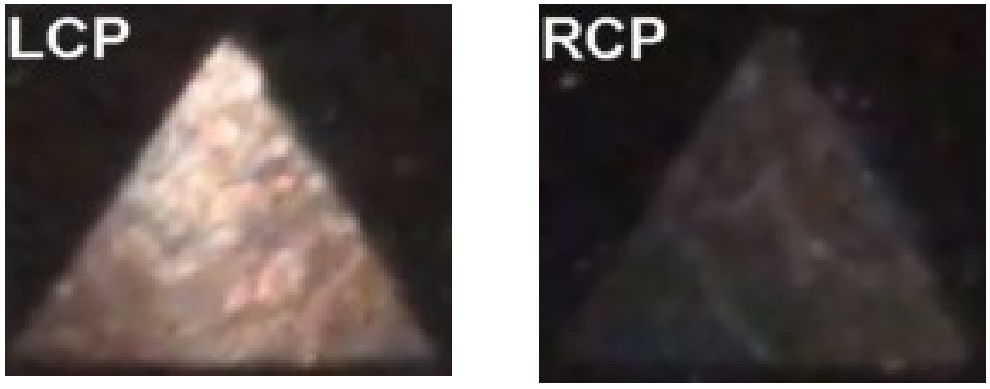


**Figure 7-2**. NCC taggants seen through left-handed circular polarizer (LCP) and right-handed circular polarizer (RCP).

The second advantages of the chirality test is that the set up using the reflective mode over the transmission mode discussed later (see Figure 7-6). The reflective mode allows one to authenticate the genuineness of the NCC taggants without need to remove the NCC taggant from the protected product's surface.

The third advantage is that this feature can be used to distinguish NCC from other polymer materials, including polymer films based on the difference of optical birefringence between the two materials: NCC has circular birefringence (chirality) while polymer film usually displays linear birefringence, and this distinction can be performed in transmission mode. The set up using a cross-linear polarizer to distinguish conventional polymer film from NCC taggant is shown in Figure 7-3.

When no sample or an isotropic sample is put on the sample holder, no light passes through as the light is blocked by the crossed polarizers. When a polymer film or NCC film is put on the sample holder and rotated, some light will pass through the second linear polarizer due to the material's birefringence, but the angular dependence will be different. Other materials that may give similar optical response to NCC will be discussed in section 7.3.2.

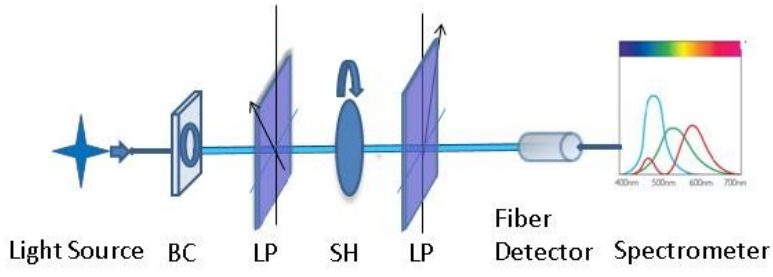


**Figure 7-3**. Schematic of NCC authentication setup. LP: linear polarizer; SH: sample holder; BC: beam size controller. Light source is 438 nm monochromatic light, fiber detector refers to multimode fiber with 200 um core diameter guided detector, and spectrometer refers to the Ocean Optic 2000 spectrometer.

The main characteristic of polymer film is that the birefringence has angular dependence, and the transmitted light intensity displays significant variation when the film is rotated (see Figure 7-4); In contrast, for NCC, the transmitted light intensity change is relatively small (see Figure 7-5).

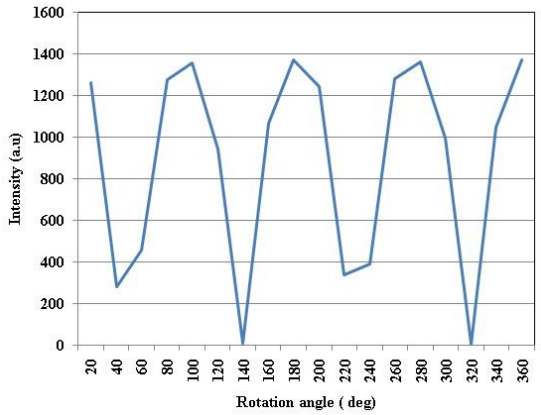


**Figure 7-4**. Transmitted light intensity from polymer film sandwiched between crossed polarizers as a function of polymer film rotation angle.

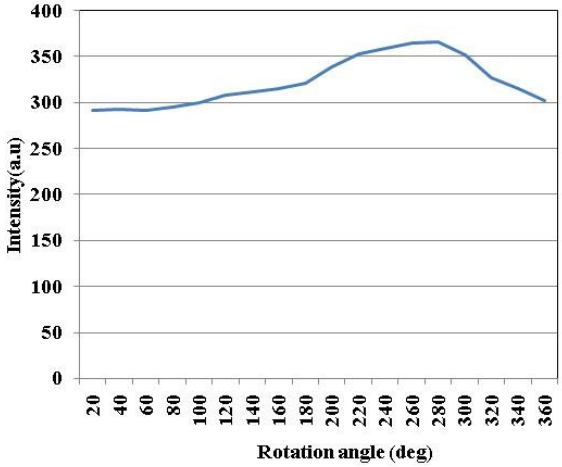


**Figure 7-5**. Transmitted light intensity from NCC taggant sandwiched between crossed polarizers as a function of NCC rotation angle.

The explanation lies in the fact that a polymer film can be thought of as a phase retarder; when sandwiched between the two crossed polarizers (previously set to null), the retarder will change the polarization state of the light passing from the first linear polarizer. The changed polarization is due to the birefringence, which is induced by stress formed during the pulling process of the film when it was manufactured. As a result, some light will be able to pass through the second polarizer and allow the image to be seen through the second linear polarizer. The Jones matrix operation can be used to calculate the intensity that passed through the polymer film and the second linear polarizer (analyzer).

For light going through the first linear polarizer (horizontal linear polarizer), the electric field vector can be written as ***E,***

$$\boldsymbol{E}=\begin{bmatrix}1\\0\end{bmatrix} \qquad (7\text{-}2)$$

For a linear phase retarder with retardation δ measured in radians and with fast axis at angle θ measured in degrees to the horizontal, the Jones matrix is

$$\begin{bmatrix} C^2{}_1 + S^2{}_1 e^{-i\delta} & C_1 S_1 (1 - e^{-i\delta}) \\ C_1 S_1 (1 - e^{-i\delta}) & C^2{}_1 e^{-i\delta} + S^2{}_1 \end{bmatrix} \qquad (7\text{-}3)$$

where $C_1 = \cos\theta \quad S_1 = \sin\theta$

And the analyzer Jones matrix is,

$$\begin{bmatrix}0 & 0\\0 & 1\end{bmatrix} \qquad (7\text{-}4)$$

therefore the output light amplitude of the image passing through the system will be

$$\boldsymbol{E}\mathrm{o}=\begin{bmatrix}0 & 0\\ 0 & 1\end{bmatrix}\begin{bmatrix}\mathrm{C^2}_1+\mathrm{S^2}_1\mathrm{e}^{-\mathrm{i}\delta} & \mathrm{C_1S_1}(1-\mathrm{e}^{-\mathrm{i}\delta})\\ \mathrm{C_1S_1}(1-\mathrm{e}^{-\mathrm{i}\delta}) & \mathrm{C^2}_1\mathrm{e}^{-\mathrm{i}\delta}+\mathrm{S^2}_1\end{bmatrix}\begin{bmatrix}1\\0\end{bmatrix} \qquad (7\text{-}5)$$

$$\boldsymbol{E}\mathrm{o}=\begin{bmatrix}0\\ \mathrm{C_1S_1}(1-\mathrm{e}^{-\mathrm{i}\delta})\end{bmatrix} \qquad (7\text{-}6)$$

The output light intensity will be the Jones matrix of Eo premultiplying the transpose of its complex conjugate which is $[0\ \mathrm{C_1S_1}(1-\mathrm{e}^{\mathrm{i}\delta})]$

therefore the output intensity will be,

$$\mathrm{I_{out}}=S^2{}_1C^2{}_1\left(1-e^{-i\delta}\right)(1-e^{i\delta}) \qquad (7\text{-}7)$$

replacing $C_1 = cos\theta \quad S_1 = sin\theta$ into Equation (7-7)

$$\mathrm{I}_{\mathrm{out}}=\frac{1}{2}sin\,2\theta\,(1-cos\,\delta) \qquad (7\text{-}8)$$

As δ depends on the birefringence of the material, and for a fixed material it is a constant value, therefore the output light intensity is modulated by the rotation angle, it is not difficult to see that there will be four maxima and four minima which is consistent with the experimental result, shown in Figure 7-4.

When a NCC taggant is used as a filter, the film can be thought as a right-handed circular polarizer as the transmitted light takes the right-handed circular polarization state [5].

The electric field vector of transmitted light will be

$$\boldsymbol{E}\mathrm{o}=\begin{bmatrix}0 & 0\\ 0 & 1\end{bmatrix}\begin{bmatrix}1 & i\\ -i & 1\end{bmatrix}\begin{bmatrix}1\\ 0\end{bmatrix} \qquad (7\text{-}9)$$

$$\mathrm{I}_{\mathrm{out}}=1 \qquad (7\text{-}10)$$

Ideally the transmited output light intensity will not change as a function of angle; however, as the limitation of the uniformity of the NCC material, therefore, some intensity variation may be observed when light spot size is large (see Figure 7-5).

Preliminary studies also indicate a strong correlation between the iridescent colour of the NCC and the degree of chirality. This provides a further level of confidence as to the genuiness of the tag in the event that counterfeiters attempt to use other iridescent materials which do not possess chirality, such as holograms, or other chiral material with different chirality, such as chiral polymer film to duplicate the appearance of the proposed NCC taggant., A simple chirality test setup (see Figure 7-6) can be used to authenticate quantitatively the genuine nature of the taggant.

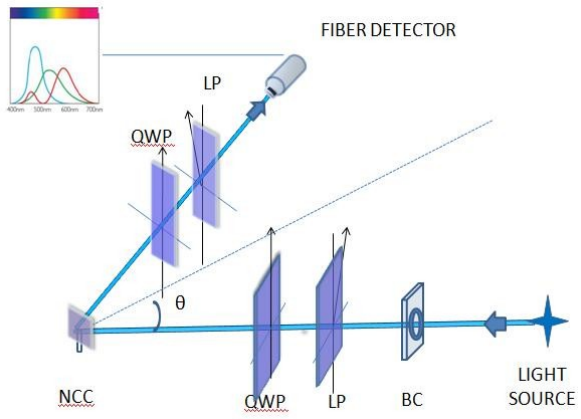


**Figure 7-6**. Schematic of the setup for chirality testing in reflection mode (BC: beam controller, LP: linear polarizer, QWP: Quarter-Wave Plate, linear arrow is faster optical axis of the wave plate).

Circular polarized light is obtained by passing a 480 nm monochromatic light first through the beam controller (0.75 $cm^2$) then the linear polarizer (LP) with axis at 45° , and then the Quarter-Wave Plate(QWP). When QWP fast axis is vertical (Figure 7-6), this results in a left-handed circular polarization state; by rotating the QWP 90 degrees clockwise, the transmitted light will change to right-handed circular polarized light. output polarizers can select either left-hand circular polarization(LHCP) or righ-hand circular polarization(RHCP), depending on the orientation of the QWP and polarizer, and that by measuring the relative intensity of LHCP and RHCP one can calculate the chirality

We list the chirality test results of three different taggants using our reflection-mode setup, as follows. The iridescent NCC taggants and their chiralities are shown in Figure 7-7 and Table 7-1.

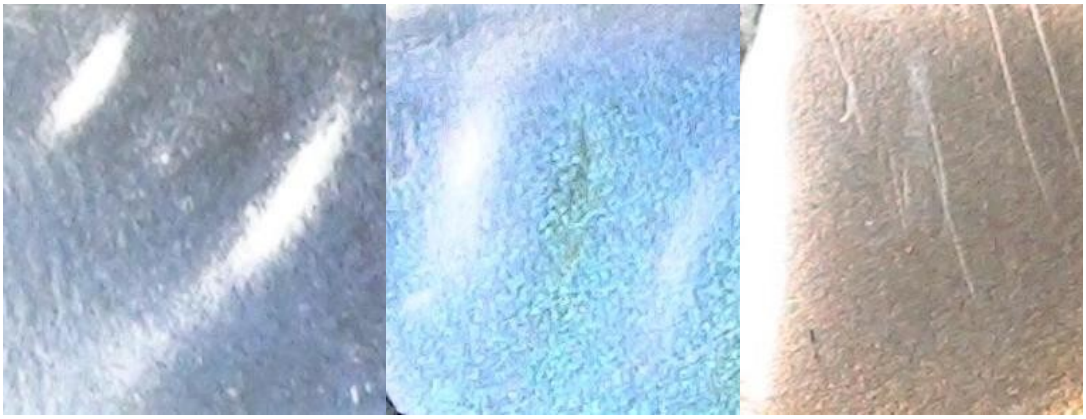

**Figure 7-7**. Iridescence displayed by different NCC films.

**Table 7-1. Chirality of NCC films from Figure 7-7**

| Film | Blue NCC | Blue-yellowish NCC | Reddish NCC |
|---|---|---|---|
| Chirality | 0.05±0.008 | 0.03±0.01 | 0.02±0.01 |

These preliminary results show that NCC taggants with a reddish reflection exhibit a smaller chirality as defined previously, while taggants with a bluish reflection have larger chirality. The combination of chirality and iridescence provides a fingerprint that allows the origin of NCC to be assured.

### *7.3.1.3 Covert Security–UV Fluorescence and Authentication*

UV fluorescence is another covert security feature. The iridescent NCC taggant will fluoresce blue under UV illumination. UV fluorescence is one of the widely used and significant security features on the market. It has been implemented in the protection of

banknotes or many other products. The security is accomplished by embedding trace amounts of fluorescent dye within the products, authenticated by evaluating its UV fluorescence spectrum.

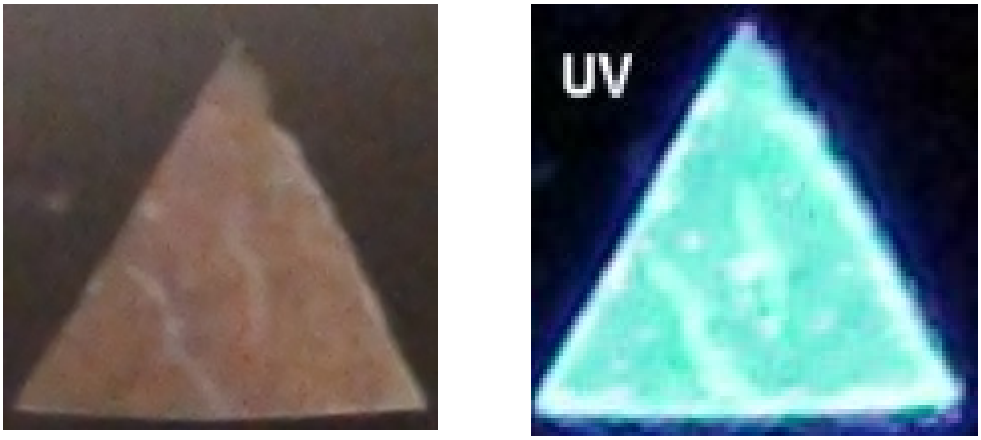


**Figure 7-8**. Iridescent NCC taggants under room light ( Left) and UV ( Right) illumination.

OBA is an ultraviolet fluorescent dye conventionally used in the pulp and paper industry to increase the whiteness of the paper products. Due to the high affinity of NCC for OBA, trace amounts of OBA can yield strong UV fluorescence. Since OBA has a unique UV fluorescence spectrum (as previously described in Chapter 5), it can be used as a taggant to trace the material being doped. In this sense, OBA can be used to trace NCC. When UV fluorescence is considered together with other security features of NCC taggants, such as selective reflection, iridescence, and unique white-light diffraction, taggants made from NCC are more secure than conventional security techniques, such as holograms, which have limited security features.

Furthermore, preliminary results indicate that the UV fluorescence from OBA-doped NCC is circularly polarized. The polarization state of the UV induced fluorescence was measured with a circular polarization analyzer which is composed of a quarter-wave plate and a linear polarizer. Figure 7-9 shows a scheme of the polarization state variation setup of OBA-doped NCC

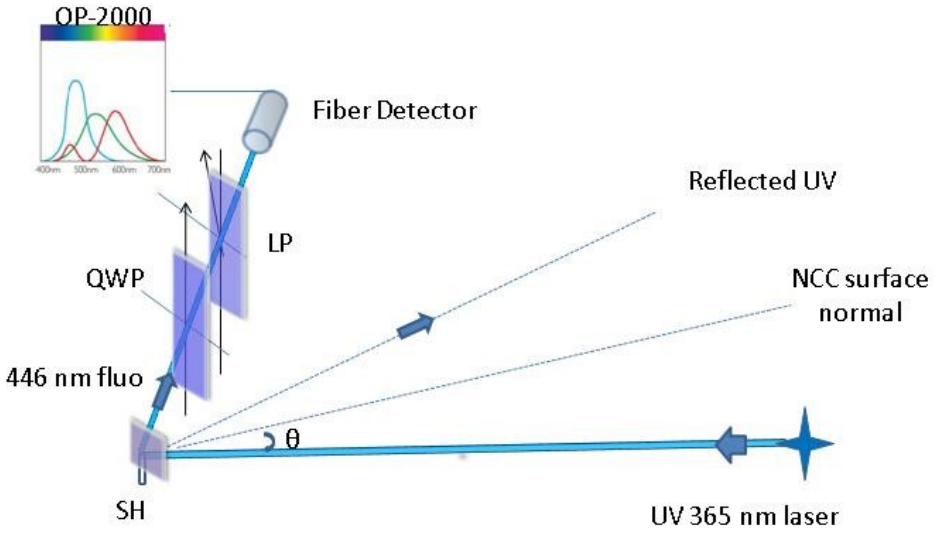


**Figure 7-9**.UV fluorescence polarization state examination setup ( SH refers to sample holder, QWP is quarter-wave plate, LP is linear polarizer, OP-2000 is Ocean Optics 2000 spectrometer).

When OBA-doped NCC taggants were illuminated by a 365 nm UV laser at a 22.5 degree incident angle, most of the UV light was reflected at 45 degrees to the laser incident direction, and a strong blue-colored fluorescence with a maximum at 446 nm was observed at 80 degrees to the laser incident direction. The fluorescence polarization state over the 360-degree range was examined by rotating the QWP from 0 degree to 360

degrees while keeping the LP position fixed. The fluorescence emission was collected by a multi-mode fiber guided detector and recorded using an Ocean Optics 2000 spectrometer.

It is well known that the fluorescence of material is usually not polarized if the molecules are randomly oriented, and this can be confirmed by a pure OBA film fluorescent polarization state examination using the above setup. Because the UV fluorescence from pure OBA is not polarized, when a quarter-wave plate was rotated from 0 to 360 degrees, no significant change in the fluorescent intensity can be seen, and our results showed it is the case (see Figure 7-10).

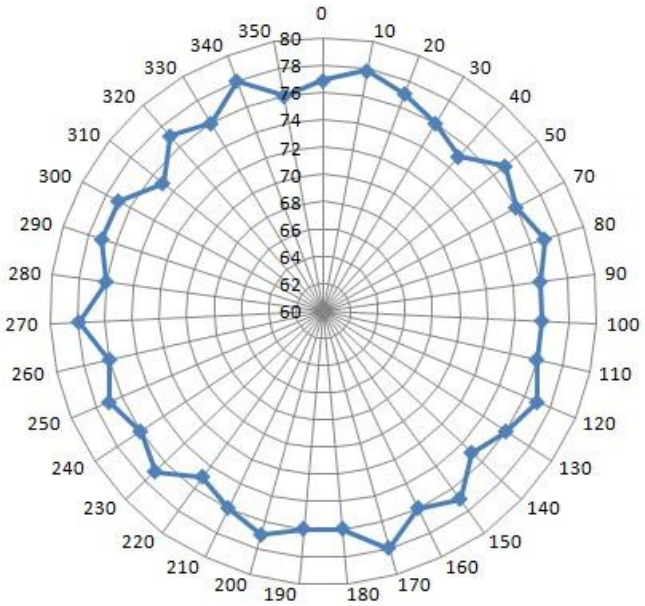


**Figure 7-10**. Radar graph of pure OBA 446 nm UV fluorescent emission polarization state distribution over 360 degrees.

In contrast, when OBA was added to NCC, UV fluorescence becomes partially circularly polarized. We propose that the circular polarization arises from the strong interaction between the OBA molecule and the chiral nematic NCCs. The reason is the strong affinity of OBA for NCC; OBA tends to align parallel along the molecule axis of NCC [6]. As NCC forms a chiral nematic structure, the aligned OBA will have a strong tendency to form circularly polarized fluorescence. The polarization state distribution is shown in Figure 7-11. This circular polarization property could be used as a security technique to authenticate OBA-doped NCC.

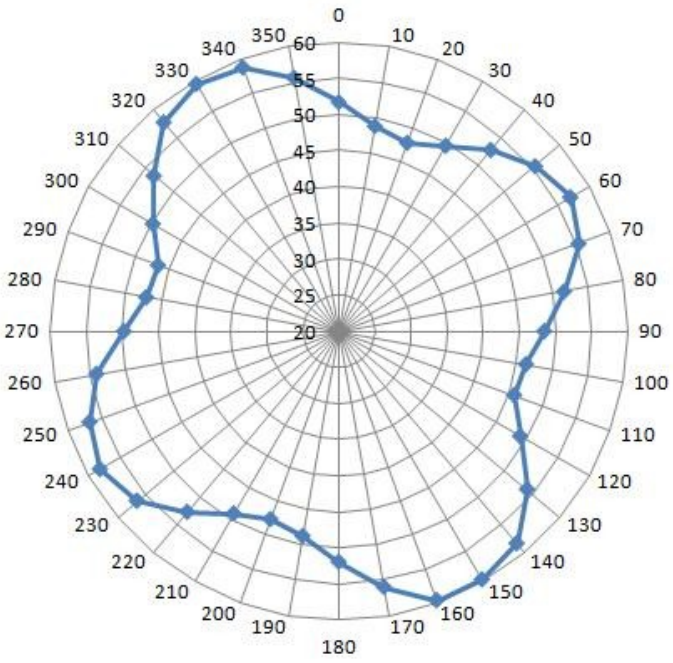


**Figure 7-11**. Circular polarization state of OBA-doped NCC over 360 degree range. Note that right-handed circularly polarized light (at 50 deg) and the left-handed circularly polarized light state( at 140 deg) has significant fluorescence intensity difference at 446 nm.

#### *7.3.1.4 Covert Security–Morphology, White Light Diffraction Pattern and water induced color change*

The unique morphology of the NCC taggant can also be used as a covert security measure, and authenticated using a microscope or a low-cost magnifier with a magnification higher than 100X. A picture of the surface structure of the NCC film is shown in Figure 7-12.

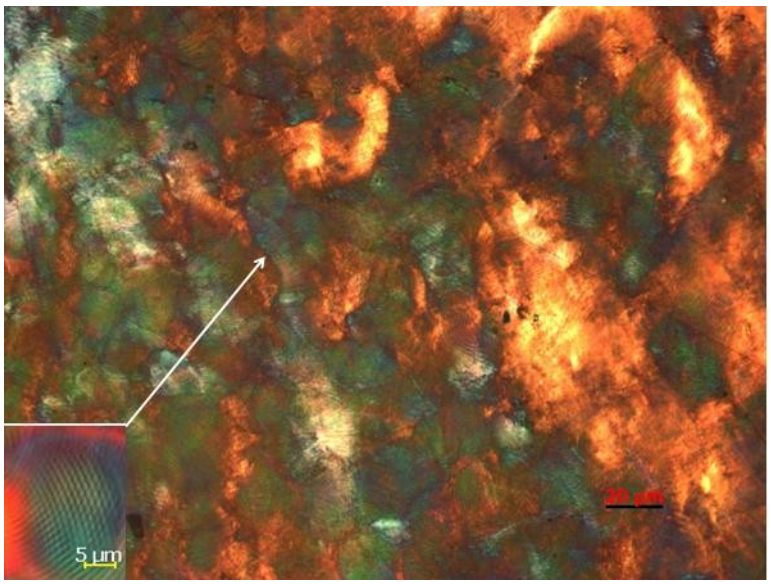


**Figure 7-12**. Morphology of NCC film. Inset is a magnified typical cross-overlayed structure.

Figure 7-12 shows that a cross-overlaid structure is formed during the casting process when the water of the NCC suspension is evaporated. These structures originate from the tactoid structure formed by the self-assembly of the NCC molecules. About 20 min after the 4 % NCC suspension was placed into a Petri dish with a diameter of 3 cm and under ambient humidity and room temperature (23 ºC). These cross-overlaid structures formed by the emergence of tactoids and the overlaying of tactoids by each other. When the water

evaporated, these structures remained. These structures can be used as security feature to characterize the NCC taggant, and can be authenticated using polarized light microscope equipped with a 530 nm retarder plate.

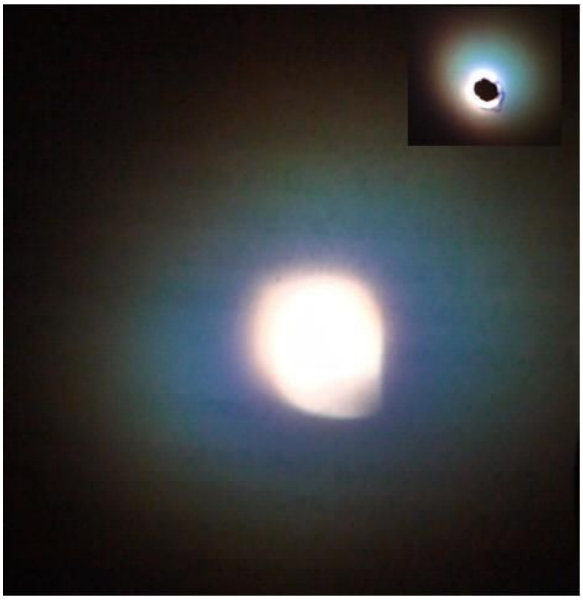

**Figure 7-13**. White light diffraction pattern of NCC taggant projected 15 degrees from the normal of the NCC surface ( inset is the diffraction pattern under normal illumination projected on white screen and the dark spot in the center of the image is a small hole cut on the screen to let the light pass).

When this taggant was illuminated with white light and projected onto a white screen, a unique white diffraction pattern can be seen. Figure 7-13 shows a typical white light diffraction pattern example. Figure 7-13 shows that the projected white-light diffraction pattern of NCC for light normally incident on the NCC surface is very similar to the diffraction pattern obtained for light that is incident at 15 degrees to the NCC surface

normal. Therefore, one can use off-axis illumination in order to authenticate the genuineness of the taggant by observing that the diffraction pattern is present.

Moreover, in Chapter 3, we showed that by controlling the casting environment, one can obtain a line type white-light diffraction pattern which is different from this circular diffraction pattern showed in previous paragraph. This means different NCC taggants can be made using different casting processes. These various white light diffraction patterns certainly can be used as a security feature. Future work will be focused on how to produce unique code from these white light diffraction pattern images and make a database for security authentication on a base of track and trace technology. The genuineness of the taggant will be confirmed by comparing the diffraction image on-site with the image saved in the database.

Finally, in Chapter 6, a humidity color indicator has been demonstrated. Upon contact with water, the NCC film was shown to change color from blue to reddish. A reversible process, color change from reddish to blue, occurs when the water was evaporated, and this reversible process can happen many times as long as the film is not damaged. As water is easy to access, therefore, one can use water as simple method to authenticate the genuineness of the NCC taggant. Though many other materials also possess color change on wetting with water, they do not have the other security features, such as selective reflection and polarized fluorescence, therefore, water can be used as an additional tool together with other security authentication tools to authenticate the genuineness of NCC taggant.

In summary, these unique optical properties of NCC taggants, such as iridescence, selective–reflection, polarized fluorescence, unique morphology, white light diffraction, and water induced color variation, provide strong security base for this material. Furthermore, all these security features can be authenticated using simple tools. Taking all these features together, the proposed NCC taggant could be considered to be a sophisticated security technique. The NCC provides a material that possesses unique measureable features and which are hard to copy. Its security can be then further enhanced by applying additional security techniques such as 2D barcode, RFID.

### 7.3.2 Possible strategies to duplicate NCC optical response

For an anti-counterfeiting technique, security is the key to success. To increase the security of the technique, a strategy has been proposed in this work. The strategy includes three key points: first, increase the numbers of the covert security features; second, to increase its visibility by extending the taggant design concept and making the taggant visible in contrast to conventional taggants which are not visible to the naked eye, and finally to design more covert security feature which can be authenticated by ordinary consumers.

At present, many security techniques exist on the market, including holograms, taggant, security ink, and biometric techniques, have one or two security features, some may have security feature that is similar to one of the features of the NCC taggant, and thus possess

a possibility of duplicating of NCC taggant. A comparison of security features between NCC taggant and the popular security techniques is provided in Table 7-2.

**Table 7-2.Authentication techniques for various materials for security applications**

| Security feature / Material | Iridescence | | Selective-reflection | | Polarized-Fluorescence | | Unique morphology | | White-light diffraction | | Water–induced color change | |
|---|---|---|---|---|---|---|---|---|---|---|---|---|
| NCC taggant | √ | Naked-eye | √ | Low-cost analyzer | √ | Simple UV source or UV+ analyzer | √ | Low-cost magnifier or Image readout | √ | White –laser pen | √ | Naked-eye |
| CLC Security ink | √ | Naked-eye | √ | Low-cost analyzer | | | | | | | | |
| Hologram | √ | Naked-eye | | | | | √ | Image readout | | | | |
| Security Taggant | | | | | † | Scanner | | | | | | |
| Polarized hidden image | | | √ | Low-cost analyzer | | | √ | Image readout | | | | |
| Cotton fiber | | | | | | | √ | Image readout | | | | |
| biometric | | | | | | | √ | Image database | | | | |
| Fluorescent fiber | | | | | † | Simple UV source | | | | | | |

Note: √ refers to possession of the security feature. † refers to partial possession of the security feature. Scanner refers to optical spectrometer

From Table 7-2, one should note that the entire approaches list here are based on the material structures and properties rather than device level approaches, such as barcode, track-trace technology, and RFID which involve complex database systems. The material structures and properties approaches are chosen because they have several advantages: firstly they have high visibility by nature. Like most popular holograms, they can be easily seen by naked eye. Studies have shown that, among all of the information that one

obtains, 80% is visually acquired [7]; secondly, optical features can be distinguished by consumer even by naked eye.

Moreover, from Table 7-2, one can see that NCC taggant has more security features than other approaches, but there is still a risk of being attacked. The possible strategies to duplicate NCC optical response will be discussed.

From the literature review, we know that among the conventional security techniques list in Table 7-2, a security ink highlighted with a brown background color posses a high potential to mimic some of the security features of the NCC taggant, such as iridescence and selective reflection. This is because the security ink technique uses a similar material: chiral liquid crystal. One typical example is the novel pigment developed by Chelix Technologies using Cholesteric Liquid Crystal (CLC) polymers.

Jiang et al. [8] of Chelix Technologies disclosed the security features of their pigment made from CLC film flakes. These CLC flakes possess iridescence and circular polarized reflectance similar to the NCC taggant. The liquid crystal polymer molecule is also chiral and could form a planar structure inside the CLC film during polymerization. However, a key difference between the CLC film formation process and the NCC process is that the CLC film is developed by doping CLC molecules with nematic LC followed by a polymerization process; in contrast, the NCC taggant is made from pure chiral nematic NCC by casting whch is relatively simple. Since the polymer CLC film mentioned above has a chiral liquid crystal material component, they may have a similar optical response to incident polarized light as would the NCC taggant, and pass the chirality test discussed in

section 7.3.1.2; however, polymer CLC film has not been shown to possess other security features, such as polarized fluorescence, unique morphology, white light diffraction pattern, and the water induced color change. According to Tsai et al. [9], polymer CLC film was made based on a highly ordered planar structure that hinders the formation of tactoids, and as a result it is very unlikely that polymer CLC film has unique white light diffraction pattern. Moreover, after the polymerization process at a high temperature, polymer CLC films consist of a glassy matrix, which prevents their pitch from changing in response to the changes in relative humidity like the NCC does. Therefore it is unlikely polymer CLC films will display a water-induced color change.

The possibility of using other materials to duplicate the optical response of NCC taggant should also be considered. A hologram is the most popular security technique in the market, and can display a similar iridescence as a NCC taggant, however, since holograms do not incorporate chiral material, they would not have the same polarization response as the NCC. Fluorescent fiber, though it exhibits fluorescence as the NCC taggant does, only has one limited security feature.

Other optical security techniques, like conventional security taggant, polarized hidden image, cotton fiber, or biometric techniques listed in Table 7-2, are covert security techniques; therefore it is difficult for a counterfeiter to duplicate NCC taggants using these techniques before they can duplicate the overt iridescence of NCC.

In short, although with the CLC security ink approach, one may partially mimic the security feature of NCC taggant in terms of iridescence and selective reflection, to

replicate other security features such as polarized fluorescence, unique morphology, white light diffraction pattern, and water-induced color change, the counterfeiter must make a large investment and needs to acquire the knowhow to construct the unique structure of NCC. One may mimic the NCC taggant in part, but as a whole assembly, however, NCC taggant cannot be duplicated presently to the best of our knowledge.

### 7.3.3 Assessment of conventional optical security techniques and proposed NCC taggants by five criteria

In a study of the effectiveness of anti-counterfeiting techniques, Anjan Das proposed five criteria [10] for assessing anti-counterfeiting techniques: consumer empowerment, cost and value, forensics and interdiction, simplicity and adaptability, and value-added features.

Consumer empowerment refers to security techniques designed so that they can be authenticated by the consumer at the point of sale on the retail level. The reason for this requirement is that, first, the consumer is at the end of the product consumption chain, and safety and purchase value are the customer's primary concerns. Therefore, if the consumer cannot authenticate the genuineness of the product at the selling point, then suspicion will prevent him or her from purchasing further products. Second, for the brand owner, a well-protected product will have an edge in leading the market and promoting the selling of its products. Third, consumer verification at the time of purchase shields the owner from any culpability, and fourth, consumer empowerment marshals a very large field force of independent agents to combat the counterfeiting problem.

The second criterion is cost and value, which refers to devising a solution at the lowest cost and which offers the highest value proposition. Investments for security are sensitive to brand owners; too high or too low an investment is unfavorable. High-cost investment will create an obstacle to the development of products; low-cost techniques, by contrast, cannot provide enough security for products, so in these instances, the investment may become a heavy loss. The rule of thumb for selecting anti-counterfeiting technology is that the total investment for security should not exceed 1% of the product's value.

Forensics and interdiction refer to security techniques needing to provide sufficient deterrence that makes counterfeiting risky. Interdiction is an outcome that only occurs if the technology has sufficient forensics. Thus, a good technique is one that can effectively differentiate a genuine from a fake item. When the consumer can distinguish the genuineness of the product at the point of sale, and no experts are needed to verify it in the lab, then the technique is ideal and should be promoted. In fact, however, many security techniques need labs to perform forensic tests. In this sense, a technique has high forensic applicability if it can provide quantitatively evident data. These data certainly are crucial to the brand owner if a prosecution procedure is required.

Simplicity and adaptability are other criteria, which refer to how easy it is to implement security techniques and whether they have long-term stability. Brand owners are always seeking solutions that produce less disruption to their on-going product manufacturing. A more flexible technique that can be used either at the product level or the packaging level, while providing sufficient security capability, is an ideal one. The fifth criteria, value-

added features, refer to security techniques being able to provide other applications or value-added features, other than anti-counterfeiting, to the brand owner.

These criteria have been selected, according to the author, on the basis of numerous interviews with industry leaders, security specialists, and various providers of anti-counterfeiting technologies. Additionally, there has been a significant review of information in the public domain, most notably from Internet sources. Moreover, the five golden criteria were recognized by Killingsworth et al. [11], from the University of Alabama in Huntsville, when presenting at DMSMS 2009 on the topic of how their practice is preventing counterfeiting in defense supply chains.

These five criteria provide more proper guidance for selecting of the proper anti-counterfeiting technology; here, we adapt the five criteria to assess the conventional security techniques, as well as the NCC taggant.

#### *7.3.3.1 Consumer Empowerment*

Many conventional security techniques provide some consumer empowerment. Holograms are a typical example. The advantage of holograms is that consumers can distinguish the genuineness of products by observing color-change properties with the naked eye. It has been successfully adopted by some very famous brand owners, including MasterCard@, and it is still being used today. Because holograms have limited covert security, they are vulnerable to counterfeiters.

CLC Security ink, another popular technique, provides similar features to holograms, such as iridescence, and can be identified by consumers. Moreover, it includes a covert

security feature, selective reflection, to provide enhanced security. Polarized-hidden images are another example for promoting covert security features, though they can be authenticated by consumers using simple solution, such as polarizers, their limited covert security features have made them less favorable for brand owners.

Other security techniques, such as security taggants and biometrics, usually require high-end instruments or scanners to verify the genuineness of products; therefore, they are also less favorable to brand owners.

NCC taggant, by contrast, provides many security features, such as iridescence, selective reflection, fluorescence, unique morphology, white light diffraction pattern and water induced color change. All of these features can be authenticated by the consumer, either with the naked eye or with simple solutions described above. Although some features are new to ordinary consumers, a security information advertizing campaign may enhance consumer's awareness, and to facilitate the authentication process. As these features can be used by consumers at the point of sale, the NCC taggant, in this instance, does provide consumer empowerment.

#### *7.3.3.2 Cost and Value*

Cost is a sensitive topic for brand owners when selecting security techniques, as it is directly related to profitability. Cost includes both the security features and the costs of authentication tools. Low-cost and efficient techniques are clearly sought. Among conventional security techniques, holograms have relative low costs due to their possibility of mass production. Other low-cost techniques include security ink and hidden

images; however, as they have limited covert security features, these techniques are more vulnerable to counterfeiters. Biometric techniques and taggants are much more secure, as they are unique and very hard to mimic. However, these techniques usually require expensive authentication tools, such as spectrometers and image databases. NCC taggant, by contrast, offers low-cost authentication solution, and this is true for either overt security or covert security.

In summary, NCC taggant technique has several advantages over other security techniques in terms of cost and value: NCC taggants not only provide multiple security features but also offer low-cost investment for authentication. If law enforcement authorization is needed, a more accurate quantified test, either on site or in the lab, can be provided.

#### *7.3.3.3 Forensic and Interdiction*

Forensic security features are crucial for product protection because they provide much accurate authentication by using special designed tools. The forensic security feature of an NCC taggant is polarized fluorescence which can be authenticated using specifically designed spectrometer and an optical analyzer kit to verify the unique fluorescent emission peak and the polarization state. Moreover, another unique optical property, the white light diffraction pattern provides a second forensic security feature and this feature not only can be identified by ordinary consumer at the point of sale, but also can be identified with a spectrometer when law-enforcement evidence is needed. Whilst other conventional security techniques, such as holograms, security ink, tanggants, may also provide forensic security, intrinsic material-based nature of the security features of the

NCC taggant, together with the large number of unique features, suggest that the NCC taggant is an attractive option.

#### *7.3.3.4 Simplicity and Adaptability*

The fourth quality concerns the properties of anti-counterfeiting technology that ensure ease of implementation and long-term stability. Among all of the conventional security techniques listed above, NCC taggants are worth noting. As taggants are usually made as invisible particles mixed with products, concern may result if the mixing has any side effects for the products. Other security techniques, such as holograms, security ink, emphasize their visibility; therefore, they are usually attached to products externally, so they incur fewer side effects during security technique implementation, NCC taggants take the same approach, and can be attached to various products with fewer side effects.

#### **7.3.3.5** *Value-added Features*

This feature concerns the extra value that can be added to products of the brand owner. Because the brand owner has already invested in security techniques for his or her products, if a security feature can bring extra value, then it will be more attractive. For example, holograms can increase visibility and attract customers, so they have often been adopted on the security market. Other techniques, such as security ink, can also attract customers with their unique iridescence. NCC taggant is designed in such a way that it not only possesses stunning iridescence but also possesses other unique optical properties, such as UV fluorescence, selective reflection, and white light diffraction, and all of these

features can be authenticated by consumers using simple method. These features could also be used for products decoration purpose, and so provide value-added benefits.

In summary, NCC Taggant is a sophisticated security technique. It not only has more covert security features, but it also includes a simple authentication method. It not only provides consumer empowerment and forensic features, but it also possesses simplicity and value-added features. Although it is required to optimize the NCC taggant , to develop mass production method, and to validate the repeatability and durability of the the material, the NCC taggants, as a newly developed security device, offers low cost and practical security choices for brand owners.

## 7.4 Conclusions

We have performed and assessed the possibility of using NCC as a security taggant. By using a technique described in this thesis, many unique optical security features including iridescence, selective reflection, UV fluorescent iridescence, unique morphology, white-light diffraction pattern, and water induced color variation can be accomplished and be combined into one taggant. The result is a single system that can support multiple security features. These security features are properties of the unique NCC material. Therefore, any attempt to counterfeit would require the counterfeiters to recreate the NCC synthesis process, which requires advanced chemistry techniques. Moreover, some of these techniques— such as the relationship between chirality of NCC and iridescence—require knowhow not available in the literature—hence increasing its security. Finally, consumers

have the advantages of a simple, low-cost authentication method and convenient simple equipment unless further lab examination is required.

## 7.5 References

[1]. P.N. Newton, R McGready, F. Fernandez, M.D. Green, M. Sunjio, C. Bruneton, et al., "Manslaughter by fake artesunate in Asia-will Africa be next?" PLoS Med.;3(6):e197 (2006)

[2]. www.aamva.org/WorkArea/DownloadAsset.aspx?id=804, "AAMVA security framework_Feb2004(2).pdf"

[3]. P. Lowe and S.Matz, "Anti-counterfeiting technology-a guide to protecting and authenticating products and documents"(2001)

[4]. http://en.wikipedia.org/wiki/Taggant

[5]. J. F. Revol, L. Godbout and D. G. Gray, "Solid self-assembled films of cellulose with chiral nematic order and optically variable properties," J. Pulp Pap. Sci. 24, 146–149 (1998)

[6]. D. P. Craig, F.R.S., E. A. Power, and T. Thirunamachandran, "The dynamic terms in induced circular dichroism," Proc. B. Soc. Lond. A. 348, 19-38 (1976)

[7]. http://www.visionandlearning.org/whatisvision08.html

[8]. Y. Jiang, B. Wilson, A. Hochbaum, J. Carter, "Novel Pigment Approaches in Optically Variable Security Inks Including Polarizing Cholesteric Liquid Crystal(CLC) Polymers," Optical Security and Counterfeit Deterrence Techniques IV, SPIE 4677 (2002)

[9]. M. L.Tsai, S. H. Chen, and S. D. Jacobs, "Optical notch filter using thermotropic liquid crystalline polymers," Appl. Phys. Lett. 54, 2395 (1989)

[10]. A. Das, "Technology Solutions:A Primer for Combating Counterfeiting & Piracy," Confederation of Indian Industry (2008)

[11]. W. R. Killingsworth and K. W. Sullivan, "An Integrated Approach to Preventing Counterfeits in Defense Supply Chains," DMSMS (2009)

# Chapter 8

# CONCLUSIONS AND SUGGESTIONS FOR FUTURE RESEARCH

## Conclusions

In this thesis, the possibility of using NCC to make a security taggant has been assessed. The assessment was conducted by following a series of experiments: namely, synthesis of NCC, study of the iridescence-formation in the chiral liquid crystal phase, and study of the origin of the iridescence in the solid film. This was followed by an exploration of the optical properties of the iridescent NCC film with one investigation of polarized light reflection, one examination of the unique morphology, one investigation of white light diffraction, and a study of color response to the change of relative humdity. Finally, an ultraviolet fluorescent dye (OBA) was added to the NCC to create further covert UV fluorescence security. As a result, multiple security features including iridescence, selective reflection, UV fluorescence, unique morphology, and white light diffraction patterns have been built into one NCC taggant. Due to the complexity of the creation of each security feature, we suggest that the proposed NCC taggant is very hard to mimic. The detailed conclusions for these experiments are as follows:

- By optimizing the sulfuric acid hydrolysis process, NCC that can be used to form iridescence. These conditions include the careful selection of key parameters, i.e., wood species, hydrolysis time, pH, and sonication power.

- Ordering plays a key role in the formation of iridescence. Ordering of the NCC is affected by an external force, such as gravity, and environmental conditions, such as

temperature, relative humidity, container shape, stability of the container supporter, and manner of NCC suspension injection. When an NCC suspension was injected into a rectangular-shaped container in a controlled manner, and left standing for a long period of time, for example, one week, a linear type long-range order phase formed, and this linear planar liquid crystal phase can yield iridescence in the liquid phase under white light illumination (see Chapter 3). When the NCC suspension was poured into a circular petridish, by contrast, a circular-shaped diffraction pattern was observed (see Chapter 4); therefore one can obtain different diffraction patterns by controlling the casting environment conditions.

- Iridescence of the solid film is of interest because it can be used as an overt security feature. The iridescence originated from a combination of multilayer selective interference and surface relief grating diffraction. The presence of the surface gratings was confirmed by AFM study of the NCC surface. These gratings had a pitch of about 2 microns. The multiple layer structure was confirmed with cross-section ananlysis of the film structure under SEM.

- The iridescent NCC film discussed in the thesis has a strong selective reflection property, that is when the material was illuminated using non-polarized light, the film can create a circularly polarized light reflection intensity contrast: it has stronger reflection for left-handed circularly polarized light than for right-handed circularly polarized light, and this light intensity contrast can be distinguishable using a low–cost circular polarizer. As a result, this property can be used as a method to identify whether the taggant is chiral NCC or not. By measuring the chirality using a chirality test setup built during this work, one can authenticate the genuineness of the taggants.

- An Optical Brightening Agent (OBA) is a fluorescent dye that is used conventionally in the pulp and paper industry for increasing the whiteness of the pulp and paper. Here we added OBA to the NCC suspension and by doing so, we demonstrated that a covert security feature, UV fluorescence, can be incorporated into the iridescent NCC film. We found that the amount of OBA addition is a key factor. An optimized amount yielded fluorescence without affecting the overall iridescence of the NCC film; an over-dosed OBA, however, affected the optical reflection property by broadening the CD spectrum and creating a red shift of the reflection wavelength. This was confirmed by examining the circular dichroism (CD) spectrum shape and CD peak position of the OBA-doped NCC film. In addition, our preliminary result showed that the fluorescence from OBA-doped NCC was circularly polarized.

- A reversible humidity color indicator has been demonstrated. The color change is attributed to the pitch tuning induced by the water sorption on the surface of NCC and inside the film. This water induced color change can be used as a tool to authenticate the genuineness of the NCC.

- By combining these unique optical properties, multiple security features can be embedded into one NCC taggant, making the NCC taggant very sophisticated. In contrast, conventional security devices, such as holograms, contain only one or two security features. Moreover, the security features demonstrated in this study can be authenticated using low-cost tools, which is very important for brand owners. In the thesis, a simple setup for further security authentication tests is also described.

It is worth pointing out that given enough time and money, people can counterfeit anything that people can make. The aim of this study is attempt to provide a Phase I security solution that is one step ahead of the counterfeiters. Futher development is needed for fine tuning of this proposed technique.

## 8.2 Suggestions for Future Research

Although our study found many attractive features, significant improvements can be made to the performance of the NCC taggants. The improvements are divided into two parts: One is targeting on the material development and the other is targeting on new security features.

- **Material development**

- Mass production is key to the commercial success of the proposed security techniques.

Mass production involves making many copies of the product in a relatively short period. That a material can be mass-produced means that one can effectively control the production process and that it has good repeatability; as a result, an assembly machine line could be used to reduce labor costs and, in turn, reduce the overall cost of making the material. Therefore, investigating techniques for the mass production of chiral NCC is essential. Recently, Celluforce [1], a Quebec joint venture of Domtar Corporation and FPInnovations, has demonstrated the first mass production plant in the world that can produce one tonne per day of NCC. It will be important to evaluate weather it would be possible to adapt the production process to achieve desirable NCC properties that we have identified in this thesis.

- Stability is another key parameter for the security application. Objects to be protected by these taggants, such as documents and security certificates, may be required to endure more than 100 years, therefore, a study of how environmental parameters, such as temperature and humidity, affects the long-term optical and material properties of the chiral NCC is needed. Accelerated aging test [2], developed in pulp and paper industry, probably can be used for this purpose. Accelerated aging is testing that uses aggravated conditions of heat, oxygen, sunlight, vibration, etc. to speed up the normal aging processes of items. It is used to estimate the useful lifespan of a product or its shelf life when actual lifespan data is unavailable.
- The Chirality test is a method proposed in this thesis to evaluate the capability of the selective reflection of the NCC, and it can be used as a method to distinguish the genuineness of the NCC material. A higher chirality will yield a higher circularly polarized light intensity contrast, which favours the authentication, therefore it is necessary to find the method to enhance this property.
- Whitelight diffraction pattern of the NCC film is another proposed security feature. It is would be usful to investigate the method to control the diffraction pattern by studying the self-assembly process.

➢ **Security feature development**

- Functionalizing NCC should be attempted. Our study demonstrated that, by adding OBA to NCC, one can obtain a fluorescent and iridescent NCC material, indicating that the surface of NCC could be an effective site for other chemical molecules. In a paper published in Nature Technology, Olsson et al. [3] demonstrated that ferromagnetic cobalt

ferrite nanoparticles could be successfully grafted onto cellulose material, which possesses high potential for security applications.

- Our study demonstrated that NCC can be used to form iridescent film, which is accomplished by casting NCC in a petri dish; therefore, understanding whether we can create iridescent film through direct printing of NCC on the substrate is interesting as it would eventually be desirable to produce chiral NCCmaterial via a roll-to-roll method in order to increase throughput.
- By controlling the chiral nematic pitch of NCC, we demonstrated that one can obtain a different color, but this is a static effect. Thus, the question remains as to whether one can change the color by dynamically controlling the pitch change. A dynamic color change not only provides enhanced security by increasing the difficulty of duplication but also extends its applications into different areas, such as the color display industry. Without a doubt, electric or magnetic fields are potential tools to dynamically change the pitch.

## 8.3 References

[1]. CelluForce press release, "CelluForce celebrates the inauguration of the world's first NanoCrystalline Cellulose demonstration plant," Embargo January 26, 2012

[2]. X. Zou, T. Uesaka and N. Gurnagul, "Prediction of paper permanence by accelerated aging I. Kinetic analysis of the aging process," Cellulose 3, 243-267 (1996)

[3]. RT. Olsson, MA. Azizi Samir, G. Salazar-Alvarez, L. Belova, V. Ström, LA.

Berglund, O. Ikkala, J. Nogués, UW. Gedde, “Making flexible magnetic aerogels and stiff magnetic nanopaper using cellulose nanofibrils as templates,”Nat Nanotechnol.5(8):584-8. Epub (2010)